Lithos 239 (2015) 186–216

Contents lists available at ScienceDirect

Lithos

journal homepage: www.elsevier.com/locate/lithos

Invited review article

What can we learn from melt inclusions in migmatites and granulites?

B. Cesare [a], A. Acosta-Vigil [a], O. Bartoli [a], S. Ferrero [b,c]

[a] Department of Geosciences, University of Padova, Italy
[b] Department of Earth and Environmental Sciences, University of Potsdam, Germany
[c] Museum für Naturkunde (MfN), Leibniz-Institut für Evolutions- und Biodiversitätsforschung, Berlin, Germany

ARTICLE INFO

Article history:
Received 3 June 2015
Accepted 28 September 2015
Available online 24 October 2015

Keywords:
Melt inclusions
Migmatites
Granulites
Granites
Crustal melting
Nanogranitoids

ABSTRACT

With less than two decades of activity, research on melt inclusions (MI) in crystals from rocks that have undergone crustal anatexis – migmatites and granulites – is a recent addition to crustal petrology and geochemistry. Studies on this subject started with glassy inclusions in anatectic crustal enclaves in lavas, and then progressed to regionally metamorphosed and partially melted crustal rocks, where melt inclusions are normally crystallized into a cryptocrystalline aggregate (*nanogranitoid*).

Since the first paper on melt inclusions in the granulites of the Kerala Khondalite Belt in 2009, reported and studied occurrences are already a few tens. Melt inclusions in migmatites and granulites show many analogies with their more common and long studied counterparts in igneous rocks, but also display very important differences and peculiarities, which are the subject of this review. Microstructurally, melt inclusions in anatectic rocks are small, commonly 10 μm in diameter, and their main mineral host is peritectic garnet, although several other hosts have been observed. Inclusion contents vary from glass in enclaves that were cooled very rapidly from supersolidus temperatures, to completely crystallized material in slowly cooled regional migmatites. The chemical composition of the inclusions can be analyzed combining several techniques (SEM, EMP, NanoSIMS, LA–ICP–MS), but in the case of crystallized inclusions the experimental remelting under confining pressure in a piston cylinder is a prerequisite. The melt is generally granitic and peraluminous, although granodioritic to trondhjemitic compositions have also been found.

Being mostly primary in origin, inclusions attest for the growth of their peritectic host in the presence of melt. As a consequence, the inclusions have the unique ability of preserving information on the composition of primary anatectic crustal melts, before they undergo any of the common following changes in their way to produce crustal magmas. For these peculiar features, melt inclusions in migmatites and granulites, largely overlooked so far, have the potential to become a fundamental tool for the study of crustal melting, crustal differentiation, and even the generation of the continental crust.

Contents

http://dx.doi.org/10.1016/j.lithos.2015.09.028

Prologue

The reader may be interested in a "historical" background to the birth and development of research in this topic.

Everything began by a serendipitous encounter with G. Venturelli (University of Parma, Italy), who owned some extraordinary thin sections of metapelitic enclaves from the dacite of El Hoyazo (Betic Cordillera, SE Spain) and offered the senior author (BC) to take part in a research project on those volcanic rocks and their crustal enclaves. The enclaves turned out to contain abundant, undevitrified glassy inclusions in most of their minerals, and in particular in garnet; for such peculiarity they can be considered unique in the world. Although El Hoyazo is visited by dozens of geologists yearly, this aspect had been completely neglected. The melt inclusions (MI) in the enclaves of El Hoyazo, and subsequently of Mazarrón, have turned out to shelter a small geological treasure and are still undergoing a thorough microstructural and chemical characterization (Acosta-Vigil et al., 2012a and references therein). Having recognized that MI were trapped by the growing host minerals during melting of the enclaves (Cesare and Maineri, 1999), and that they could be analyzed to gain information on the chemical composition of crustal anatectic melts (e.g., Cesare et al., 2003a), the consequential following step has been to look for similar MI in regionally metamorphosed anatectic rocks such as migmatites and granulites, in order to understand if MI entrapment was an exceptional feature of enclaves or a common process during crustal anatexis.

After a few years of search, the first finding of MI (*nanogranites*) in regionally melted rocks came from a granulite of the Kerala Khondalite Belt (India, Cesare et al., 2009a). Since then, some tens of occurrences have been recorded in metapelitic, metapsammitic and metagranitoid migmatites and granulites worldwide, providing the justification for this paper.

1. Introduction

This is a review of the state of the art of knowledge on melt inclusions (MI) in migmatites and granulites. Research on MI in high-grade anatectic rocks would have started earlier if the report of inclusions in garnet and the insightful interpretations made by Hartel et al. (1990; unknown to the writers until 1999) had been followed by further, detailed studies. But it was not the right time, yet, and the first paper where MI are extensively described and discussed appeared a few years later (Cesare et al., 1997).

Although MI are well known since Sorby (1858) and have been extensively used in igneous petrology, geochemistry, volcanology and economic geology (reviews in Roedder, 1984; Frezzotti, 2001; Audétat and Lowenstern, 2014), until recently they have been observed and studied exclusively in intrusive and extrusive igneous rocks. Conversely, apart from a few notable exceptions (e.g., Chupin et al., 1998, 2001), they have been overlooked in partially melted crustal rocks such as migmatites, granulites and enclaves or xenoliths in lavas.

Such lack of recognition of MI outside igneous systems is still so well established that MI are defined as "droplets of silicate melt that are trapped in minerals during their growth in a magma" (Audétat and Lowenstern, 2014; Clocchiatti, 1975). This incomplete definition needs to be modified, and the perspective on related processes widened, as MI also occur in crustal rocks that have undergone partial melting, and in host minerals (e.g., garnet, hercynite, ilmenite) from rocks which clearly do not have an igneous origin. A review about a novel topic such as MI in high-grade anatectic rocks is therefore timely and useful for crustal petrology and related disciplines.

Reviewing the literature produced mainly by the research group of the writers, this paper discusses in detail the origin by incongruent melting of MI in migmatites, granulites and anatectic enclaves, outlining the fundamental differences between these inclusions and those formed during magma crystallization. It provides an exhaustive description of the optical and electron microscope features of MI, from totally glassy to fully crystallized, and reviews the analytical techniques adopted for the microstructural and chemical characterization of MI, discussing analogies and differences with respect to analysis of MI in igneous rocks. Then the paper outlines the key microstructural and chemical information that can be obtained from MI, and reports some significant examples of how this new approach has impacted on our views of crustal anatexis. Finally, after a comment on the problems and pitfalls of studies on MI and of data interpretation, and a reply to the main objections raised in the recent literature against our approach, we highlight some of the directions where research on MI in crustal rocks should focus in the next decade.

2. What are melt inclusions?

Research on MI has a long history, and continues to provide key information for our understanding of, among others, igneous processes, volcanism, ore formation, and even the origin of the solar system. Being by far more common in igneous rocks, especially volcanic, it is easy to understand why MI have been fully exploited in these systems, and why conversely they have been neglected in granulites and migmatites where they are more rare, difficult to recognize, and were not expected to occur until recently.

MI in most cases contain silicate phases (minerals or quenched glass) but may also display other more exotic compositions (e.g., carbonatite or metal liquids). This paper implicitly refers to silicate-melt inclusions, although several of the concepts presented here could apply to a wider compositional range. We also implicitly refer to *primary* MI, i.e., those trapped during the simultaneous growth of the mineral that contains them (the *host*), rather than to the *secondary* MI that are trapped after the growth of the host (Roedder, 1984).

Given that (primary) MI can be trapped by a host growing both from and with a melt phase (as detailed in the next section), we propose to redefine MI as "small droplets of melt that are trapped in minerals during their growth in the presence of a melt phase" (Cesare et al., 2011). This more comprehensive definition accounts for MI entrapment during both igneous and metamorphic/anatectic processes.

The general characteristics, modes of entrapment, textural features, post-entrapment changes and common ways of characterization of MI in igneous rocks, have been extensively and thoroughly reviewed and regularly updated to the state of the art of knowledge (Audétat and Lowenstern, 2014; Clocchiatti, 1975; Danyushevsky et al., 2002; Frezzotti, 2001; Roedder, 1984; Schiano, 2003; Sobolev and Kostyuk, 1975; Webster, 2006). Here we briefly review some basic information from igneous MI that is applicable also to MI in migmatites and granulites, in order to focus on the peculiar features of the latter in the following sections.

Melt inclusions are hosted in many, virtually all, igneous-related minerals, but are mostly studied in those minerals where they are more abundant and/or better preserved and/or more visible. It follows that common host minerals are quartz and plagioclase in felsic igneous rocks, and olivine, pyroxene and plagioclase in mafic/ultramafic igneous rocks. The host phases where MI have been observed in metamorphic/anatectic rocks are reported in Table 1 and discussed later.

Melt inclusions size commonly ranges from a few to a few tens or, less frequently, a few hundreds of micrometers, the lower limit being dictated by the spatial resolution of optical microscopes, making the smaller inclusion not usable for most routine analytical techniques. In order to be easily studied by optical methods, and to allow application of most analytical techniques, a minimum size of c. 20 μm is recommendable. Such size is common in MI from igneous rocks (Audétat and Lowenstern, 2014), but very rare in migmatites and granulites (compare Cesare et al., 2003a with Bartoli et al., 2013b).

The shape of MI varies from highly irregular to a perfect "negative crystal" defined by facets parallel to rational crystallographic orientations of the host (e.g., bipyramid in quartz, dodecahedron in garnet; Fig. 1). The negative crystal shape results from post-entrapment readjustment of the MI shape, by a process of dissolution–reprecipitation that is argued not to change the volume of the inclusion (e.g., Roedder, 1984) or its composition (Frezzotti, 2001; Manley, 1996).

The post-entrapment modifications that may take place in MI depend on the complex interplay between several factors: P–T conditions and variations, time, deformation, melt composition and chemical refractoriness of the host. The main changes that MI may undergo after the primary conditions of entrapment are the diffusional exchange with the host or with the external magmas/rock matrix through the host (e.g. Fe and H; Danyushevsky et al., 2000; Gaetani et al., 2012), the partial to complete crystallization of the melt (Frezzotti, 2001), the nucleation of bubbles by volume contraction during cooling and crystallization (Lowenstern, 2003; Moore et al., 2015; Roedder, 1979a), the breakage of the cavity (decrepitation) when the pressure within the MI significantly exceeds the pressure on the host (e.g., Tait, 1992; Touret and Huizenga, 2012), or when the host is undergoing strain and microfracturing affects the MI (Ferrero et al., 2012). All the above processes, plus the crystallization of the host on inclusion walls (e.g., Frezzotti, 2001), may affect to different extents the capacity of MI to retain information on the original melt composition and on the conditions of entrapment.

From a microstructural point of view, the most solid evidence for a primary trapping is when MI are distributed in zonal arrangements (Roedder, 1979b) that reflect the progressive, often concentric growth of the host. This is a typical microstructure in phenocrysts of lavas (Fig.2a) but is also observed in porphyroblasts of migmatites (Fig. 2b). Primary entrapment is also suggested when MI occur isolated or in clusters with random distribution in the host mineral (Fig. 2c,d). When support in favor of a primary entrapment exists, a close genetic relation between melt and (part of) the host mineral can be established, and consequently, unless there have been significant post-entrapment modifications, the chemical compositions of MI and host are related and provide petrogenetic information.

Analysis of the mineralogical and chemical compositions of crystallized to glassy MI can be difficult and time-consuming due to the small size of these entities, which in some cases prevents from using conventional methods. However, a number of analytical techniques, both destructive and non-destructive, can be successfully applied to measure the major and trace element concentrations, including the fluid species (e.g., H, C, B), and the isotope ratios of the melts, as well as to determine the nature of the solids or of the (immiscible) fluids that may coexist with the melts. These techniques have recently been reviewed by Audétat and Lowenstern (2014) and below we will only focus on those that are of special interest for the small MI in migmatites and granulites. In the case of partially or totally crystallized MI, it is necessary to re-homogenize them by heating under controlled settings (Danyushevsky et al., 2002; Esposito et al., 2012), in order to bring the MI back to the original trapping conditions, i.e., to a homogeneous melt that is then quenched to glass by rapid cooling. Then, the chemical composition of this glass, assumed to represent that of the original trapped melt, can be measured by electron microprobe, Laser Ablation Inductively Coupled–Plasma Mass-Spectroscopy (LA–ICP–MS), Secondary Ion Mass Spectrometry (SIMS) and other tools depending on the size of MI and on the parameter of interest.

3. Entrapment of melt inclusions during incongruent melting

In order to form MI, a host mineral must grow in the presence of a melt phase. The most common geological process that fulfills these conditions is magma crystallization, but another one, less noted but equally important, is incongruent melting.

The hypothesis that minerals may trap MI during anatexis was first made by Cesare and Maineri (1999), discussing the origin of glassy inclusions in the residual metapelitic enclaves of El Hoyazo. In these rocks primary MI are found most frequently within garnet and plagioclase, but also within most other phases; moreover, glass in the matrix is intimately intergrown with acicular sillimanite. The interpretation of these microstructures was that crystals in the solid framework of the enclave had grown in the presence of melt during the prograde anatexis of the enclaves. Chupin et al. (2006a) and Madyukov et al. (2011) reached the same conclusions for some granulite xenoliths from the Pamir diatremes.

Due to the incongruent nature of many melting reactions in the continental crust (recently reviewed by Weinberg and Hasalovà, 2015), the entrapment of MI during (crustal) anatexis should appear as a common process in the genesis of migmatites and granulites. In a model incongruent reaction:

$$A\ (+B)\ =\ C\ +\ M$$

with A, B and C representing solids and M a liquid phase, C is produced (grows) together with M, thereby creating the necessary conditions for primary entrapment of MI. Geological examples of incongruent melting range from the well-known, ideal reaction

$$En\ =\ Fo\ +\ melt,$$

Table 1
Published occurrences of MI in migmatites and granulites. n.a.: not available. n.d.: not determined. *) if P–T conditions of MI intrapment are not specified, we report estimated or inferred P–T conditions at peak.

	Occurrence			
Reference	Locality	Rock type	Assemblage	T, P conditions*
Acosta-Vigil et al. (2007)	El Hoyazo (Spain)	Metapelitic enclave	Bt–Grt–Sil–Pl–Ilm–Gr-melt	850 ± 50 °C, 5–7 kbar
Acosta-Vigil et al. (2010)	El Hoyazo (Spain)	Metapelitic enclave	Bt–Grt–Sil–Pl–Ilm–Gr–melt	700–750 °C, 850 ± 50 °C, 5–7 kbar
Acosta-Vigil et al. (2012a)	El Hoyazo (Spain)	Metapelitic enclave	Bt–Grt–Sil–Pl–Ilm–Gr–melt	700–750 °C, 850 ± 50 °C, 5–7 kbar
Acosta-Vigil et al. (2014)	Istán, Ronda (Spain)	Grt-leucosome in migmatites	Qz–Kfs–Pl–Grt–Ms–Sil–Tur	675–685 °C, 3–3.5 kbar
Álvarez-Valero and Kriegsman (2008)	Mar Menor (Spain)	Metapelitic enclave	Crd–Sil–Spl–Pl–And–Bt–Kfs–Opx–Gr–Ilm-melt	850–900 °C, 2–3 kbar
Álvarez-Valero and Kriegsman (2010)	El Hoyazo, Mazarrón and Mar Menor (Spain)	Metapelitic enclave	Not provided	850 ± 50 °C, 4–7 kbar
Álvarez-Valero et al. (2005)	El Hoyazo (Spain)	Metapelitic enclave	Grt–Sil–Crd–Bt–Spl–Kfs–Pl–Ilm–Gr–melt	850 ± 50 °C, 5.5–7 kbar
Álvarez-Valero et al. (2007)	El Hoyazo and Mazarrón (Spain)	Metapelitic enclave	Spl–Crd–Bt–Grt–Sil–melt–Kfs–Pl–Ilm–Gr	850 ± 50 °C, 4–7 kbar
Álvarez-Valero et al. (2014)	Beni Bousera (Morocco)	Metapelitic granulites	Grt–Bt–Ky–Rt–Kfs	710–830 °C, 5–12 kbar
Axler and Ague (2015)	Bigelow Brook Fm. (USA)	Felsic granulites	Grt–Sil–Kfs–Qz–Crd–Bt ± Spl	1000 °C, 10 kbar
Barich et al. (2014)	Jubrique, Ronda (Spain)	Mylonitic gneisses and porphyroblastic gneisses	Grt–Qz–Pl–Kfs–Ky–Sil–Crd–Bt–Rt–Ilm–Spl–Gr	750–850 °C, 5–14 kbar
Bartoli et al. (2013a)	Ojén, Ronda (Spain)	Quartzo-feldspathic metatexite	Qz–Pl–Kfs–Bt–Sil–Grt–Ms–Gr–Ap–Ilm	680–750 °C, 4.5–4.8 kbar
Bartoli et al. (2013b)	Ojén, Ronda (Spain)	Quartzo-feldspathic metatexite	Qz–Pl–Kfs–Bt–Sil–Grt–Ms–Gr–Ap–Ilm	700 °C, 5 kbar
Bartoli et al. (2013c)	Ojén, Ronda (Spain)	Quartzo-feldspathic metatexite	Qz–Pl–Kfs–Bt–Sil–Grt–Ms–Gr–Ap–Ilm	660–700 °C, 4.5–5 kbar
Bartoli et al. (2014)	Ojén, Ronda (Spain)	Quartzo-feldspathic metatexite	Qz–Pl–Kfs–Bt–Sil–Grt–Ms–Gr–Ap–Ilm	660–700 °C, 4.5–5 kbar
Bea and Montero (1999)	Kinzigite Formation, Ivrea (Italy)	Metapelitic migmatite	Grt–Bt–Sil–Qz–Pl–Ilm–Rt	n.a.
Bento dos Santos et al. (2011)	Ribeira Fold Belt (Brazil)	Granulites	n.a.	n.a.
Carosi et al. (2015)	Kali Gandaki (Nepal)	Metasedimentary granulites and migmatites	Qz–Pl–Bt–Grt–Ky–M ± Sil	n.a.
Cesare (2008)	El Hoyazo, Mazarrón and Mar Menor (Spain)	Metapelitic enclave	Grt–Pl–Bt–Sil–Gr–glass ± Ilm ± Crd ± And ± Kfs ± Spl	850 ± 50 °C, 5–7 kbar
Cesare and Acosta-Vigil (2011)	El Hoyazo (Spain); Kerala Khondalite Belt (India); Ronda (Spain)	Metapelitic enclave; felsic granulite; migmatite	Grt–Bt–Sil–Pl–Gr-glass	700–750 °C, >900 °C
Cesare and Gómez-Pugnaire (2001)	El Hoyazo and Mazarrón (Spain)	Metapelitic enclave	Bt–Grt–Sil–Pl–melt–Ap–Gr ± Crd ± Ilm ± Spl ± Kfs; Grt–Bt–Sil–Pl–Crd ± Spl; Crd–And–Sil–Bt–Pl–Spl ± Kfs	850 ± 50 °C, 4–7 kbar; 900–950 °C, ≥5 kbar
Cesare and Maineri (1999)				
Cesare et al. (1997)	El Hoyazo (Spain)	Metapelitic enclave	Bt–Grt–Sil–Pl–Ilm–Gr–melt	850 ± 50 °C, 5–7 kbar
Cesare et al. (2003b)	El Hoyazo and Mazarrón (Spain)	Metapelitic enclave	Bt–Pl–Grt–Sil–Spl–Kfs-glass–Ilm–Gr ± Crd; Crd–Kfs–Sil–Bt–Pl–Ilm–Spl–Gr-glass	850 ± 50 °C, 7 kbar; 800–900 °C, 4 kbar
Cesare et al. (2003a)	Mazarrón (Spain)	Metapelitic enclave	And–Sil–Spl–Crd–Bt–Pl-glass–Gr ± Kfs ± Qz	615–725 °C
Cesare et al. (2005)	El Hoyazo (Spain)	Metapelitic enclave	Bt–Grt–Pl–Sil-glass-Gr ± Crd ± Kfs ± Ilm ± Qz	850 ± 50 °C, 5–7 kbar
Cesare et al. (2007)	El Hoyazo and Mazarrón (Spain)	Metapelitic enclave	Crd–Sil–Pl–melt–Ilm–Gr ± Bt ± Grt ± Spl ± Qz ± Kfs ± And	850 ± 50 °C, 4–7 kbar
Cesare et al. (2009a)	Kerala Khondalite Belt (India)	Felsic granulite	Qz–Kfs–Grt–Crd–Sil–Bt–Spl	>900 °C, 6–8 kbar
Cesare et al. (2011)	El Hoyazo and Mazarrón (Spain); Lipari (Italy); Kerala Khondalite Belt (India); Ronda (Spain); Ivrea and Ulten Zones (Italy); Himalaya (Nepal)	Metapelitic enclave; felsic granulite; migmatite; gneiss		
Chen et al. (2013)	Sulu (China)	UHP quartzite	Qz–Grt–Amp–Spn–Hem	n.a.
Chen et al. (2014)	Sulu (China)	UHP Eclogite	Grt–Omp–Qz–Zo–Pg–Ky–Rt	820–840 °C, 18–21 kbar
Chen et al. (2015)	Dabie (China)	Leucosome in migmatite	Qz–Pl–Kfs–Zrn–Ttn–Ap–Amp–Mag–Bt–Chl	n.d.
Chupin and Kosukhin (1982)	Aldan Shield, Siberia (Russia)	Granulite facies anatectites	Not provided	5–7 kbar
Chupin et al. (1993)	Anabar and Aldan Shields, Siberia (Russia); Uivak, Canadian Shield (Canada); SE Pamir	Tonalite–trondhjemite gneisses; granulitic, eclogitic and pyroxenitic xenoliths	Hyp–Grt–Bt–Sil; Grt–Sil–Crd–Bt	850–950 °C, ≥6–8.5 kbar; >1050 °C, >15 kbar
Chupin et al. (1998)	Witwatersrand Basin and Limpopo Belt (South Africa)	Quartzites and orthogneisses	Not provided	Greenschist facies and granulite facies
Chupin et al. (2010)	SE Pamir	Granulitic and eclogitic xenoliths	Grt–Opx-Cpx; Grt–Bt–Opx; Grt–Ky; Grt–Cpx–Pl; Grt–Bt–Opx; Grt–Bt	940 °C, ≥12–13 kbar

Chupin et al. (2006a)	SE Pamir (Tajikistan)	Granulitic xenolith		≈1000 °C, ≈15 kbar
Chupin et al. (2006b)	Kola (Russia)	Trondhjemite plagiogneiss	Not provided	Not provided
Chupin et al. (2010)	SE Pamir	Granulitic xenoliths	Grt–Cpx–Pl; Grt–Ky	940–1000 °C, >12 kbar
Clarke et al. (2005)	Mazarrón (Spain)	Metapelitic enclave		
Darling (2013)	W Adirondacks (NY, USA)	Metapelitic granulite	Grt–Bt–Sil–Qz–Pl–Kfs	≈850 °C, ≈7 kbar
Darling et al. (1997)	Gore Mountain (NY, USA)	Mafic granulite	Grt–Amp-	800 °C, 8 kbar
Di Martino et al. (2011)	Lipari (Italy)	Metasedimentary xenocrysts		725–900 °C, 4–4.5 kbar
Dolgov et al. (1984)	Aldan Shield (Russia)	Amphibolite and granulite-facies migmatites	Not provided	700–900 °C, 5–7 kbar
Ferrando et al. (2005)	Donghai, Su-Lu (China)	Quartzite and eclogite	Qz–Ky–Ph-Tpz-Pa-Py-Brt–Rt–Zrn–Ap; Grt–Cpx–Amp–Phe–Ky-Pg-Qz–Rt–Ap–Zrn–opaque ore	840 ± 50 °C, 35–40 kbar
Ferrero et al. (2011)	El Hoyazo (Spain)	Metapelitic enclave	Grt–Pl–Bt–Sil-melt–Gr–Ap–Zrn–Mnz–Ilm ± Crd ± Spl ± Qz; Grt–Crd–Spl–Bt–Sil–melt ± Ilm ± Kfs ± Qz	850 ± 50 °C, 5–7 kbar
Ferrero et al. (2012)	Kerala Khondalite Belt (India); Ojén, Ronda (Spain); Ivrea and Ulten Zones (Italy); Barun, Himalaya (Nepal)	Khondalites; migmatites; gneisses	Qz–Grt–Crd–Sil–Bt–Ilm–Spl–Kfs–Pl; Qz–Pl–Kfs–Bt–Sil–Grt–Crd–Gr–Ilm; Bt–Sil–Pl–Qz–Grt–Ky–Kfs	≈900 °C, 6–8 kbar; 700–800 °C, 5–8 kbar; 800–860 °C, 8 kbar
Ferrero et al. (2014)	La Galite (Tunisia)	Tonalitic and garnetitic enclaves	Pl–Qz–Grt–Bt–Kfs–Ilm–Zrn–Mnz ± Spl; Grt–Qz ± Kfs	770–820 °C, 5 kbar
Ferrero et al. (2015)	Orlica-Śnieżnik Dome, Bohemian Massif	Felsic Granulite	Grt–Ky–Qz–Msp–Pl + Rt + Ttn ± Ep	875 °C, 27 kbar
Frezzotti et al. (2004)	Vulcano (Italy)	Quartz xenoliths	Qz (Kfs–Opx-Pl)	980–1100 °C, 3.5–5.5 kbar
Ganzhorn et al. (2014)	Western Gneiss Region (Norway)	UHP Eclogite	Grt–Omp–Qz–Ep	≈800 °C, >30 kbar
Gao et al. (2012)	Dabie (China)	UHP Eclogite	Grt–Omp–Rt–Pl–Amp–Ph–Spn–Brt	≈830 °C, 24 kbar
Gao et al. (2013)	Dabie (China)	Eclogite	n.a.	n.d.
Gao et al. (2014)	Dabie (China)	UHP Eclogite	Grt–Omp–Qz/Coe–Rt	750–850 °C, >33 kbar
Georgieva et al. (2005)	Central Rhodope (Bulgaria)	Grt–Ky Schists	n.a.	n.a.
Groppo et al. (2012)	Barun (Nepal)	Metasedimentary anatectic gneisses	Qz–Pl–Kfs–Bt–Grt–Ky–Sil–Rt–Ilm–Ap–Gr	>800–810 °C, >7.8–8.5 kbar
Harley and Nandakumar (2014)	Kulappara, KKB (India)	Leucocratic vein in UHT migmatite	Qz–Afs–Pl–Grt	>800 °C, 5(?) kbar
Hartel et al. (1990)	W Sulawesi (Indonesia)	Granulite–facies metapelite	Qz–Grt–Pl–Sil	>700 °C, >8 kbar
Hiroi et al. (2014)	Highland Complex (Sri Lanka)	(U)HT granulites	Grt–Bt–Sil–Qz–Ilm	950 °C, 9 kbar
Hwang et al. (2001)	Erzgebirge (Germany)	UHP Gneiss	Grt–Qz–Phe–Ky–Ab–Rt	n.a.
Kawakami et al. (2013)	Ryoke Belt (Japan)	Metapelitic migmatites	Grt–Bt–Crd–Qt–Kfs–Pl	700–750 °C, 6–4 kbar
Korsakov and Hermann (2006)	Kokchetav (Kazakhstan)	Marbles	Cc–Dol–Cpx–Grt–Ol–Spl–Kfs–Zrn–Rt–Ttn-Dia-Amp–Bt	1000 °C, 43–60 kbar
Kotkova et al. (2014)	N Bohemian Massif	UHP Felsic Granulite	Grt–Ky–Fsp–Qz–Dia	n.d.
Lang and Gilotti (2007)	NE Greenland	UHP metapelites	Grt–Ky–Phe–Qz–Bt	970 °C, 36 kbar *
Liu et al. (2013)	Dabie (China)	UHP Eclogite	Grt–Omp–Qz–Rt–Mag–Ap	800 °C, 15 kbar
Liu et al. (2014)	Dabie (China)	UHP Calc–gneiss	Grt–Ph–Ep–Qz–Pl–Kfs–Bt–Cal–Chl	650–800 °C, 10–20 kbar
Madyukov et al. (2011)	SE Pamir (Tajikistan)	Granulitic xenolith	Grt–Cpx–Sa–Ttn–Scp–Qz	≈1000 °C, ≈15 kbar
Malaspina et al. (2006)	Dabie (China)	Grt orthopiroxenites	Opx–Grt–Cpx–Ti Chu–Ti Chn–Ol	870 ± 50 °C, 40 ± 10 kbar
Massonne (2014)	Jubrique, Ronda (Spain)	Migmatite gneisses	Grt–Bt–Sil–Ky–Qz–Pl–Kfs–Rt–Ilm–Gr	>650 °C, 13 kbar
Mosca et al. (2012)	Kangchenjunga (Nepal)	Anatectic metapelites	Grt–Bt–Ky–Qz–Pl–Kfs–Ms	670 °C, 8 kbar
Stöckhert et al. (2001)	Erzgebirge (Germany)	UHP Gneiss	Grt–Qz–Pl–Phe	≥1000 °C, >45 kbar
Stöckhert et al. (2009)	Erzgebirge (Germany)	Saidenbachite (UHP gneiss)	Grt–Qz–Pl–Phe	≥1000 °C, >45 kbar
Wang et al. (2015)	Nyalam transect (Nepal)	Metapelitic migmatite	Grt–Bt–Ms–Ky–Qz–Pl–Ilm–Rt	≈700 °C, ≈10 kbar
Zeng et al. (2009)	Sulu (China)	Eclogite	Grt–Omp–Rt	≈830 °C, 24 kbar

Table 1 (*continued*)

Reference	Occurrence			Characterization								
	Host phase	Glassy	Crystallized	Optical	SEM	Phases in MI	Remelting	EMP	LA–ICP–MS	Raman	nanoSIMS–SIMS	Other info-comments
Acosta-Vigil et al. (2007)	Grt, Pl, Bt, Crd, Kfs, Ilm, Ap	X		X	X	Glass, Kfs, Ilm, Gr, Sil		X				
Acosta-Vigil et al. (2010)	Pl, Grt, Zrn, Mnz	X		X	X	Glass			X			
Acosta-Vigil et al. (2012a)	Pl, Grt	X		X	X	Glass, Kfs, Bt, Mag			X			
Acosta-Vigil et al. (2014)	Grt		X	X								
Álvarez-Valero and Kriegsman (2008)	Crd, Pl, Grt, Spl, And	X		X		Glass		X				
Álvarez-Valero and Kriegsman (2010)	Pl, Crd, Spl	X		X		Glass						
Álvarez-Valero et al. (2005)	Grt	X		X	X	Glass						
Álvarez-Valero et al. (2007)	Crd, Spl, Pl, Grt	X		X	X	Glass		X				
Álvarez-Valero et al. (2014)	Grt, Zrn	X		X	X	Glass						
Axler and Gue (2015)	Grt		X	X	X	Qz, Phl, Ms, glass (phase-CV)		X				
Barich et al. (2014)	Grt, Qtz	X	X	X	X	Qz, Pl, Afs, Kfs, Bt, Ms, glass, Phl, Als, Gr, Rt, Ilm, Spl, Cc, Ap, Zrn, Mnz						
Bartoli et al. (2013a)	Grt	X	X	X	X	Bt, Ms, Qz, glass	X	X		X		SIMS for H_2O
Bartoli et al. (2013b)	Grt	X	X	X	X	Bt, Ms, Qz, glass	X	X		X		
Bartoli et al. (2013c)	Grt	X	X	X	X	Bt, Ms, Qz, Pl, Kfs, glass, liquid H2O	X	X				
Bartoli et al. (2014)	Grt	X	X	X	X	Bt, Ms, Qz, Pl, Kfs, glass	X				X	
Bea and Montero (1999)	Mnz		X		X	Qz,Kfs, Ab						Growth from leucosome melt
Bento dos Santos et al. (2011)	Grt	X	X	X		Glass, n.d.						
Carosi et al. (2015)	Grt		X	X	X	Qz, Na–Pl, Ms, Chl, Ca–Pl, Ilm, Rt, Ap, Zrn, Mnz,	X	X				
Cesare (2008)	Pl, Grt, Crd, Bt, And, Qtz, Crn, Ilm, Spl, Mnz, Zrn	X		X	X	Glass, Afd, Ilm, Gr		X				
Cesare and Acosta-Vigil (2011)	Pl, Grt, Crd, Ilm	X	X	X	X	Glass, Qz, Afs, Bt, Pl	X	X	X			
Cesare and Gómez-Pugnaire (2001)	Pl, Grt, And	X		X		Glass		X				
Cesare and Maineri (1999)												
Cesare et al. (1997)	Grt, Pl, Bt, Crd, Ilm	X		X		Glass		X				
Cesare et al. (2003b)	Grt, Crd, Ap, Zrn, Mnz	X		X	X	Glass						
Cesare et al. (2003a)	And	X		X		Glass ± aqueous solution		X	X			
Cesare et al. (2005)	Pl, Crd, Ilm	X		X	X	Glass		X				
Cesare et al. (2007)	Pl, Crd	X		X		Glass		X				
Cesare et al. (2009a)	Grt	X	X	X	X	Qz, Kfs, Na–Pl, Bt, Ap, Rt, Zrn, Ttn, Fe oxide	X	X		X		
Cesare et al. (2011)	Grt,Pl, Bt, Crd, Spl, Kfs, Qtz, Ilm, Zrn,Mnz, Ap, Crn	X	X	X	X	Glass, Qz, Kfs, Bt, Ms, Ap, Ilm, Gr, Rt, Ttn	X	X	X	X		
Chen et al. (2013)	Zrn		X	X		Qz, Ms, Pl, Kfs				X		
Chen et al. (2014)	Grt, Omp		X	X	X	Qz, Pl, Kfs,Brt			X	X		
Chen et al. (2015)	Zrn		X	X	X	Qz, Pl, Hem, Cal, Kfs, Ep, Bt, Ap				X		
Chupin and Kosukhin (1982)	Qtz		X			Not provided						

Chupin et al. (1993)	Zrn, Ky, Qz, Grt	X	X	X		Glass, minerals not provided	X	X		X		
Chupin et al. (1998)	Zrn		X	X		Not provided	X	X				remelting at ambient P
Chupin et al. (2010)	Ky, Grt, Opx, Cpx, Sa, Qz, Ap, Zrn	X	X			Glass, heterogeneous bubble, microcrystallites	X	X				SIMS for trace elements and H_2O
Chupin et al. (2006a)	Grt, Cpx, Scp, Zrn, Ap, Ttn, Pl, Qz, Kfs	X		X		Glass	X	X		X		SIMS, remelting in HT stage
Chupin et al. (2006b)	Zrn	X	X	X		Glass, fluid phase, minerals not provided	X	X				Zrn interpreted to grow from the trapped melt
Chupin et al. (2010)	Grt, Cpx, Opx,Ky, Scp, Ttn, Qz, Ap, Zrn, Mnz	X	X	X		Glass, gas bubble, microcrystallites	X	X				
Clarke et al. (2005)	And	X		X		Glass						
Darling (2013)	Grt		X	X	X	Qz, Bt, Kfs, Ab, Zrn		X				
Darling et al. (1997)	Grt		X	X		Crs, Ab, Ilm		X		X		
Di Martino et al. (2011)	Grt, Crd	X		X	X			X		X		
Dolgov et al. (1984)	Qz		X			Not provided						
Ferrando et al. (2005)	Grt, Ky		X	X	X	Pg, Ms, Anh, Alu-type sulfate, Amp, Pl, Crn, Dsp, Zrn, Ap, ilmeno hematite, Mag, Spl, Py, Cc, Chl, Brt	X					
Ferrero et al. (2011)	Grt, Pl, Crd, Bt, Spl	X		X		Glass		X				
Ferrero et al. (2012)	Grt, Ilm	X	X	X	X	Qz, Pl, Kfs, Ms, Bt, glass, Ap, Rt, Spl	X	X		X		
Ferrero et al. (2014)	Grt	X	X	X	X	Glass, Na–Pl, Kfs, Qz, Bt, Ap, Ilm, Spl	X					
Ferrero et al. (2015)	Grt		X	X	X	Qz, Pl, Kfs, Bt	X	X		X		
Frezzotti et al. (2004)	Qz	X		X		Glass	X	X		X	X	
Ganzhorn et al. (2014)	Grt		X	X	X	Pl, Kfs, Bt		X				
Gao et al. (2012)	Grt		X	X	X	Qz, Pl, Kfs		X		X		
Gao et al. (2013)	Grt		X	X	X	Qz, Kfs, Ep, Aln			X	X		
Gao et al. (2014)	Grt		X	X	X	Cal, Qz, Kfs, Pl, Mag			X	X		
Georgieva et al. (2005)	Grt		X		X	Qz, Bt, Ms, Kfs, Ap, Rt, Zrn						Abstract
Groppo et al. (2012)	Grt		X	X	X	Qtz, Bt, Kfs, Na–Pl, Ap						
Harley and Nandakumar (2014)	Zrn		X	X	X	Qz, Kfs						Hosts crystallized from met?
Hartel et al. (1990)	Grt	X	X	X		Glass		X		X		Abstract
Hiroi et al. (2014)	Grt		X	X	X	Qz, Pl, Kfs, Fsp,		X		X		
Hwang et al. (2001)	Grt		X	X		Qz,Pa, Phl, Dia, Ap				X		TEM
Kawakami et al. (2013)	Zrn	X			X	Glass						TEM–EDS
Korsakov and Hermann (2006)	Grt, Cpx, Ttn		X	X	X	Mg-Cal, Dia, Gr, Dol, Aln, Phe, Bt, Kfs, Cpx, Grt, Ttn	X	X				
Kotkova et al. (2014)	Grt		X	X	X	Qz, Phl, kumdykolite		X		X		
Lang and Gilotti (2007)	Grt		X	X		Qz,Ky,Pl, Bt		X				
Liu et al. (2013)	Grt		X	X	X	Qz, Kfs (Pl, Phe, Amp)		X	X			
Liu et al. (2014)	Grt, Ep		X	X	X	Qz, Kfs, Bt, Pl, Ph,		X				
Madyukov et al. (2011)	Grt, Cpx, Scp, Zrn, Ap, Ttn, Pl, Qz, Kfs	X		X		Glass	X	X		X		SIMS, remelting in HT stage
Malaspina et al. (2006)	Grt		X	X	X	Spl, Amp,–Chl ± talc ± Phl ± Ap ± FeNi sulfide	X	X	X			
Massonne (2014)	Grt		X		X	Qz, Fsp						
Mosca et al. (2012)	Grt		X		X	Qz, Bt, Wm, Chl, Ap, Rt						
Stöckhert et al. (2001)	Grt		X	X	X	Qz, Pg,Ky, Pl, Phe, Ap, Rt, Dia						
Stöckhert et al. (2009)	Grt		X	X	X	Qz, Pg,Ky, Pl, Phe, Ap, Rt, Dia, Gr		X				
Wang et al. (2015)	Grt		X	X	X	Qz, Pl, Ms, Bt						
Zeng et al. (2009)	Grt, Omp		X	X	X	Qz, Kfs, Ab		X				

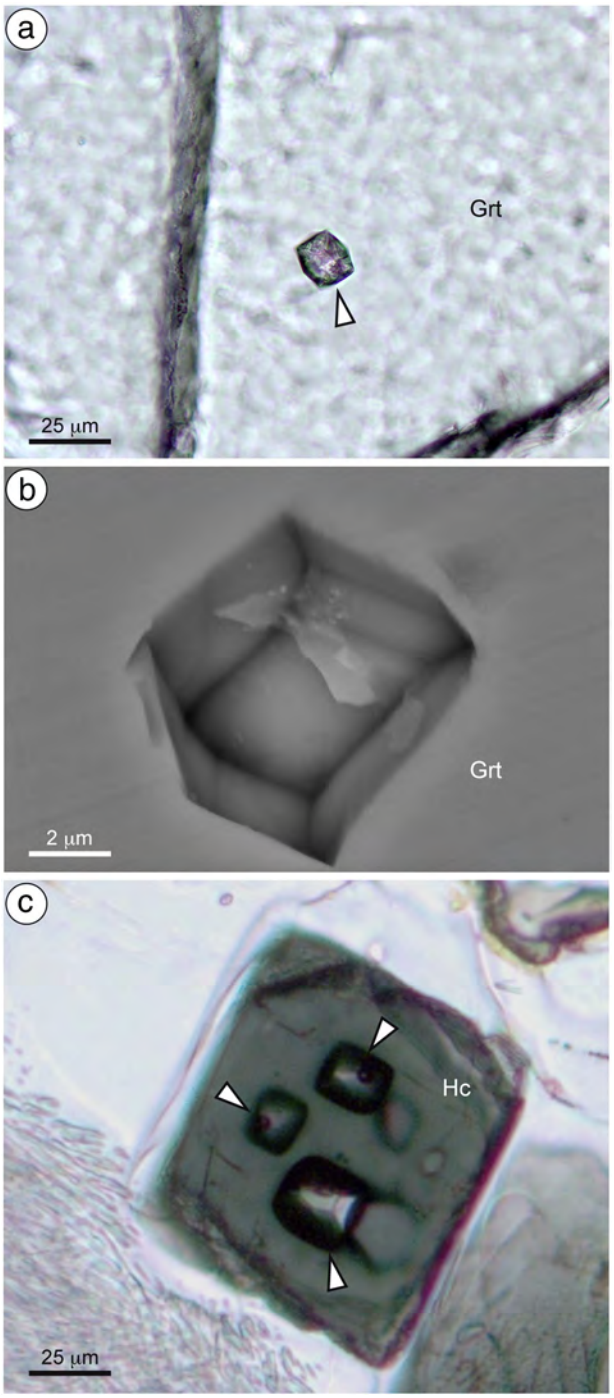

Fig. 1. Negative crystal shape of MI in migmatites and granulites. a) plane-polarized light photomicrograph of a *nanogranite* inclusion in garnet from the metapelitic granulites of the Kerala Khondalite Belt, India. From Cesare et al., 2009a. b) Secondary electron SEM image of a dodecahedral MI in garnet from the migmatites of Kali Gandaki (Nepal). The inclusion was mechanically emptied during sample preparation and polishing. c) plane-polarized light photomicrograph of a hercynitic spinel in a corona around garnet in the metapelitic enclaves of Mazarrón, Spain. Arrows point to square (octahedral) inclusions of rhyolitic glass, each with a shrinkage bubble. From Cesare (2008).

to the more complex (Vielzeuf and Holloway, 1988)

$$\mathrm{Bt} + \mathrm{Pl} + \mathrm{Qz} + \mathrm{Sil}\ (\pm \mathrm{fluid}) = \mathrm{Grt} + \mathrm{melt}\ (\pm \mathrm{Kfs}).$$

The latter is of particular relevance to metapelites, as it would explain the occurrence of MI in peritectic garnet.

Indeed, primary MI do exist in garnet and in other minerals from many granulites and migmatites, especially in their melt-depleted melanosome portions. Their primary nature is demonstrated by unequivocal microstructures such as the zonal arrangement of MI, which may form clusters located either at the cores or randomly distributed throughout the crystals, or internal annuli, both in garnet (Bartoli et al., 2013b; Carosi et al., 2015; Ferrero et al., 2012) and in zircon (Cesare et al., 2003b; Kawakami et al., 2013).

Along with the natural occurrences, the process of incongruent melting is also reproduced in experiments, and despite the extreme fine grain-size of run products, seldom exceeding 20 μm and therefore unsuited for the formation of frequent and/or large inclusions, the occurrence of MI in garnet and plagioclase has been reported in the experimental products of the melting of a metagreywacke (Fig. 3; see also Gardien et al., 2000) and of a cordierite gneiss (Koester et al., 2002). These examples highlight the fundamental property of MI trapped during incongruent melting, i.e., that their mineral hosts grow with the coexisting melt phase, as opposed to the growth from (or in) a melt that is typical of hosts from igneous rocks.

The twofold nature of MI entrapment can be visualized in a schematic T–t diagram (Fig. 4) representing an ideal path during which a rock exceeds its solidus, melts, reaches a thermal peak and then cools down into the subsolidus region (see also Cesare et al., 2011). For the sake of simplicity, variations in pressure during the T–t path have not been considered; however, this does not diminish the general validity of the conclusion drawn from Fig. 4. Along such path, if anatexis takes place by incongruent reactions, peritectic minerals may trap MI. This mode of entrapment should occur primarily along the up-temperature part of the path (labeled 1 in Fig. 4), where most melting reactions are normally crossed. Conversely, the melt that has formed and segregated into in situ leucosome, or extracted from the source area into larger dikes or plutons, or even rapidly extruded on the Earth surface, will in general remain in the liquid state until cooling starts, during the down-temperature part of the path (labeled 2 in Fig. 4). It is during this down-temperature path that major crystallization takes place in the partially melted portions of migmatites and in the associated felsic intrusions and lavas. This process – crystallization on cooling – provides the conditions for the entrapment of MI and indeed represents the most common trapping process (e.g., Webster, 2006). Note the first and fundamental difference between the two modes of MI trapping: MI are trapped during *melt-producing processes* along path 1, whereas they are trapped during *melt-consuming processes* along path 2.

The peculiar trapping process by incongruent melting during the prograde part of a metamorphic/anatectic path has some major implications on where these MI can be found and on what petrogenetic information they preserve. First of all, these MI will occur in peritectic minerals of rocks that have crossed their solidus and have partially melted. Confining our attention to the Earth's continental crust such rocks are represented by migmatites and granulites, forming at T exceeding c. 650 °C and variable pressure (Sawyer et al., 2011), from middle continental crust down to UHP conditions (Hermann et al., 2013). The peritectic host mineral varies depending on the bulk composition of the anatectic rock and on P–T conditions, but the most common is expected to be garnet, as it constitutes the product of melting reactions in a wide P–T–X range, from medium- to high-P and in both felsic and mafic protoliths (Baxter et al., 2013).

A second, and probably most important implication of the peculiar nature of the trapping process, is that the melt being trapped in the peritectic mineral during the melting of the rock is a pristine primary anatectic melt. Thus, in the metasedimentary migmatites where they have been thoroughly characterized so far, these droplets of melt (and their crystallized counterpart, see below) have been shown to be the witnesses of the unmodified, primary embryos of S-type granites (Bartoli et al., 2014) before the processes of segregation, collection, mixing and migration to upper crustal levels create the much more familiar leucosomes and/or felsic intrusions/volcanic rocks. On the

contrary, MI in igneous rocks are unlikely to provide chemical information on pristine anatectic magmas, because these undergo variable degrees of mixing, entrainment of residual/peritectic/exotic material and differentiation, both before and during their crystallization, such that MI will trap variably evolved, residual melt compositions.

Incongruent melting, with the new growth of minerals together with melt, is the main mechanism for the formation of MI in migmatites and granulites, but probably it is not the only one. In fact, some reactanct minerals in the rock matrix may recrystallize and equilibrate with the melt, and possibly trap MI even if they contribute to the melt and their modal amount decreases. This mechanism has been described for the case of plagioclase during melting experiments (Johannes, 1989; Johannes and Holtz, 1992; Fig. 5 of Acosta-Vigil et al., 2006a), where the more sodic starting plagioclase crystals/rims dissolve into, and reprecipitate from the melt to form more calcic portions. Another example of common textural readjustment that may lead to the entrapment of MI upon heating and melting of anatectic rocks is the coarsening of crystals, where some grains grow at the expenses of others. The shift of grain boundaries may induce the formation of MI, if some melt is present along the boundary itself.

Dealing with MI entrapment, a mineral deserving further attention is zircon, which based on current observations (see Table 1) is probably the second most common host for MI after garnet. Like monazite, zircon in migmatites is expected to dissolve during partial melting, and to crystallize when the anatectic melt becomes saturated in Zr (Kelsey et al., 2008; Rubatto et al., 2006). This means that zircon should normally crystallize during the cooling path 2 of Fig. 4. However, Cesare et al. (2009a) and Kawakami et al. (2013) have shown that both in enclaves and in regional migmatites the zircons enclosed in peritectic garnet grew and were able to trap MI early in the melting history of metapelites or near their metamorphic peak. Therefore, the MI trapped in zircon occurring in migmatites, especially in their melanosome, can be compared in origin to those found in peritectic minerals.

A thorough discussion of the differences between MI trapped during heating (by peritectic reactions) vs. cooling (by magma crystallization) has been made by Bartoli et al. (2014) with reference to the MI hosted in basalts, which are by far the most common in igneous environments. MI coming from these two contrasting modes of trapping not only differ in the associated reactions and processes, but also in the *P–T* ranges and general *P–T* evolution of their host rocks, with near adiabatic decompression to almost ambient pressure for MI hosted in volcanic rocks (Fig. S1). These marked differences have important implications for the ability of MI to preserve and document the composition of pristine magmas, and to retain the fluid component of the trapped melts: while MI in volcanic rocks turn out to be the most suitable system for diffusional re-equilibration and volatile loss, those in migmatites and granulites are expected in many cases to preserve their primary fluid content. Along with the diffusional aspects explored by Bartoli et al. (2014), the loss of volatiles by decrepitation is favored in MI of volcanic settings, because of the elevated internal overpressures produced in the MI during abrupt near-isothermal decompression of associated magmas (Fig. S1; see also Ferrero et al., 2011; Touret and Huizenga, 2012).

Another major difference between MI in peritectic hosts and those in minerals formed during magma crystallization is the extent of crystallization of the host on inclusion walls upon cooling: host mineral crystallization is not expected in the former, whereas in the latter it is almost the rule (Danyushevsky et al., 2002; Frezzotti, 2001), the reason being the different topological relations among host and melt in the two

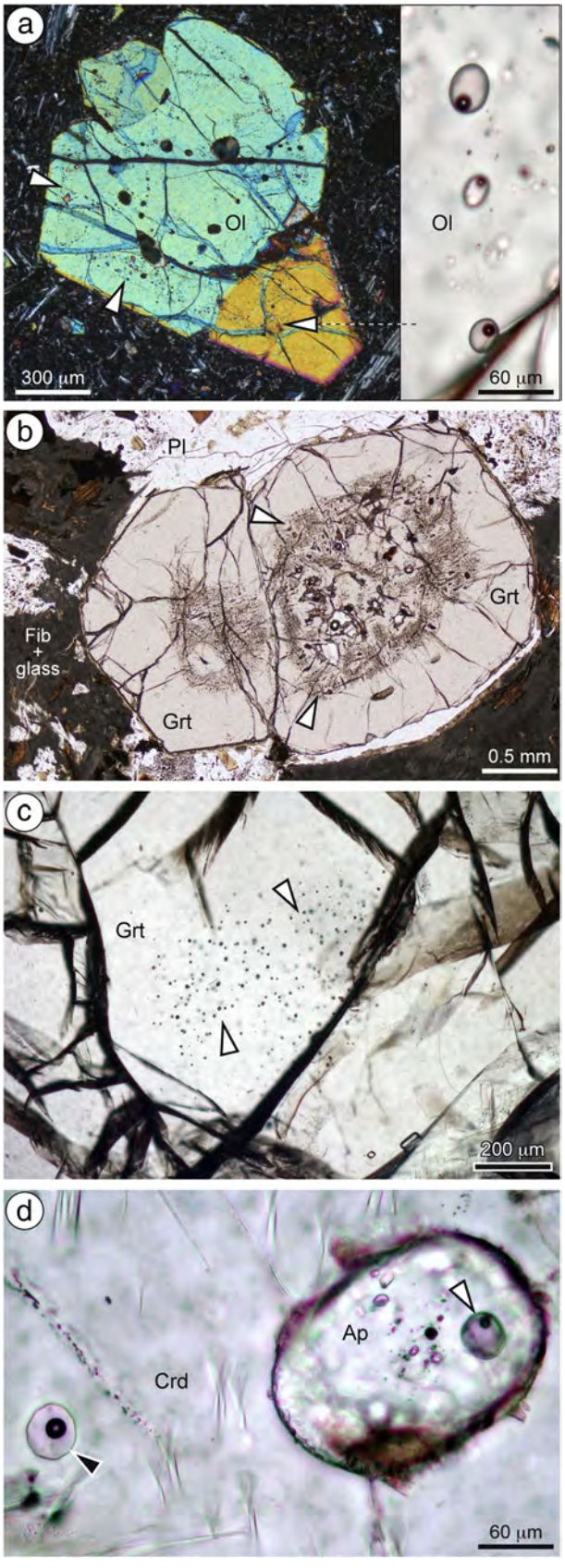

Fig. 2. Photomicrographs with examples of microstructures strongly supporting a primary origin of MI. a) Left: glass inclusions define thin concentric growth shells (arrows) in a phenocryst of olivine in an alkali lava from East Island, Crozet archipelago (sample kindly provided by C. Meyzen). Right: close-up view of one of the growth shells. Inclusions contain fresh colorless glass and one shrinkage bubble. b) MI-rich cores (arrows) in garnet porphyroblasts from a partially melted pelitic enclave in the dacite of El Hoyazo, Spain. From Cesare et al. (2011) c) Small cluster of crystallized MI (*nanogranites*) in a garnet from a metapelitic granulite (*khondalite*) of the Kerala Khondalite Belt. Most of the garnet is clear and inclusion-free. d) Isolated glass inclusion (black arrow) in a cordierite crystal from a partially melted pelitic enclave in the dacite of Mazarròn. The cordierite includes a crystal of apatite that in turn contains an isolated glass inclusion (white arrow). From Cesare et al. (2003a).

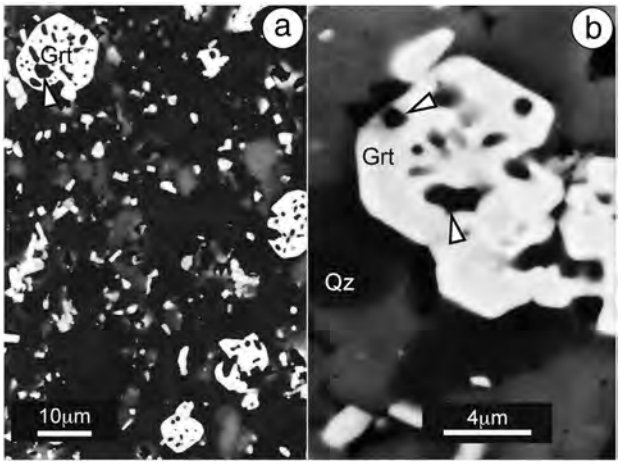

Fig. 3. Inclusions of anatectic melt, now quenched as glass (arrows) in runs of experimental melting of a pelite. BSE images courtesy of Veronique Gardien. See also Gardien et al. (1995). a) experiment performed at 900 °C, 20 kbar, without added H_2O. b) experiment performed at 900 °C, 20 kbar, with 2 wt.% added H_2O.

scenarios, as discussed by Bartoli et al. (2013a). Although in migmatites and granulites small volumes of the host are predicted to dissolve during equilibration at lower temperatures, from our experience such dissolution does not seem to take place or is rarely recorded by clear-cut microstructures (see below).

4. How are melt inclusions identified and microstructurally characterized?

4.1. Preliminary identification of MI by optical microscopy

The identification of anatectic MI in partially melted rocks is challenging due to their small diameter, often <20 μm (Bartoli et al., 2013b; Cesare et al., 2011; Ferrero et al., 2012); based on the case studies so far investigated, we propose two main microstructural criteria.

1) *Shape*: a fully-developed negative crystal shape, e.g. isometric in garnet (Cesare et al., 2009a) and more elongated or tubular in other phases (e.g. andalusite, Cesare et al., 2003a), is very common in MI of partially-melted rocks, especially for small-sized (<10 μm) inclusions. Larger inclusions tend to only develop straight walls (Fig. in 2 in Ferrero et al., 2015).

2) *Polycrystalline/glassy nature*: anatectic MI may present extremely variable degrees of crystallization, from glassy to fully crystallized (*nanogranites* after Cesare et al., 2009a; *nanogranitoids* after this work, see below). Crystallized MI appear often brownish under optical observation and may be mistaken for defects of the thin section surface. Crossed-polarizers observation allows to directly verify the presence of multiple birefringent phases in case of *nanogranites* (e.g. Ferrero et al., 2012), or of an isotropic, homogeneous phase in case of glassy inclusions (e.g. Cesare et al., 2009a). Moreover, MI must be fully enclosed in the crystal under microscope observation, to ensure that they are not portions of larger embayments. The use of thick (100–200 μm) doubly-polished sections is recommended to allow simultaneous inspection of a large number of inclusions and of their spatial arrangement (Ferrero et al., 2012).

4.2. High-resolution techniques and sample preparation

The microstructures of MI can be successfully characterized with back-scattered electron (BSE) imaging, using Field Emission Gun (FEG)-based electron microscopes. Uncovering and polishing the MI is however a crucial problem: while glassy inclusions are generally easy to polish because of their homogeneous nature, the polishing of crystal-bearing MI often results in the complete or partial mechanical removal of the inclusion content (see Fig. 1b). This is due to the polycrystalline nature, the small size of the enclosed crystals (commonly 0.1–5 μm) and, especially for garnet-hosted inclusions, the large difference in hardness between inclusion crystals and the host. Moreover, MI in well-developed euhedral, crack-free hosts are easier to polish than those in skeletal porphyroblasts (Ferrero et al., 2012). The best results have been obtained by polishing with a colloidal suspension of silica ("Siton") in crack-free hosts or by following the diamond-paste metallographic preparation. Al_2O_3-powder polishing is also a reliable alternative when diamond contamination should be avoided, e.g. in the preparation of UHP samples.

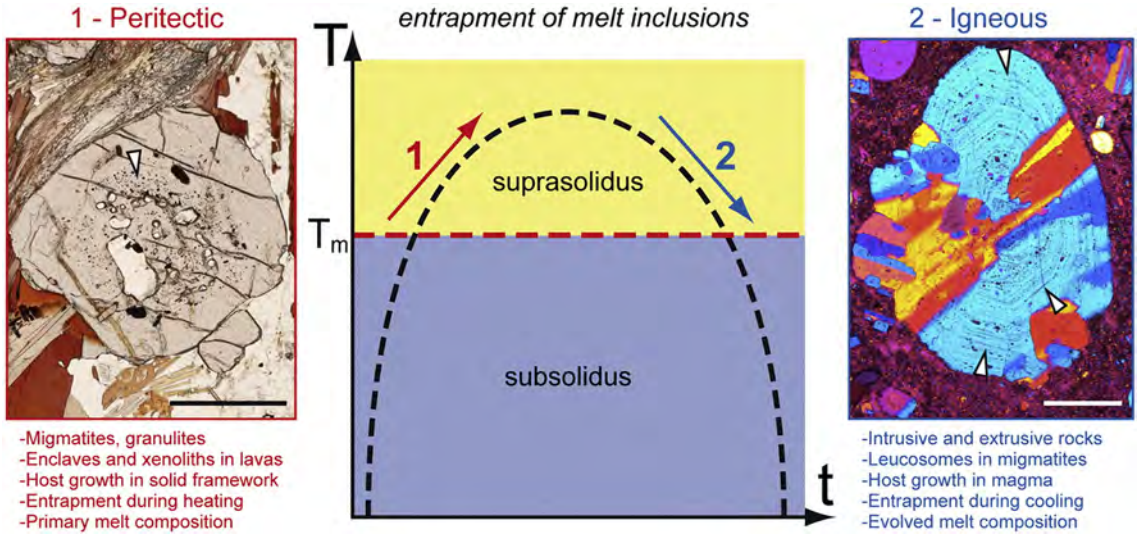

Fig. 4. Schematic T–t diagram, modified from Cesare et al. (2011), illustrating the differences between MI entrapment during peritectic melting and igneous crystallization. On the left a Bt–Grt–Sil migmatite (*kinzigite*) from the Ivrea Verbano Zone, Italy, showing a garnet porphyroblast with a MI-rich core (arrow). On the right a glomerocryst of plagioclase in an andesite from Cabo de Gata, Spain. The larger plagioclase of the glomerocryst (light blue) contains abundant MI arranged in concentric shells (arrows) outlining the progressive growth of the phenocryst. Scale bars = 1 mm. See text for further details.

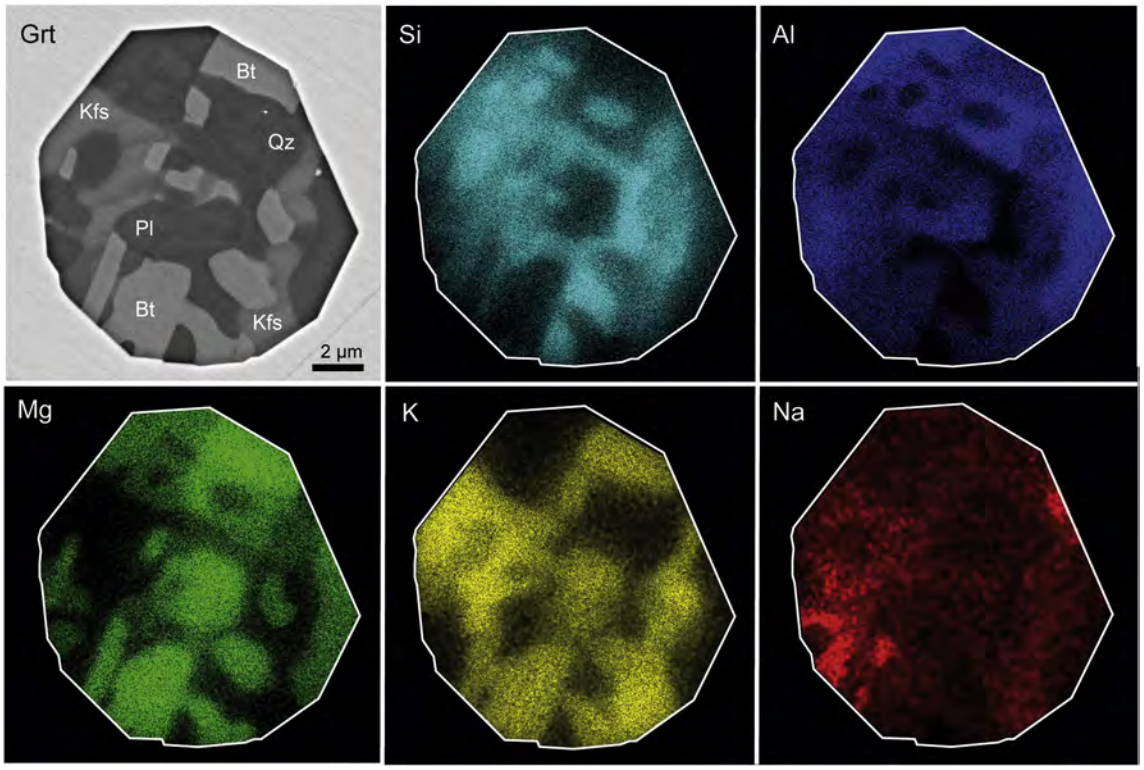

Fig. 5. SEM backscattered image (top left) and X-rays maps of the distribution of Si, Al, Mg, K and Na in a *nanogranite* inclusion in garnet of a metapelitic granulite (*khondalite*) from the Kerala Khondalite Belt.

4.3. Microstructural characterization

Melt inclusion-forming crystals, and in some cases the residual glass, can be identified by acquiring EDS spectra and/or X-ray maps of the major elements (Fig. 5; see also Cesare et al., 2009a; Ferrero et al., 2012, 2015; Darling, 2013; Chen et al., 2014). Daughter minerals found within the inclusions studied so far are, obviously, consistent with the products of granitoid magma crystallization: quartz, alkali feldspar, plagioclase, biotite and/or muscovite (Fig. 6; see also Ferrero et al., 2012, 2014; Barich et al., 2014). Other minerals commonly found in MI are solid inclusions trapped during MI formation, such as accessory minerals (e.g. graphite, ilmenite, rutile, zircon and monazite: Cesare and Maineri, 1999; Ferrero et al., 2012; Darling, 2013), and rock-forming minerals present in the matrix and as single inclusions in the host, e.g. Al_2SiO_5 in metapelites (Barich et al., 2014; see Table 1 for a complete list of daughter minerals and solid inclusions). In both cases, solid inclusions can be easily distinguished from the melt crystallization products because they are usually larger and often indent the MI walls (Fig. 6e, f; Ferrero et al., 2012). Porosity and sub-micrometric pseudomorphs after melt films may also be observed (Fig. 6b,d). Further microstructural data, e.g. the high spatial resolution three-dimensional (3D) reconstruction of small crystal-bearing single MI (Fig. 7), can be obtained through the dual-beam focused ion-beam–scanning electron microscope (FIB–SEM), as suggested by Anderson and McCarron (2011).

Given the small size of the crystals, Micro Raman spectroscopy (MRS) represents a rapid way to identify the phases and different polymorphs in MI (Table 1; see also Darling et al., 1997; Hwang et al., 2004, 2009; Ferrero et al., 2015). MRS mapping has revealed also the presence of liquid H_2O in micro- and nanopores of *nanogranites* located below the surface of the studied thin section, i.e. entirely enclosed within the host (Bartoli et al., 2013b). Glassy inclusions (Cesare et al., 2009a) and residual glass in partially crystallized inclusions (Ferrero et al., 2015) may also be identified via MRS. When the size of MI is >10 μm, SEM (BSE) and electron microprobe (EMP) imaging and analysis are well suited for the characterization of phases within MI (Barich et al., 2014).

4.4. Different degrees of crystallization, and coexistence with fluid inclusions

MI are mostly glassy in anatectic enclaves in volcanic rocks (Acosta-Vigil et al., 2007) and in garnet xenocrysts in granitoids (Ferrero et al., 2014), consistent with the rapid cooling below the solidus of shallow intrusions and extrusions (Cesare and Gomez-Pugnaire, 2001). Surprisingly, MI with different degrees of crystallization – from fully glassy to fully crystallized – have been recognized in slowly cooled high-grade terrains already in the first study of MI in granulites, i.e. in the Kerala Khondalite Belt (Cesare et al., 2009a). As the number of case studies increases, glassy MI in classic migmatitic terrains appear to be always present, though in very low proportions, while partially crystallized MI are quite common regardless of the pressure at which the melt was trapped. In fact, they occur in migmatites formed both at shallow crustal levels (e.g., Ronda migmatites, Bartoli et al., 2013c) and at mantle depths (e.g., Orlica-Śnieżnik Dome — Bohemian Massif, Ferrero et al., 2015). Cesare et al. (2009a) demonstrated that *nanogranites* in KKB granulites are generally larger (average diameter ≈ 13 μm) than the coexisting preserved glassy MI (≈8 μm), and argued that crystallization was probably inhibited in the smaller inclusions (see also Holness and Sawyer, 2008).

Primary COH fluid inclusions associated in clusters together with primary MI occur in peritectic minerals of either rapidly exhumed anatectic enclaves in the Neogene Volcanic Province, Southern Spain (Cesare et al., 2007), or constituting xenocrysts within granitoids from La Galite Archipelago, Tunisia (Ferrero et al., 2014). This association provides a strong microstructural evidence for fluid-melt immiscibility during partial melting, and allows (1) identification of fluid-present anatexis, (2) direct chemical characterization of the immiscible fluids, and (3) evaluation of the role of fluids in the anatexis of the crust (see also Section 8.4). Similar new occurrences have been recently recognized in metasediments from different localities in the western part of the Bohemian Massif (Moldanubian Zone), and represent the first direct evidence of fluid-melt immiscibility during partial melting in regional granulites (Fig. 8).

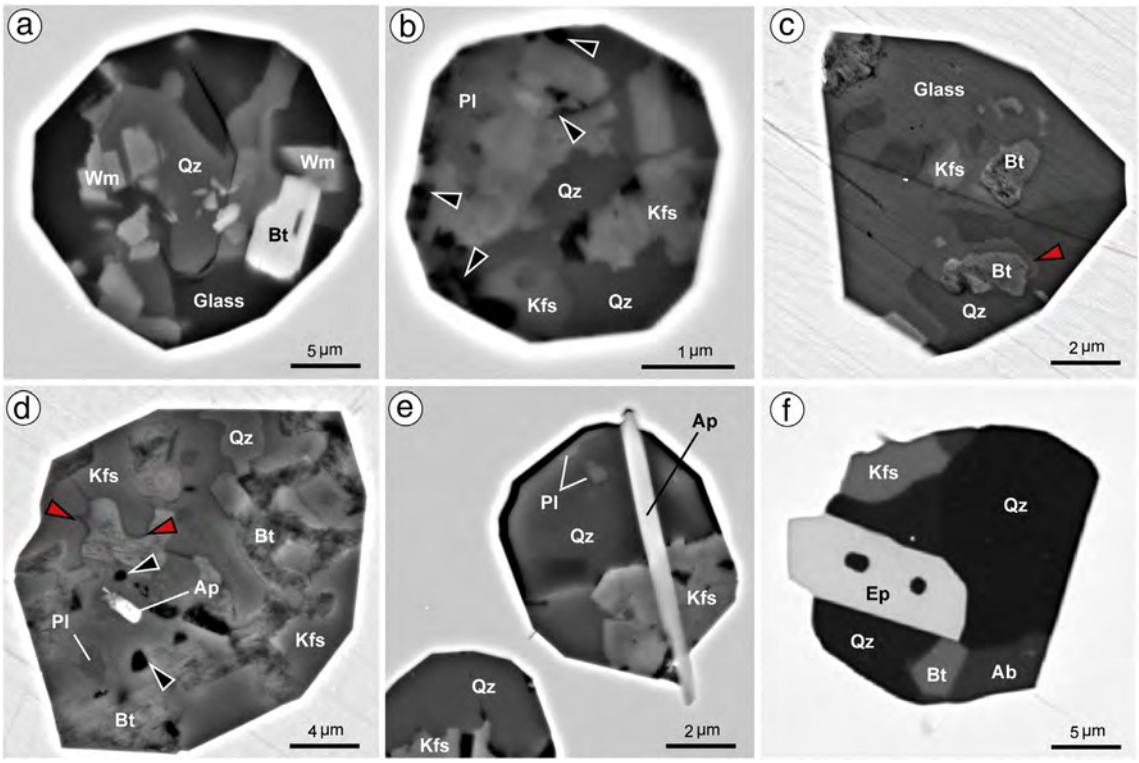

Fig. 6. SEM backscattered image of *nanogranites*. a) fully crystallized *nanogranite* in Ronda metatexites. b) *nanogranite* from the same location of (a) showing internal porosity (black arrows). c) partially crystallized inclusion, Kerala Khondalite Belt. Glass is still present, forming microstructures that are clear precursor of pseudomorphs after melt (red arrow). d) fully crystallized *nanogranite* with internal porosity (black arrow) from the same location of (c). Red arrow: sub-micrometric melt pseudomorphs of possible plagioclase. From (Cesare et al., 2009a). e) and f) *nanogranites* with trapped accessory phases indenting the inclusion walls. Samples from Ronda metatexites (e) and from the Orlica-Śnieżnik Dome in the Bohemian Massif (f).

4.5. Evidence for decrepitation

Since after entrapment MI behave as a (quasi)isochoric system, whose internal pressure and temperature cannot vary independently, pressure gradients between MI and the surrounding rock may be generated during the post-entrapment history of the sample, and in particular during exhumation (see above). The magnitude of such gradients depends on the nature of the P–T path followed by the rock (e.g. clockwise

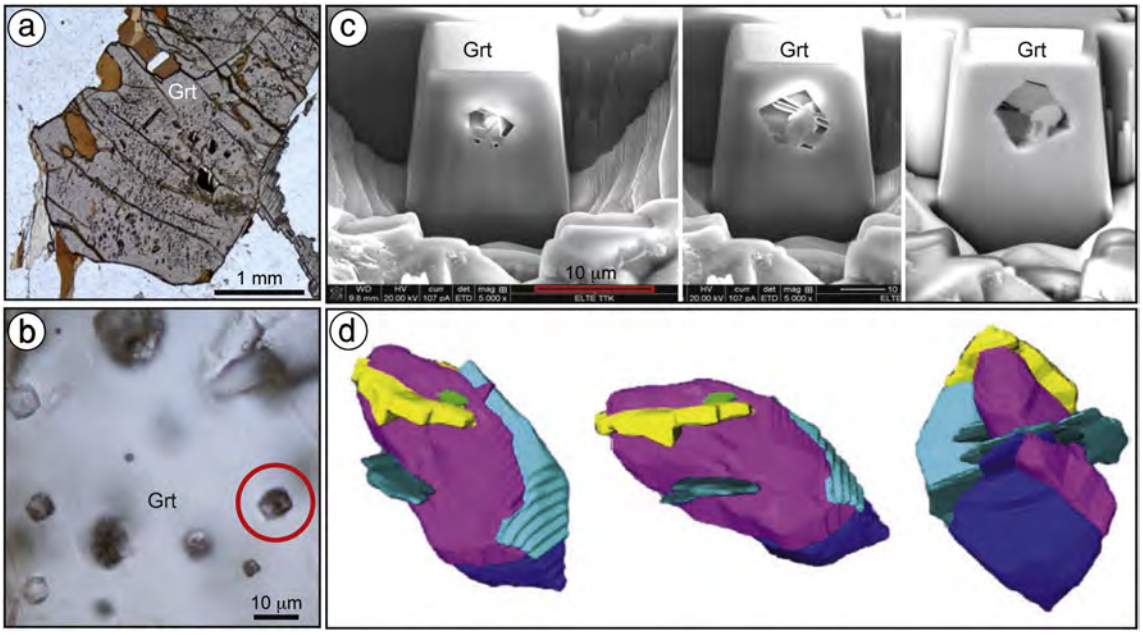

Fig. 7. 3D reconstruction by FIB–SEM serial sectioning of one MI in garnet from the metapelitic migmatites of Kali Gandaki. a) polarized light photomicrograph of a garnet porphyroblast rich in MI. From Carosi et al. (2015) b) close-up view of an area rich in MI. Red circle locates the MI used for serial sectioning. c) SE and BSE (rightmost) SEM images of three sequential stages of the sectioning process. From left to right the MI is progressively uncovered by the FIB milling. d) 3D representation of the polycrystyalline aggregate filling the MI. The three views are slightly rotated with respect to each other. Phases have not been identified in this test experiment. FIB–SEM images and reconstruction courtesy of Laszlo Elod Aradi and Lithosphere Fluid Research Lab, Institute of Geography and Earth Sciences Eötvös University Budapest, Hungary.

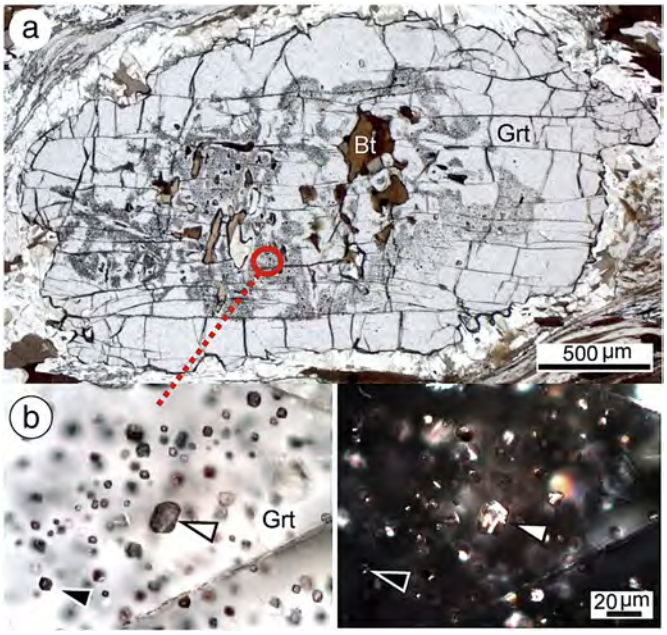

Fig. 8. Evidence for primary fluid-melt immiscibility during partial melting. (a) Peritectic garnet in stromatic migmatites (Zeilengneise) from Oberpfalz, Moldanubian Zone (Bohemian Massif). Clusters of micrometric inclusions are visible in the inner part of the crystal, along with residual biotite; (b) close-up of (a) where primary fluid inclusions (black arrow) coexist with *nanogranite* inclusions (white arrow), recognizable for the presence of multiple birefringent phases (right: crossed polarizers image).

vs. counterclockwise; Ferrero et al., 2012), and the differential P may overcome the strength of the host and cause MI decrepitation (Bodnar, 2003; Stöckhert et al., 2009). The most common microstructural evidence for this process are offshoots filled with minerals similar to those in the MI (Fig. 9), as reported by Stöckhert et al. (2001) in diamond-bearing inclusions from Erzgebirge granulites. Another evidence is the presence of cracks reaching the external boundary of the host (Ferrero et al., 2015). Decrepitation can also occur in natural glassy inclusions brought to considerably higher temperatures after their entrapment, or be induced experimentally by overheating the sample (Fig. 9, see below). In the presence of these microstructures, fluid loss and element exchange with the surrounding matrix are expected to have occurred, hampering experimental re-homogenizationof MI due to a likely irreversible change in the bulk composition of the trapped melt. Verifying the absence of any evidence for decrepitation in the MI is thus a necessary step before proceeding with their experimental re-homogenization.

5. How can melt inclusions be analyzed?

5.1. Re-homogenization strategies and problems

Recovering complete compositional data, including the volatile contents, requires the heating and remelting of the crystallized MI to a

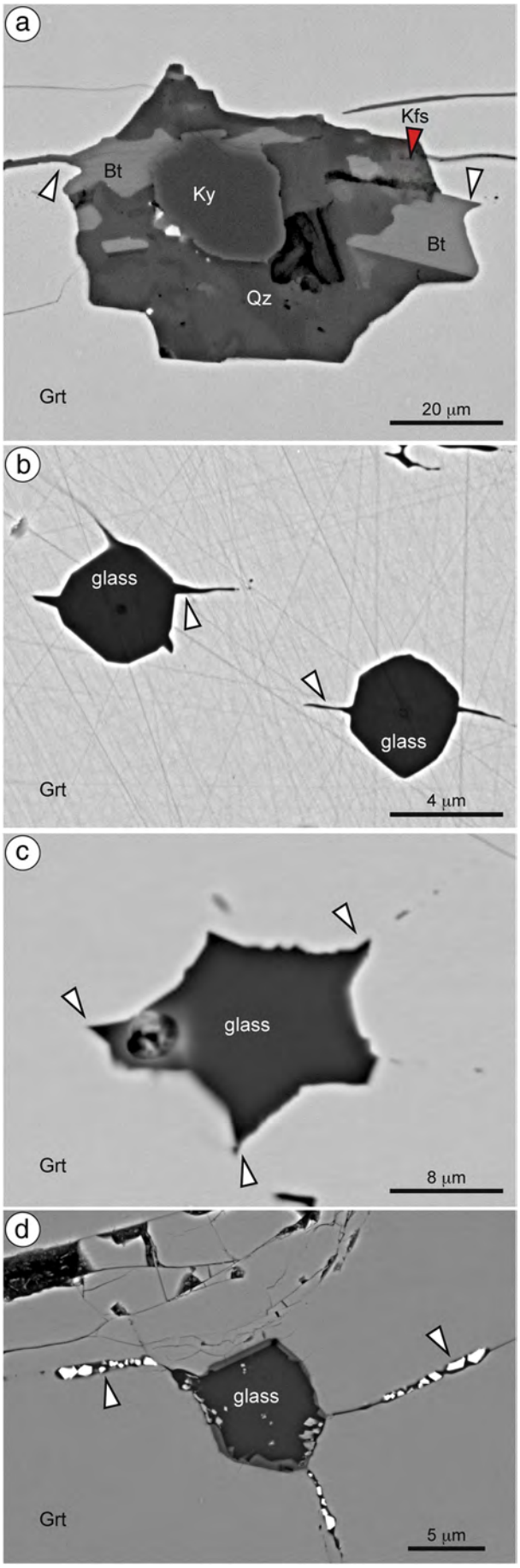

Fig. 9. BSEM images showing examples of natural and experimental decrepitation of MI. All are hosted in garnet. a) Polycrystalline MI from migmatites of Jubrique, showing cuspate offshoots filled with biotite (white arrows) that also fills the inclusion. This inclusion, together with most MI in the samples from Jubrique, contains a large crystal of kyanite (Ky) that is interpreted as a trapped solid inclusion. b) Two MI from Ojén experimentally remelted at 750 °C and 5 kbar. The experimental heating at temperatures exceeding (of about 50 °C) the trapping values has caused the decrepitation of MI, with microfractures filled with glass. c) glassy inclusion in garnet from the Bt–Grt–Sil enclaves of El Hoyazo. The cusps of MI, pointing towards garnet and to thin nanofractures, suggest the decrepitation of these inclusions by the natural process of heating of the enclaves from 700–750 °C (the entrapment conditions of MI) to 850–900 °C (the maximum temperatures attained by enclaves in the dacite. d) a MI from the Kerala Khondalite Belt, experimentally remelted at 1050 °C and room pressure. During the experiment the inclusion decrepitated, and the host garnet has melted in the offshoots, with formation of new peritectic phases, probably hercynite.

homogeneous liquid, reversing the phase changes that occurred along the cooling path after their entrapment, i.e. crystallization of daughter phases and fluid exsolution. For crystallized MI in migmatites and granulites, remelting has been accomplished in two ways: i) using a one atmosphere heating stage, and ii) under a given confining pressure using a piston cylinder apparatus.

In the case of the microscope-mounted heating stage, the heating is usually conducted in an inert atmosphere of He to prevent sample oxidation (see Esposito et al., 2012). Rock wafers containing MI-bearing minerals (e.g. garnet) are separated from double-polished thick (commonly 100–250 μm) sections. Different heating rates and ramps have been applied to the different case studies (see Ferrero et al., 2012). The obvious disadvantage of the remelting experiments at room pressure is the large overpressure generated in the MI. Indeed, during heating the P–T conditions within the MI follow the isochore defined by the density and composition of the exsolved fluid (Fig. S2). This generates an internal pressure much greater than the external room pressure, so that MI often decrepitate before remelting, with loss of volatiles. As a consequence of the H_2O loss, the re-homogenization of crystallized MI occurs at temperatures higher than the trapping conditions, favoring incongruent melting of host crystal, production of new peritectic phases by melt–host interaction, and melt contamination. This is why MI experimentally remelted by the heating stage are commonly characterized by i) irregular walls, ii) decrepitation cracks filled with melt, iii) presence of new crystals (i.e., not observed in the starting material, such as iron oxides and orthopyroxene) close to the MI walls or within cracks, and iv) the presence of one or more empty (vacuum) bubbles formed to accommodate the volume lost by H_2O and melt leaving the inclusion (Fig. S2).

Homogenization under confining pressure using a piston cylinder apparatus (Fig. 10) may overcome the problems described above, but is much more time consuming. MI-bearing samples are loaded into Au or Pt capsules (external diameter of 3 and 5 mm) together with powdered silica, to isolate the fragments from each other and from the capsule walls. In addition, water can be added to some capsules to evaluate the potential effects of H_2O exchange with MI during experiments (Bartoli et al., 2013a). Because the abundance and the microstructural distribution of MI in host crystals vary from sample to sample, different strategies can be adopted during experimental rehomogenization. When MI are present in all peritectic crystals (e.g., garnet), pure crystal concentrates can be obtained (Fig. 10a) after rock crushing using conventional heavy liquids and magnetic techniques. On the other hand, when the samples are characterized by the scarcity of MI-bearing crystals, by the presence of MI-bearing crystals having a low number of MI, or by an inhomogeneous distribution of MI within large porphyroblasts, the occurrence and location of MI have to be carefully verified first for any crystal under the microscope using thick (0.1–1 mm) sections. Then, wafers of MI-bearing crystals can be cut and loaded into the experimental capsules (Fig. 10b). Alternatively, the MI-rich portions of crystals can be extracted using a microdrilling technique (Fig. 10c). Because we have recently documented systematic variations in the composition of MI as a function of the location of the host crystal (e.g., in leucocratic versus melanocratic domains; Bartoli et al., 2014), we recommend to adopt those approaches which permit to control the precise microstructural location of the investigated MI, in order to have robust microstructural constraints for the interpretation of compositional data.

The P–T conditions at which the first exploratory piston-cylinder experiments are run are usually based on available estimates of anatectic conditions in the rock. Conditions of further experiments will be

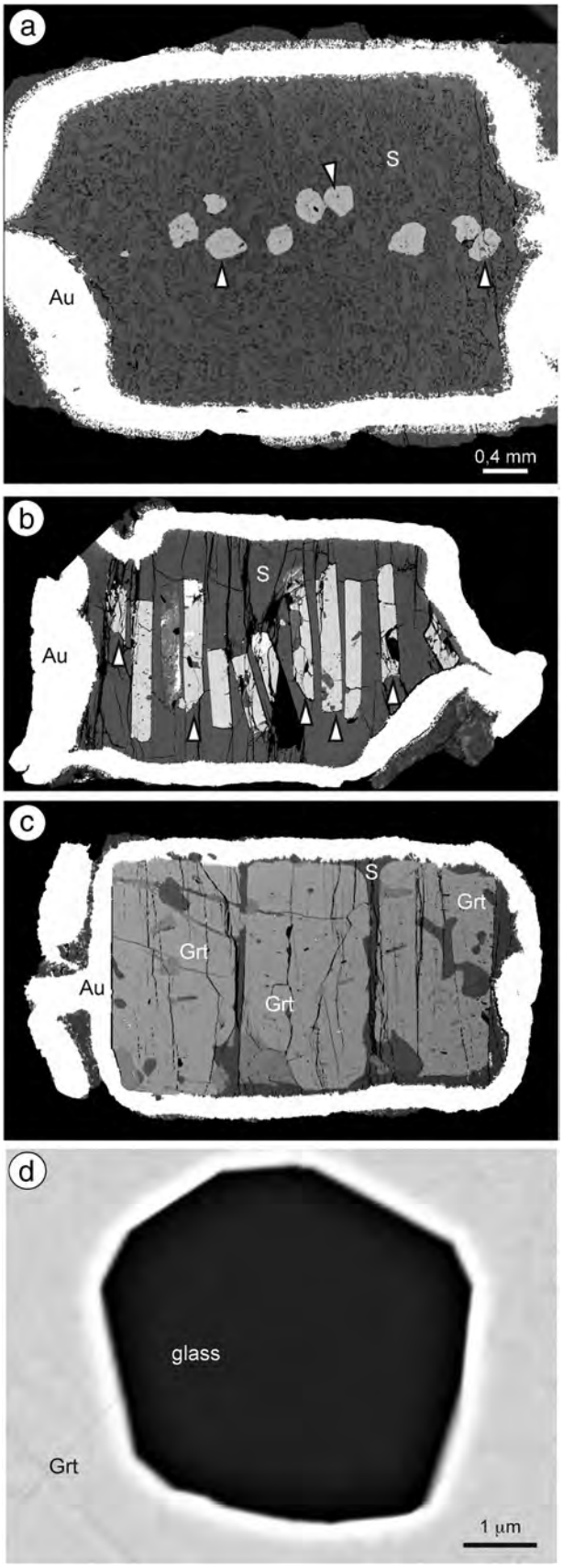

Fig. 10. BSE images of the polished surface of gold (Au) capsules filled with silica powder (S) and garnet (arrows, Grt) used for the experimental rehomogenization of MI. Based on garnet dimensions, abundance and microstructural occurrence of MI, three different setups have been used and are illustrated: a) single, small, garnet crystals (arrows) separated from crushed rock (sample from Ronda); b) wafers of garnet (arrows), c. 200 μm thick, stacked into the capsule, approximately orthogonal to its elongation (sample from Jubrique); c) three cylindrical cores of garnet, c. 1.5 mm-thick, filling the experimental capsule (sample from Ivrea Zone). All capsules have c. 2,5 mm external diameter. d) example of a successfully remelted MI from Ojen migmatites. This sample was experimentally remelted in a piston cylinder, at 700 °C and 5 kbar for 24 h. The glass has a peraluminous granitic composition (see text for details). From Bartoli et al. (2015).

dictated by the results in these exploratory experiments (see Bartoli et al., 2013a; Ferrero et al., 2015). Indeed, the main disadvantage of using a piston-cylinder apparatus is that the MI cannot be directly observed during remelting experiments. Thus, it is not possible to stop the heating at the moment of homogenization, and this can result in overheating of the MI. Using a piston cylinder, identification of overheated MI requires compositional and/or microstructural criteria, such as the presence of irregular or cuspate inclusion walls and/or cracks and bubbles (Fig. 9b,d), or remarkably high concentrations of elements present in the host crystal (Bartoli et al., 2013a). Since melting kinetics play a central role during reheating experiments, the MI homogenization process depends also on the duration of heating (Sobolev and Danyushevsky, 1994; Thomas, 1994; Thomas and Klemm, 1997). So far MI in migmatites and granulites have been successfully re-homogenized with run durations between 24 and 48 h (Fig. 10d), but MI from other anatectic terranes might require longer or shorter duration runs, i.e., time-resolved experiments may be required along with temperature- and pressure-resolved ones.

Despite the trial-and-error nature of this experimental approach, much better quality compositional data can be obtained using a piston-cylinder because several MI-bearing crystals, and in turn a large number of MI, can be rehomogenized simultaneously, once the trapping conditions are determined. While other experimental equipments such as cold-seal or internally heated vessels and pressurized microscope stages, are appropriate to re-homogenize MI from igneous rocks under low confining pressure (see Bodnar and Student, 2006 and references therein), only solid media apparatus such as a piston cylinder will allow to reach the high-pressure conditions appropriate for the deep crust and upper mantle, up to approximately 40 kbar in the case of an end-loaded piston cylinder (e.g., Ferrero et al., 2015; Malaspina et al., 2006; Perchuck et al., 2008).

5.2. Chemical investigation

Glassy or re-homogenized MI can be analyzed for most elements in the periodic table. The EMP has been routinely used to analyze major elements of MI exposed on the crystal surface (Table 1). A problem that needs to be considered during EMP analysis of hydrous felsic glasses, however, is the alkali migration from the inclusion target, which increases by focusing the beam size and increasing the beam current (Morgan and London, 1996, 2005). When the size of the investigated MI is too small to use the recommended 15–20 μm beam diameter, and/or to move constantly the inclusions under a defocused beam (see Di Martino et al., 2011; Madyukov et al., 2011; Morgan and London, 1996, 2005), the problem may be overcome following the recommendation of Morgan and London (2005), and using correction factors for Na, K, Si and Al obtained from the analysis of secondary glass standards conducted in the same analytical session. Recommended standards for such correction are leucogranitic glasses of known composition with H_2O contents as close as possible to the analyzed samples (e.g., Acosta-Vigil et al., 2007; Bartoli et al., 2013a,b; Ferrero et al., 2012). An alternative method for minimizing the alkali loss is the use of a N_2-cooled cryostage (Stevens et al., 1997).

H_2O is the major volatile dissolved in crustal anatectic melts, and can be quantified on exposed glassy MI in migmatites and granulites by several approaches including EMP-difference method (i.e., deficiency from 100% in the EMP analysis after alkali loss correction; Acosta-Vigil et al., 2007; Ferrero et al., 2011, 2014), Raman spectroscopy (Bartoli et al., 2013b; Ferrero et al., 2015), secondary ion mass spectrometry (SIMS) (Chupin et al., 2006a; Madyukov et al., 2011) and NanoSIMS (Bartoli et al., 2014). Although Fourier Transform Infrared (FTIR) spectroscopy is considered a routine approach in the characterization of large (≥100 μm) MI in igneous rocks (e.g., Anderson et al., 2000; Bachmann et al., 2010), the large spot size of FTIR and the requirement of sufficient sample thickness to allow precise absorbance measurements, make this technique unsuitable for small MI such as those in migmatites and granulites. Conversely, NanoSIMS and Raman spectroscopy only need MI exposed on one side of the host crystal, and the H_2O content can be determined with a high spatial resolution (1–2 μm; see Thomas, 2000; Bartoli et al., 2014). Different protocols were explored and proposed for the acquisition and processing of Raman spectra from MI in igneous rocks, with variable success (e.g., Behrens et al., 2006; Chabiron et al., 2004; Le Losq et al., 2012; Thomas, 2000; Zajacz et al., 2005). In addition, Thomas et al. (2006) developed a technique for using micro-Raman spectroscopy to measure H_2O in unexposed glassy MI. Other volatiles occurring in minor concentrations can be quantified by SIMS/NanoSIMS in the case of F, S and Cl (Bartoli et al., 2013a), by EMP in the case of F and Cl (e.g., Acosta-Vigil et al., 2007; Cesare et al., 2007; Di Martino et al., 2011; Ferrero et al., 2012), and by LA–ICP–MS in the case of B (e.g., Acosta-Vigil et al., 2010; Cesare et al., 2003a).

LA–ICP–MS is also used to measure trace element contents of MI. In the case of glassy MI ≥ 20 μm in anatectic enclaves, analyses are obtained by ablation of material coming exclusively from the MI. Any contamination from mineral inclusions, fractures or host, can be detected by monitoring several elements and integrating only the "clean" portion of the signal (Acosta-Vigil et al., 2010, 2012a; Cesare et al., 2003a). For MI ≤ 10–15 μm in migmatites and granulites, analyses so far have been conducted by drilling crystallized MI entirely enclosed in the host (Bartoli, unpublished data; Gao et al., 2013, 2014). When also the host mineral is ablated with the MI, quantification of the MI composition needs deconvolution of the mixed signal (Halter et al., 2002). This procedure is critical because it affects the accuracy of the MI composition. One of the major elements determined by EMP analyses in glassy or re-homogenized MI can be used as internal standard to separate the signals from MI and host mineral. Alternatively, Gao et al. (2013, 2014) and Chen et al. (2014) obtained the absolute abundances of trace elements in their crystallized MI calculating the mass ratio between each analyzed inclusion and the host. In this case, uncertainties associated with volume estimates by BSE images may be considerable, and the approach has turned out to be not precise enough (Halter et al., 2002). Trace element concentrations of exposed glassy MI have also been measured by SIMS (e.g. Madyukov et al., 2011).

6. What can we learn from melt inclusions? Microstructural information

6.1. That (part of) a mineral grew in the presence of melt

Because the requirement to form MI is the growth of a mineral in the presence of a melt phase, the occurrence of primary MI definitively testifies that the MI-bearing portion of the host mineral grew in the presence of melt at some point during anatexis of the rock. Garnets from migmatites in the Kali Gandaki valley (Himalaya, central Nepal) are characterized by a core clouded with inclusions of plagioclase and ilmenite, whereas hundreds of MI show a systematic distribution in an annulus around that core containing also rutile (Fig. 11). This distribution matches the concentric chemical zoning of the garnet: MI-rich areas show a slight and gradual decrease in Ca and Mn and enrichment in Fe and Mg with respect to the core (Carosi et al., 2015). These microstructures demonstrate that the MI-rich annuli certainly formed above the solidus during incongruent melting of the host rock. Concerning the absence of MI in the garnet core or outermost rim, one cannot rule out a possible suprasolidus origin also for these crystal portions, since the entrapment of MI may be promoted by other factors in addition to the presence of melt (e.g. the rapid growth of the host phase to form embayments that can accommodate that melt).

Another example comes from MI-bearing garnets present in the Jubrique granulites, on top of the Ronda peridotites (Betic Cordillera, S Spain). Previous metamorphic studies concluded that anatexis of these rocks occurred during decompression and in the field of sillimanite, corresponding with growth of Sil-bearing garnet rims. Recent MI studies on these rocks have demonstrated that anatexis started at medium-to-high

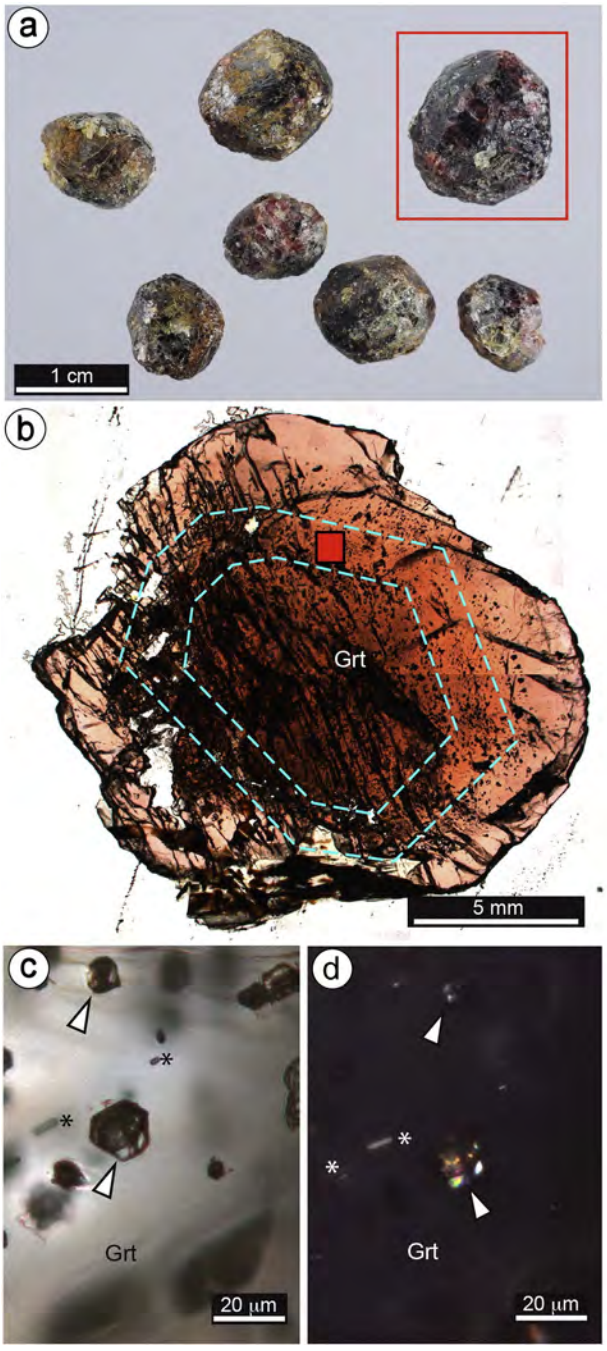

Fig. 11. MI in internal annuli in garnets from Kali Gandaki. a) garnet porphyroblasts separated from metapelitic migmatites. Red box identifies the crystal illustrated in images (b) to (d). b) plane-polarized photomicrograph of the equatorial section of the porphyroblast from (a), showing a distinct chromatic zoning confirmed by SEM X-ray mapping (details in Carosi et al., 2015). Dashed blue lines define the annulus of garnet containing MI. Red box: area enlarged in (c) and (d). c) and d) are respectively plane-polarized and crossed polarizers photomicrograph showing crystallized MI (arrows) within the annulus outlined in (b). In this region garnet also contains elongate, subparallel rutile crystals (stars).

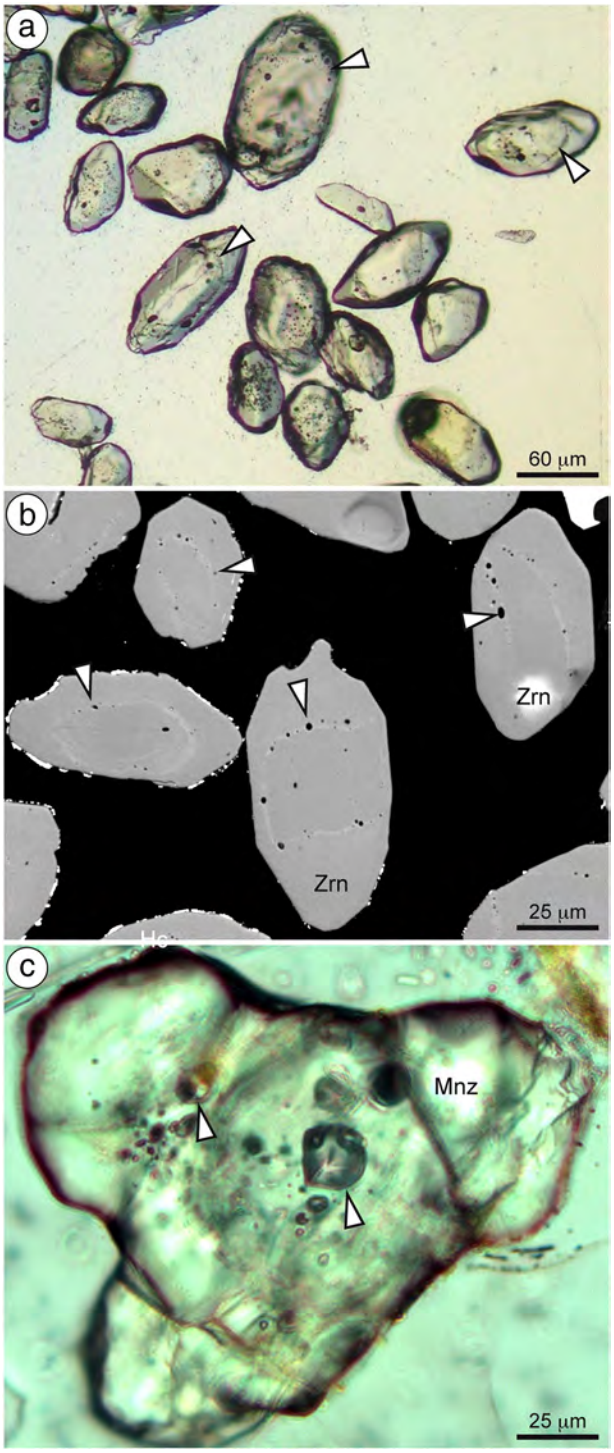

Fig. 12. a) plane-polarized photomicrograph of zircon crystals separated from a metapelitic enclave in the dacite at El Hoyazo. b) SEM backscattered image of a detail of the same separate. A very thin, BSE-bright annulus containing μm-sized glassy inclusions (arrows) separates inherited cores from euhedral overgrowths, grown in the presence of melt. c) Cluster of primary glassy inclusions (arrows) with shrinkage bubble at the core of a monazite crystal from Mazarrón. From Cesare (2008).

pressure conditions and in the field of kyanite, as primary MI are present throughout the entire garnet crystals (Barich et al., 2014). In fact, the core of large garnets show MI associated with kyanite and rutile (Fig. 9a), whereas their rims and small garnets have MI coexisting with sillimanite and ilmenite. These data show that during garnet growth the (sub)assemblage changed from Grt–Ky–Rt-melt to Grt–Sil–Ilm-melt, in agreement with the decompressional history commonly proposed for the rocks (Barich et al., 2014).

6.2. That a rock has melted

There are many microstructural criteria (reviewed by Vernon, 2011) for inferring the former presence of melt in regionally metamorphosed migmatite and granulite terrains which have undergone slow cooling over millions of years. Among them, the most common are mineral

Table 2
Mean major an trace element concentrations (with associated standard deviations in parentheses) of glassy and rehomogenized melt inclusions in anatectic enclaves, migmatites and granulites analyzed up to date by our research group. Matrix glass analyses from the anatectic enclaves of El Hoyazo are also included. #K = mol. $K_2O/(K_2O+Na_2O)$. #Mg = mol. $MgO/(MgO+FeO_t)$.

Location, unit	El Hoyazo	El Hoyazo	El Hoyazo	El Hoyazo	El Hoyazo	El Hoyazo	Mazarrón	Mazarrón	Mazarrón	Mazarrón	Ronda, Ojén	Ronda, Ojén
Rock type	Grt–Bt–Sil enclave	Grt–Bt–Sil enclave	Grt–Bt–Sil enclave	Grt–Bt–Sil enclave	Grt–Bt–Sil enclave	Sp–Crd enclave	Sp–Crd enclave	Sp–Crd enclave	Sp–Crd enclave	Sp–Crd enclave	Metatexites	Metatexites
Notes	MI in Pl	MI in Grt	MI in Crd	MI in Ilm	Matrix glass	MI in Grt	MI in And	MI in Pl	MI in Qz	MI in Crd	Remelted,dry	Remelted,wet
P–T rehomog.							n.a.				5 kb–700 °C	5 kb–700 °C
Major elements (wt%)												
No. anal.	209	63	56	18	160	15	31	38	11	5	15	13
SiO_2	73.25 (1.50)	71.26 (1.44)	73.42 (0.95)	70.68 (1.30)	70.10 (1.29)	68.95 (1.65)	70.16 (2.15)	72.80 (2.02)	74.56 (0.91)	71.98 (2.51)	70.03 (2.36)	69.60 (1.86)
TiO_2	0.09 (0.04)	0.10 (0.03)	0.07 (0.05)	0.31 (0.05)	0.16 (0.04)	0.10 (0.12)	0.11 (0.13)	0.09 (0.03)	0.10 (0.05)	0.14 (0.10)	0.04 (0.07)	0.06 (0.07)
Al_2O_3	12.61 (0.86)	14.44 (0.33)	14.01 (0.39)	15.69 (0.80)	14.48 (0.75)	12.82 (1.14)	14.73 (0.83)	12.57 (0.73)	13.12 (0.64)	14.87 (1.02)	11.71 (0.89)	12.06 (0.49)
FeO_t	1.14 (0.36)	1.72 (0.51)	1.31 (0.16)	2.58 (0.19)	1.37 (0.31)	1.32 (0.40)	1.56 (0.47)	1.18 (0.27)	1.14 (0.33)	1.17 (0.49)	1.71 (0.22)	1.74 (0.25)
MnO	0.02 (0.03)	0.08 (0.05)	0.04 (0.04)	0.07 (0.05)	0.01 (0.01)	0.16 (0.17)	0.08 (0.07)	0.08 (0.06)	0.02 (0.02)	0.08 (0.02)	0.17 (0.10)	0.16 (0.10)
MgO	0.14 (0.05)	0.05 (0.04)	0.04 (0.06)	0.13 (0.04)	0.14 (0.06)	0.02 (0.04)	0.12 (0.05)	0.11 (0.03)	0.08 (0.04)	0.17 (0.22)	0.12 (0.07)	0.12 (0.07)
CaO	0.23 (0.23)	0.60 (0.10)	0.93 (0.15)	0.96 (0.13)	0.49 (0.13)	0.68 (0.16)	0.69 (0.17)	0.52 (0.18)	0.54 (0.12)	0.75 (0.17)	0.45 (0.13)	0.45 (0.10)
Na_2O	2.83 (0.46)	3.61 (0.42)	3.41 (0.39)	3.55 (0.15)	3.10 (0.22)	2.25 (0.35)	2.74 (0.47)	2.24 (0.28)	2.57 (0.31)	3.16 (0.23)	2.79 (0.37)	2.85 (0.50)
K_2O	5.00 (0.58)	4.97 (0.31)	4.92 (0.60)	4.92 (0.17)	5.43 (0.31)	4.56 (0.83)	5.57 (0.75)	5.13 (0.41)	5.77 (0.52)	5.19 (1.06)	4.05 (0.41)	4.08 (0.30)
P_2O_5	0.22 (0.11)	0.37 (0.09)	0.20 (0.17)	0.31 (0.10)	0.34 (0.11)	0.16 (0.07)	n.d.	n.d.	n.d.	n.d.	0.26 (0.24)	0.22 (0.14)
F	0.06 (0.06)	0.08 (0.07)	0.05 (0.06)	0.07 (0.10)	0.05 (0.05)	0.01 (0.03)	n.d.	n.d.	n.d.	n.d.	n.d.	n.d.
Cl	0.04 (0.09)	0.01 (0.01)	0.45 (0.08)	0.00 (0.00)	0.01 (0.01)	n.d.	0.23 (0.16)	0.30 (0.06)	0.01 (0.02)	0.18 (0.19)	n.d.	n.d.
Total	95.59 (1.11)	97.28 (1.61)	98.77 (1.00)	99.25 (0.76)	1.51 (0.35)	91.03 (1.62)	96.12 (1.88)	95.15 (1.27)	98.03 (0.76)	97.81 (1.47)	91.33 (2.26)	91.34 (2.12)
H_2O by diff.	4.4 (1.1)	2.7 (1.6)	1.3 (1.0)	0.8 (0.6)	4.3 (0.6)	9.0 (1.6)	3.9 (1.9)	4.9 (1.3)	2.0 (0.8)	2.2 (1.5)	8.7 (2.3)	8.7 (2.1)
ASI	1.21 (0.10)	1.17 (0.08)	1.11 (0.05)	1.22 (0.04)	1.22 (0.06)	1.31 (0.10)	1.25 (0.45)	1.24 (0.08)	1.15 (0.05)	1.24 (0.20)	1.20 (0.08)	1.22 (0.10)
#K	0.54 (0.06)	0.48 (0.03)	0.49 (0.05)	0.48 (0.02)	0.54 (0.02)	0.57 (0.05)	0.57 (0.51)	0.60 (0.03)	0.60 (0.05)	0.52 (0.06)	0.49 (0.04)	0.49 (0.05)
#Mg	0.18 (0.04)	0.04 (0.02)	0.04 (0.06)	0.08 (0.02)	0.15 (0.04)	0.03 (0.04)	0.12 (0.17)	0.15 (0.05)	0.11 (0.06)	0.16 (0.13)	0.10 (0.06)	0.10 (0.05)
FeO_t+MgO	1.16 (0.37)	1.76 (0.55)	1.35 (0.18)	2.71 (0.22)	1.51 (0.35)	1.44 (0.48)	1.79 (0.65)	1.39 (0.27)	1.32 (0.36)	1.47 (0.61)	1.87 (0.25)	1.91 (0.31)
*H_2O by Raman											5.1 (1.3), 24	5.0 (1.5), 19
*H_2O by SIMS											5.0 (2.3), 6	4.4 (1.2), 3
*H_2O by nanoSIMS	3.4 (0.6), 19	4.0 (1.3), 46			5.2 (0.4), 11						6.5 (1.4), 26	
Trace elements (ppm)												
No. Anal.	20–24	10–32			22–39							
Li	204 (282)	278 (105)			115 (43)							
Rb	207 (30)	225 (34)			221 (26)							
Cs	30 (5)	30 (4)			26 (3)							
Sr	28 (27)	120 (23)			68 (33)							
Ba	77 (66)	240 (62)			311 (157)							
B	317 (109)	364 (69)			184 (35)							
V	0.81 (0.58)	0.43 (0.71)			2.1 (0.8)							
Zr	25 (7)	29 (3)			44 (14)							
U	3.8 (1.3)	4.3 (0.4)			3.1 (0.7)							
Th	1.50 (0.90)	1.13 (0.17)			3.1 (1.4)							
Y	6.5 (2.1)	2.5 (1.2)			12 (6)							
La	2.3 (0.7)	4.1 (0.4)			7.1 (2.7)							
Ce	6.3 (1.1)	8.8 (0.5)			17 (6.0)							
Nd	3.3 (0.7)	3.4 (0.5)			8.3 (2.9)							
Sm	1.03 (0.28)	0.93 (0.15)			2.3 (1.0)							
Eu	0.25 (0.25)	0.87 (0.18)			0.63 (0.29)							
Gd	1.25 (0.44)	1.03 (0.35)			2.5 (1.4)							
Er	0.42 (0.21)	0.13 (0.06)			0.77 (0.34)							
Yb	0.26 (0.18)	0.05 (0.04)			0.58 (0.32)							
Lu	0.05 (0.04)	0.02 (0.02)			0.04 (0.05)							
Qz norm	36.4 (3.9)	29.48 (3.19)	32.23 (2.13)	27.8 (2.3)	29.8 (2.8)	36.2 (5.8)	29.9 (4.8)	37.1 (4.8)	35.4 (1.9)	31.0 (5.5)	36.1 (3.7)	35.3 (2.6)
Crn norm	2.4 (0.9)	2.89 (0.78)	1.88 (0.72)	3.5 (0.7)	3.3 (0.7)	3.3 (0.8)	2.9 (1.1)	2.2 (0.8)	1.7 (0.6)	2.7 (1.9)	2.4 (0.9)	2.6 (1.1)
Or norm	29.6 (3.5)	29.38 (1.80)	29.07 (3.54)	29.1 (1.0)	32.1 (1.8)	26.9 (4.9)	32.9 (4.4)	31.4 (4.1)	34.1 (3.1)	30.7 (6.2)	24.0 (2.4)	24.1 (1.8)
Ab norm	23.9 (3.9)	30.52 (3.52)	28.82 (3.31)	30.0 (1.3)	26.2 (1.8)	19.1 (2.9)	23.2 (4.0)	19.0 (2.4)	21.8 (2.6)	26.7 (1.9)	23.6 (3.1)	24.1 (4.2)
An norm	0.35 (0.97)	0.64 (0.57)	3.27 (1.05)	2.8 (1.0)	0.5 (0.6)	2.3 (1.1)	3.4 (0.9)	2.6 (0.9)	2.7 (0.6)	3.7 (0.86)	0.99 (1.20)	0.84 (0.58)

*) data reported as a (b), c, where a = mean H_2O concentration, b = standard deviation, and c = number of analyses

pseudomorphs after melt films and pools, and crystals with euhedral shapes often concentrated in veinlets and patches (e.g., Holness and Sawyer, 2008; Marchildon and Brown, 2002; Sawyer, 2008; Vernon and Collins, 1988). However, recrystallization and deformation in the subsolidus may completely erase most or all evidences of partial melting, such as in the metapelitic rocks belonging to the Austroalpine basement of the Eastern Alps and forming the contact aureole of the Vedrette di Ries pluton (Cesare et al., 2010). These rocks are polymetamorphic and polydeformed, and the microstructures (Fig. S3a,b) reflect the superposition of two regional metamorphisms – a dynamic high-temperature Variscan and a static medium-pressure eo-Alpine – followed by a contact metamorphism related to

Ronda, Ojén	Ronda, Ojén	Ronda, Ojén	KKB	KKB	La Galite	La Galite	Himalaya, Barun	Himalaya, KGD	Himalaya, KGD	Bohemia, OSD
Metatexites	Mylonites	Mylonites	Granulite	Granulite	Tonalites	Garnetites	Gneiss	Gneiss	Gneiss	Felsic Granulite
Glassy	Glassy, type I	Glassy, type II	Remelted,dry	Glassy MI	Glassy MI	Glassy MI	Remelted, dry	Remelted, dry	Remelted, dry	Remelted, dry
n.a.	n.a.	n.a.	atm–1040 °C	n.a.	n.a.	n.a.	atm–830 °C	12 kb–800 °C	12 kb–820 °C	27 kb–875 °C
3	30	8	11	3	15	8	4	25	18	18
69.69 (1.76)	76.33 (1.48)	75.97 (2.20)	73.96 (2.63)	77.72 (0.39)	73.56 (1.96)	74.53 (1.47)	73.77 (2.34)	67.13 (2.14)	66.33 (1.82)	68.71 (1.78)
0.08 (0.14)	0.05 (0.08)	0.07 (0.07)	0.11 (0.09)	0.04 (0.07)	0.06 (0.05)	0.01 (0.02)	0.09 (0.08)	0.12 (0.13)	0.19 (0.24)	0.10 (0.09)
11.78 (0.32)	11.35 (0.53)	11.30 (0.73)	12.95 (1.31)	11.90 (0.06)	12.02 (0.81)	12.11 (0.77)	12.90 (1.46)	13.67 (1.28)	13.92 (1.09)	13.58 (0.71)
1.20 (0.11)	1.60 (0.50)	1.34 (0.34)	3.03 (0.69)	1.01 (0.13)	1.31 (0.31)	1.28 (0.27)	2.51 (0.37)	1.84 (0.40)	2.68 (0.46)	2.02 (0.57)
0.09 (0.09)	0.06 (0.06)	0.08 (0.08)	0.04 (0.03)	0.04 (0.07)	0.09 (0.05)	0.07 (0.04)	0.25 (0.17)	0.07 (0.05)	0.13 (0.10)	0.00 (0.00)
0.07 (0.03)	0.17 (0.11)	0.15 (0.15)	0.65 (0.21)	0.01 (0.01)	0.13 (0.10)	0.09 (0.06)	0.53 (0.13)	0.29 (0.32)	0.45 (0.21)	0.08 (0.04)
0.39 (0.19)	0.07 (0.04)	0.14 (0.17)	0.53 (0.20)	0.03 (0.03)	0.25 (0.17)	0.28 (0.33)	0.85 (0.48)	0.61 (0.12)	2.63 (1.00)	0.76 (0.46)
3.09 (0.24)	1.96 (0.35)	3.05 (0.51)	1.10 (0.32)	0.97 (0.06)	3.33 (0.44)	3.61 (1.01)	1.94 (0.13)	2.44 (0.66)	2.59 (0.85)	4.24 (0.74)
4.19 (0.23)	5.76 (0.36)	3.98 (0.33)	6.72 (0.70)	7.60 (0.35)	5.96 (0.29)	5.79 (0.81)	4.86 (0.79)	1.52 (0.17)	1.25 (0.60)	4.50 (0.44)
0.18 (0.27)	0.23 (0.23)	0.29 (0.29)	0.03 (0.05)	0.15 (0.05)	0.08 (0.14)	0.04 (0.06)	0.02 (0.02)	0.17 (0.16)	0.25 (0.24)	0.02 (0.03)
n.d.	n.d.	n.d.	n.d.	n.d.	n.d.	n.d.	n.d.	n.d.	n.d.	n.d.
n.d.	n.d.	n.d.	0.25 (0.12)	n.d.	n.d.	n.d.	n.d.	n.d.	n.d.	n.d.
90.75 (1.61)	97.54 (1.60)	96.30 (1.08)	99.37 (1.00)	99.42 (0.73)	95.16 (1.53)	96.12 (0.92)	97.73 (1.59)	87.86 (2.44)	90.43 (1.36)	94.02 (1.34)
9.3 (1.6)	2.5 (1.6)	3.7 (1.1)	0.8 (0.8)	0.7 (0.6)	4.8 (1.5)	3.9 (0.9)	2.3 (1.6)	12.1 (2.4)	9.6 (1.4)	6.0 (1.3)
1.15 (0.09)	1.19 (0.10)	1.19 (0.12)	1.29 (0.07)	1.21 (0.05)	0.97 (0.06)	0.96 (0.06)	1.29 (0.09)	2.08 (0.39)	1.35 (0.15)	1.03 (0.07)
0.47 (0.03)	0.66 (0.04)	0.46 (0.03)	0.80 (0.05)	0.84 (0.01)	0.54 (0.03)	0.52 (0.10)	0.62 (0.05)	0.30 (0.05)	0.24 (0.11)	0.42 (0.06)
0.09 (0.04)	0.14 (0.07)	0.13 (0.12)	0.28 (0.09)	0.02 (0.02)	0.13 (0.06)	0.11 (0.05)	0.27 (0.03)	0.19 (0.09)	0.22 (0.08)	0.07 (0.04)
1.35 (0.06)	1.82 (0.61)	1.55 (0.45)	3.79 (0.69)	1.07 (0.12)	1.51 (0.43)	1.38 (0.32)	3.13 (0.51)	2.25 (0.77)	3.32 (0.61)	2.20 (0.61)
34.2 (2.9)	41.3 (2.7)	41.6 (5.1)	37.3 (5.8)	42.1 (1.4)	30.5 (3.8)	30.6 (4.3)	39.1 (5.0)	44.3 (4.8)	38.6 (5.4)	23.9 (4.3)
1.9 (0.6)	1.9 (0.9)	1.9 (1.0)	3.0 (0.7)	2.1 (0.4)	0.20 (0.41)	0.07 (0.13)	3.0 (0.8)	7.3 (1.6)	4.1 (1.6)	0.70 (0.55)
24.8 (1.3)	34.0 (2.2)	23.5 (2.0)	39.7 (4.2)	44.9 (2.1)	35.2 (1.7)	34.2 (4.8)	28.8 (4.6)	9.0 (1.0)	7.4 (3.6)	26.6 (2.6)
26.1 (2.1)	16.6 (3.0)	25.8 (4.3)	9.4 (2.7)	8.2 (0.5)	27.1 (3.7)	29.3 (7.9)	16.4 (1.1)	20.7 (5.6)	22.0 (7.2)	35.5 (5.8)
0.83 (0.72)	0.13 (0.22)	0.18 (0.23)	2.5 (1.1)	0.04 (0.07)	0.26 (0.36)	0.24 (0.49)	4.1 (2.3)	2.0 (1.2)	11.4 (5.5)	3.0 (2.6)

the intrusion of the Vedrette di Ries batholith at ≈31 Ma (Cesare, 1999; Tajčmanová et al., 2009). All other microstructures having been erased, the only evidence that these rocks underwent anatexis at some time in their complex history is represented by the occurrence of *nanogranites* within relics of Variscan garnet (Fig. S3c). This example demonstrates that MI have to be considered among the most reliable microstructural

criteria for the former presence of melt in regional migmatites and granulites.

6.3. When a rock has melted, and timeframes of melt segregation

Because MI attest to the growth of a mineral during crustal melting (see Section 6.1), in the case of hosts like zircon or monazite (Fig. 12) their occurrence allows anatectic events to be dated with unprecedented confidence. For instance, Cesare et al. (2003b) and Kawakami et al. (2013) described zircon crystals characterized by tiny glassy MI distributed in annuli at the core-overgrowth interface (Fig. 12a,b). This texture clearly indicates that overgrowths formed in the presence of a melt phase, i.e., during an anatectic event. In the case of MI-bearing zircon and monazite enclosed in peritectic garnet (indicating that garnet growth occurred during or after the growth of these accessory minerals), the monazite and zircon ages are likely to reflect the age of the anatectic event associated with the growth of peritectic garnet, or the timing of the oldest melting event in the investigated rocks (Section 3; see also Cesare et al., 2009b). At El Hoyazo, Cesare et al. (2003b, 2009b) dated by SHRIMP at c. 9 Ma those euhedral zircon rims after MI annuli. These zircons are included within peritectic Grt of metasedimentary enclaves hosted within peraluminous dacites extruded at c. 6 Ma (Zeck and Williams, 2002). Making the reasonable assumption that dacites formed due to the anatectic event recorded by the metasedimentary enclaves, Cesare et al. (2009b) concluded that melt and residue coexisted at the base of the crust for about 3 Ma.

7. What can we learn from melt inclusions? Compositional information

Chemical analysis of glassy and remelted MI allows the in situ characterization of natural primary anatectic melts. To date, approximately 600 MI, including glassy MI in anatectic enclaves and glassy MI and rehomogenized *nanogranites* in migmatites and granulites, have been analyzed using the methodology and techniques described above (Table 2). These analyses come from a variety of geologic/geodynamic/geographic environments (detailed in Table 1). It is important to notice that the composition of preserved glassy MI in migmatites and granulites is similar to that of coexisting rehomogenized MI (Bartoli et al., 2013b; Cesare et al., 2009a). The chemical dataset of MI is integrated with 160 analyses of interstitial glass from anatectic enclaves, that allow further petrological and geochemical considerations on anatectic processes in metapelites *s.l.*

The MI are hosted in Grt and Pl and, less frequently, Crd, And, Ilm and Qz, found within metasedimentary peraluminous metapelites and metagreywackes, and metaluminous (meta)igneous orthogneisses and tonalites (Table 2). These rocks are inferred to have melted at conditions varying from 670–700 to ≥900 °C and 4 to 27 kbar, with H_2O-rich fluid-present to H_2O-poor fluid-present or fluid-absent scenarios. All analyses include the concentrations of the major elements obtained by EMP, with H_2O calculated by the EMP difference method. Part of the dataset (≈30 analyses) includes H_2O directly measured by either Raman spectroscopy, SIMS or nanoSIMS, and trace elements (≈60 analyses) analyzed by LA–ICP–MS.

7.1. Major elements

Most MI correspond to granites based on their normative compositions (Fig. 13a). However, some of the remelted MI from Kali Gandaki are characterized by low K_2O (≈1–2 wt.%), CaO up to 4.0 wt.% and high H_2O (≈8–15 wt.%), plotting as granodiorites, trondhjemites and tonalites. Because of this variability beyond granitic (s.s.) compositions, we propose *nanogranitoids* as a comprehensive name for the totally crystallized MI.

In a normative Qz–Or–Ab diagram, granitic MI from each locality show some spread and, at the same time, a distinctive composition with respect to each other (Fig. 13b). They are located in most cases towards the center of the diagram and within ≈10–20% of the haplogranitic eutectic compositions. Considering that the host rocks for these MI cover a relatively wide compositional spectrum, this emphasizes that the concept of haplogranitic "*minimum melt*" compositions finds little applicability in natural migmatites, as even at low temperatures melt may significantly depart from these model compositions. Some of the granitic MI are clearly displaced towards either the Ab–Or or Qz–Or sidelines; these compositions can be explained by the effects of T, P and bulk rock composition of the host (see below). MI from Kali Gandaki are mostly tonalitic, trondhjemitic and granodioritic, plot close to the Qz–Ab sideline and show some spread in the Qz/feldspar ratio compared to their small variation in Ab/Or.

MI are metaluminous to strongly peraluminous, with most Aluminum Saturation Index values [ASI = molar $Al_2O_3/(CaO + Na_2O + K_2O)$] in the range 1.00–1.40 (Fig. 14a). These values are similar to those expected in granitic melts at equilibrium with a variety of strongly peraluminous minerals and from H_2O-saturated to low a_{H_2O} conditions (Acosta-Vigil et al., 2003). A small proportion of MI in garnet from an orthogneiss of the Bohemian Massif and the tonalitic enclaves of La Galite show an ASI of 0.90–1.00. The combination of low H_2O concentrations in melt (Acosta-Vigil et al., 2003) and the metaluminous character of the host rock can partially explain these ASI values around 1.00 (see discussion in Ferrero et al., 2014).

Most MI have $FeO_t + MgO$ concentrations in the range 0.5–2.5 wt.% (Fig. 14b). Only a small fraction (≈10%) of the dataset shows values up to 4.0 wt.%, including most of the MI in Ilm from El Hoyazo enclaves and some from the other case studies. The MI in Ilm from El Hoyazo are rather large (up to 100 μm, see Fig. 10 of Acosta-Vigil et al., 2007) and, although TiO_2 in the inclusions is also quite high (0.25–0.40 wt.%), contamination by the host during analysis does not seem an explanation for their high $FeO_t + MgO$ concentration. High T of melting might be the explanation for some extra dissolution of these components, as these MI are found in the enclaves that experienced the highest T (850–900 °C) at El Hoyazo. Regarding the rest of MI with high $FeO_t + MgO$ concentrations, which are included in Grt, there is no clear correlation between $FeO_t + MgO$ and ASI (Fig. 14a), as expected if contamination by the host Grt had occurred during analysis. MI from the Bohemian Massif and Kerala Khondalite Belt were trapped at rather high temperatures (≥875–900 °C), and this may partially explain as well their high concentrations in ferromagnesian components.

Fig. 14c and d shows that loss of alkalis during EMP analyses of the hydrated glasses either did not occur or was corrected using the analysis of secondary glass standards. Otherwise we would expect tight negative correlations between Na_2O and ASI in glasses with the lowest Na_2O concentrations (≤2 wt.%), and between K_2O and SiO_2, as loss of alkalis increases the concentrations of all other components, particularly SiO_2.

Compared to nanoSIMS, the analysis/estimations of H_2O in MI by SIMS, Raman spectroscopy and EMP difference methods provide similar ranges, though somewhat different concentrations: SIMS and Raman spectroscopy underestimate H_2O, whereas the difference method overestimates or underestimates H_2O. Nevertheless, the differences are always moderate to low: ≤20% relative on the average value (Table 2; and Bartoli et al., 2014).

The Kali Gandaki MI are distinct from the rest, and record high concentrations of H_2O and (although variable) CaO as well, high ASI and low K_2O, likely due to melting under high a_{H_2O} (Carosi et al., 2015; see also Patiño-Douce and Harris, 1998; García-Casco et al., 2003). The spread in the Qz/feldspar ratio compared to the small variation in the Ab/Or ratio is likely due to the sluggish diffusion of Si and Al versus rapid diffusion of alkalis in melt (Acosta-Vigil et al., 2006b, 2012b; Morgan et al., 2008). MI from the ultrahigh-T granulites of the Kerala Khondalte Belt have the highest K_2O (6.0–8.0 wt.%) and $FeO_t + MgO$ and the lowest Na_2O (0.5–1.5 wt.%) and H_2O, justified by their very high T of formation and the likely low Na_2O concentration of the protolith (Ferrero et al., 2012). MI from the orthogneiss of the Bohemian Massif show the highest Na_2O (3.5–5.5 wt.%) and some of the lowest #K

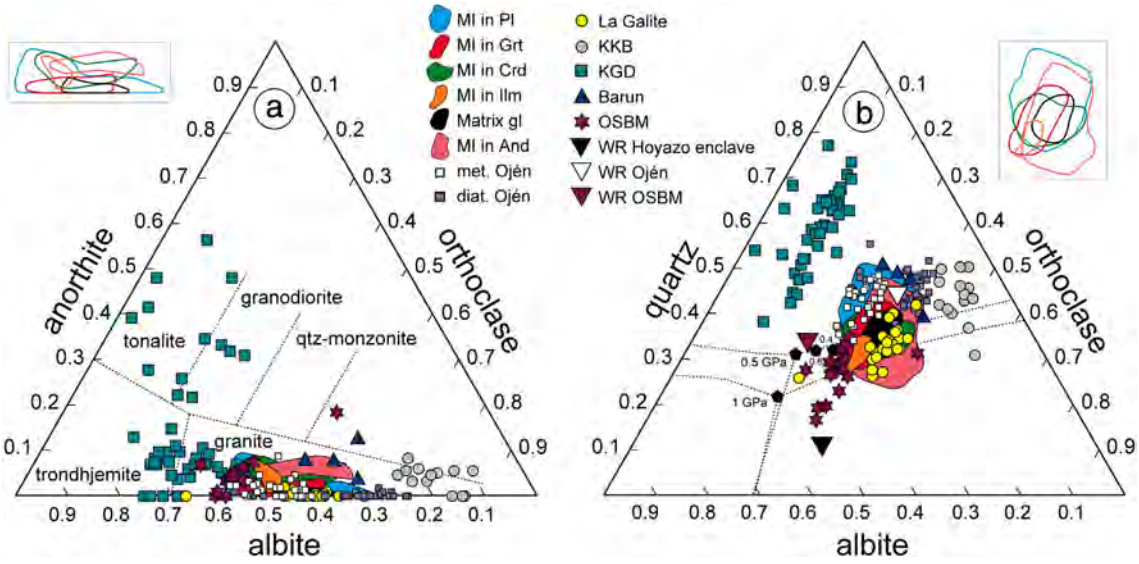

Fig. 13. Pseudoternary diagrams showing the wt.% normative An, Qz, Or and Ab compositions of all analyzed melt inclusions and matrix glasses in anatectic enclaves, and melt inclusions in migmatites and granulites. a) An–Or–Ab, with fields for granite, quartz–monzonite, granodiorite, trondhjemite and tonalite after Barker (1979); b) Qz–Or–Ab, including equilibria data (cotectic lines, stippled, and eutectic compositions at 0.5 and 1.0 Gpa and $a_{H_2O} = 1$, 0.6 and 0.4) for the haplogranite system. Colored lines to the upper right of each triangular diagram show both the entire contours of, and spatial relationships among the solid colored fields in the diagram. Met = metatexites; diat = diatexites; KKB = Kerala Khondalite Belt; KGD = Kali Gandaki; and OSBM = Orlica-Śnieżnik Bohemian Massif.

(0.30–0.45) values, explained by melting at almost ultrahigh-P (haplogranite eutectics move closer to Ab with increasing P), but also by the high T of melting (≥875 °C) of Na-rich rocks. Interestingly, these almost ultrahigh-P melts have only moderate to low H_2O concentrations (3.5–8 wt.%), strongly suggesting a low a_{H_2O} melting scenario. The rest of MI in the dataset of Table 2 relates to melting of mostly metasedimentary rocks under low a_{H_2O} conditions, and shows that melt composition is distinct for each individual sample, even if the protolith and melting conditions are similar, presumably reflecting details of melting reactions and attendant P–T-fluid conditions.

7.2. Trace elements

The more limited dataset of trace element analyses currently available shows that MI have variable, though mostly high, concentrations of elements (Li, Cs, B) partially to totally controlled by muscovite, and moderate-to-low (Rb, Sr, Ba, Nb, Zr, U, Th, REE) or very low (Sc, V, Cr) concentrations of elements hosted by feldspars, biotite, garnet and accessory minerals such as zircon and monazite. Chondrite-normalized REE patterns show flat to negative slopes, with moderate to low fractionation between LREE and HREE and mostly negative Eu anomalies in MI within Pl, and moderate to large fractionation between LREE and HREE and positive Eu anomalies in MI within Grt (Fig. 14e). These REE patterns, however, may be partially affected by syn-entrapment modifications (see Section 9.2). Nevertheless, when MI are large enough (≥50 μm) and/or when the elements of interest are incompatible with respect to the mineral host (e.g. Y in MI within Pl, or Sr in MI within Grt), the concentrations of trace elements can provide reliable information on the nature and mechanisms of crustal anatexis (see Section 8.1). For instance, the concentrations of Zr and LREE of all analyzed MI were used to calculate zircon and monazite saturation temperatures in order to link MI and potential melt-producing reactions (Fig. S4; Acosta-Vigil et al., 2010).

7.3. Comparison with experimental glasses, leucosomes in migmatites, and allochthonous granites

We have compared the compositions of MI with a datasets of ≈200 experimental glasses, ≈50 in-situ leucosomes and ≈100 crustal granites reported in the literature, all related to the partial melting of metasedimentary rocks (Fig. 14f, see caption for origin of data).

Glasses from experiments performed at P–T-a_{H2O} similar to those estimated for anatexis in the host rocks of analyzed MI are also mostly granitic and, to lower extent, tonalitic, trondhjemitic and granodioritic. For the most part they show remarkably similar compositions and ranges in concentrations with respect to the MI. Importantly, each of the experimental and MI studies provides a slightly variable though distinctive melt composition. This means that, although Thompson (1988) pointed out that the liquidus of the granite system shows a "pit" in temperature-composition space close to the pseudo-granitic composition of liquids, primary anatectic melt compositions show some variability (up to several tens of wt% in normative compositions; Figs. 14b, and 5 of Bartoli et al., 2013b) which depends on the protolith and conditions of anatexis. This shows the importance of analyzing MI in migmatites and granulites in order to retrieve the precise primary melt composition of the rock under investigation (Bartoli et al., 2013b).

The leucosome dataset includes only in-situ leucosomes (Sawyer, 2008) interpreted to possibly record primary anatectic melts. The dataset for allochthonous granites includes peraluminous leucogranites interpreted as primary anatectic melts (e.g. Himalayan leucogranites; Inger and Harris, 1992) and also strongly peraluminous mafic granites interpreted as primary melts contaminated with abundant residual material (e.g., the Layos granite, central Spain; Barbero and Villaseca, 1992). Leucosomes and granites show major and trace element concentrations mostly similar to the MI (see also Acosta-Vigil et al., 2012a). Leucosomes show somewhat higher MgO, TiO_2 and #Mg than MI. This also holds for granites, that however show a major difference with respect to MI regarding the higher FeO_t + MgO, reaching 9–10 wt.% in the more mafic strongly peraluminous varieties (Fig. 14f). Also, several leucosomes and many granites show extremely low concentrations of FeO_t (0.1–0.5 wt.%), whereas the extensive dataset for MI systematically shows $FeO_t \geq 0.5$–1 wt.%. In addition, leucosomes and granites show very good FeO_t vs. TiO_2 and FeO_t vs. MgO positive correlations, unlike MI (and experimental glasses). Granites also show good positive correlations of CaO vs. FeO_t, slightly better than in leucosomes, and much better than in MI (and experimental glasses). All these observations suggest differences in the mechanisms controlling the concentrations of ferromagnesian components, and to lower extent of Ca, in leucosomes and granites versus MI. The different mechanisms have

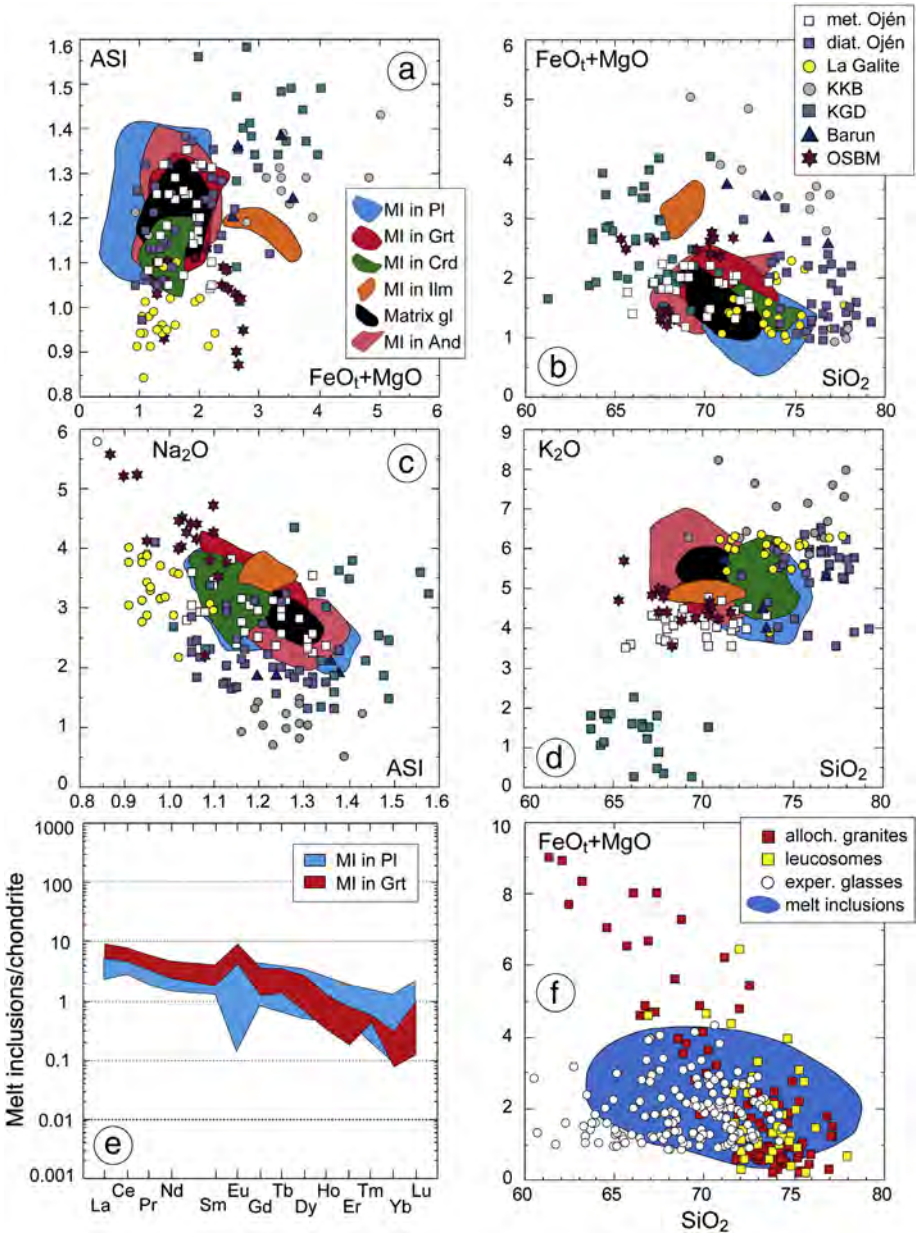

Fig. 14. Selected variation diagrams showing some major element concentrations and ASI values of melt inclusions and matrix glasses in anatectic enclaves, and of melt inclusions in granulites and migmatites: a) ASI vs. $FeO_t + MgO$; b) $FeO_t + MgO$ vs. SiO_2. c) Na_2O vs. ASI; d) K_2O vs. SiO_2. e) Chondrite-normalized Rare Earth Elements for glassy melt inclusions in plagioclase and garnet of El Hoyazo enclaves (using values from Sun and McDonough, 1989); f) Comparison among the $FeO_t + MgO$ and SiO_2 concentrations of melt inclusions, experimental glasses from the equilibrium partial melting of powdered metasedimentary rocks, leucosomes of migmatites interpreted as primary anatectic melts, and mostly allochthonous S-type granites including both peraluminous leucogranites interpreted as primary anatectic melts, and mafic strongly peraluminous granites including abundant residual material.
Data sources for experimental glasses: Vielzeuf and Holloway (1988), Holtz and Johannes (1991), Patiño Douce and Johnston (1991), Montel and Vielzeuf (1997), Patiño Douce and Harris (1998), Schmidt et al. (2004) and Hermann and Spandler (2008). Data sources for leucosomes: Weber et al. (1985), Weber and Barbey (1986), Collins et al. (1989), Barbey et al. (1990, 1996), Bea et al. (1994), Watt and Harley (1993), Barbero et al. (1995), Braun et al. (1996), Watt et al. (1996), Acosta (1998) and Acosta-Vigil et al. (2014). Data sources for S-type granites: Albuquerque (1971), Currie and Paraji (1981), Vidal et al. (1982), Barker et al. (1986), Charoy (1986), Day and Weiblen (1986), Silver and Chappell (1988), White and Chappell (1988), Collins et al. (1989), Scaillet et al. (1990), Barbero and Villaseca (1992), Nabelek et al. (1992), Montel and Abdelghaffar (1993) and Guillot and Le Fort (1995).

been recognized in a) dissolution in, and equilibration of ferromagnesian minerals and plagioclase with the melt; b) entrapment of residual/peritectic minerals, and c) fractional crystallization with formation of cumulate rocks and migration of evolved liquids (Chappell and White, 1992; Chappell et al., 1987; Clemens and Stevens, 2012; Lavaure and Sawyer, 2011; Sawyer, 1996, 2008; Stevens et al., 2007).

8. New insights on the petrology of crustal melting

The MI-based studies of the last two decades have provided significant advances in our understanding of crustal anatexis. In this section we summarize some of the most important outcomes.

8.1. Mechanisms and nature of crustal melting

The study of MI opens a new window of information into melting mechanisms and melt evolution during the prograde history of crustal anatectic rocks. Conversely, the leucosomes investigated in classic petrological and geochemical studies do not commonly and/or unequivocally represent primary melts, and the melt-related information is apparently erased due to superimposition of melting reactions, melt-residue retrograde reactions, presence of xenocrysts, melt crystallization and loss of volatiles (e.g., Sawyer, 2008).

An example of the new powerful approach allowed by MI comes from the study of the Grt–Bt–Sil anatectic enclaves from El Hoyazo:

they represent a snapshot of anatexis in the medium-to-lower crust, frozen due to the ascent, extrusion and rapid cooling of the host lava, as shown by the solidification of former melt to undevitrified glass. Hence, at El Hoyazo melt and residue can be readily indentified and analyzed. Glass is present as MI in most minerals and as intergranular films in the matrix (Cesare, 2008; Cesare et al., 1997). A detailed major and trace element study of the MI in plagioclase and garnet and of matrix glasses, in combination with a solid background on the petrology of the enclaves, has shown that MI in plagioclase constitute the earliest record of melt produced in the rocks by water-present to fluid-absent muscovite melting, and that MI were trapped at the beginning of anatexis in a context of rapid heating and melting. At that time, the melt present throughout the rock was somewhat heterogeneous both in major and trace element concentrations (Acosta-Vigil et al., 2007, 2010).

MI in garnet represent melts formed by fluid-absent melting of muscovite, trapped simultaneously to MI in plagioclase or slightly after. At this stage melt became more homogeneous due to more effective diffusion. In spite of some heterogeneity, melts were close to equilibrium with their residue regarding most trace elements and coexisting minerals, except for some undersaturation in accessory minerals zircon and monazite.

Interstitial glasses in the matrix represent the latest melts produced in the enclaves, and record the start of the fluid absent melting of biotite. Melt at this stage was quite homogeneous and at near equilibrium with most of the residue, except garnet and, to some extent, zircon and monazite (Acosta-Vigil et al., 2007, 2010; Acosta-Vigil et al., 2012a).

8.2. H_2O contents of melts and fluid regime during melting

Constraining the fluid regime during crustal melting is an issue that has received very recently renewed attention (see Weinberg and Hasalová, 2015). MI represent a valuable tool in this respect.

Based on theoretical, experimental and petrological arguments (e.g., Clemens and Watkins, 2001; Stevens and Clemens, 1993; Thompson, 1990; Yardley and Valley, 1997), the production of anatectic granitoid magmas has been traditionally considered to take place mostly under (or to evolve quickly toward) fluid-absent conditions i.e., at $a_{H_2O} < 1$. In this view, the P–T conditions normally achieved during HT metamorphism are sufficient for hydrate-breakdown (*dehydration*) melting reactions to take place in rocks of the mid to lower continental crust, where very little or no aqueous fluid is present in the intergranular pores.

H_2O-present (or *H_2O-fluxed*) melting has been successfully identified either by the presence of diagnostic mineral assemblages or by the abnormally high melting degrees at low-T, both conditions being in agreement with the presence, and abundance, of a free aqueous fluid during melting (e.g., Pattison and Harte, 1988). In his study of the leucogranodiorite gneisses of the Opatica subprovince, Canada, Sawyer (2010) describes the microstructural, petrological and oxygen isotopic features of the migmatites, concluding that up to 30% melt was produced by water-fluxed melting of quartz + plagioclase + microcline. Based on this and other studies, the recent review of Weinberg and Hasalová (2015) concludes that water-fluxed melting has been underestimated in the past and, on the contrary, may be an important process of crustal differentiation. It is apparent, also from the reactions of the scientific community (Clemens and Stevens, 2015), that the fluid regime during anatexis will remain a debated, controversial aspect until we find an easy way to access and constrain in situ, in the source region and at the moment of their production, the chemical properties of anatectic melts.

By analyzing with nanoSIMS the H content of rehomogenized MI from amphibolite-facies migmatites at Ronda, Bartoli et al. (2014) have provided the first example of what can (and should) be done. Their measurement in situ demonstrates high and variable H_2O contents (mean of 6.5 ± 1.4 wt.%) in these granitic melts which were produced at ~700 °C and ~5 kbar. They propose that the melting process progressively evolved from fluid-present to fluid-absent conditions, similarly to what proposed by Acosta-Vigil et al. (2010) in the study of MI from the anatectic enclaves of El Hoyazo. In addition, Bartoli et al. (2014) show that H_2O contents in MI from different crystals range from 5.4 to 9.1 wt.%, documenting the existence of H_2O heterogeneities in natural granitic melts at the source region.

New data from the migmatites of Jubrique (Acosta-Vigil et al., under review) indicate that H_2O contents of remelted MI may exceed 10 wt.%, thus suggesting a fluid-present melting process at mid-to-lower levels of the continental crust (4–6 kbar).

The direct measurement of H_2O in rehomogenized and glassy MI from migmatites and granulites is still in its infancy, is very time-consuming, and like other approaches can be affected by methodological and interpretive problems (see above). However, given also the possibility of analyzing C by the same method, it appears the best approach for the correct quantification of fluid contents in anatectic melts, and therefore for a correct understanding of fluid regimes during anatexis.

8.3. Placing melt in the right phase assemblage

One of the main difficulties during the modeling of partial melting is to include the melt phase in the right assemblage(s). This step is fundamental to extract reliable thermobarometric information from phase diagrams.

Microstructures such as pseudomorphs after films of melt and "string of beads" are valuable tools for identifying the former presence of melt (Hartel and Pattison, 1996; Holness and Sawyer, 2008; Sawyer, 1999). However, these delicate structures are easily erased by deformation and/or recrystallization (Holness et al., 2011). In addition they mostly occur in the rock matrix and not within single crystals, and therefore the presence of melt can be only associated with the latest assemblages developed in the rock. As they are preserved within crystals, MI can survive through the metamorphic history of the rocks. Because of their primary nature, they have furthermore the advantage of relating the presence of melt with the formation of the host, and thus with a specific assemblage.

One example of such approach is represented by the migmatitic kyanite gneisses of Kali Gandaki at the base of the Greater Himalayan Sequence. Here melting has been generally considered to take place in the decompressional phase of exhumation at about 30 Ma, and very little evidence of melting during the prograde compressional path had been reported. In these gneisses Carosi et al. (2015) have discovered MI of both granitic and tonalitic–trondhjemitic–granodioritic compositions in garnets which are texturally synchronous with kyanite (see also Section 6.1). These MI demonstrate that melting took place in the kyanite stability field during the prograde path of the metamorphic cycle (Eo-Himalayan event; Vannay and Hodges, 1996). Furthermore, in situ U–Th–Pb dating of monazite included in garnets, in the same structural positions as MI, allowed Carosi et al. (2015) to constrain the beginning of partial melting at 41–36 Ma.

A second example comes from the highly deformed granulitic gneisses of Jubrique, at the contact with the Ronda peridotite slab. These rocks have a complex and controversial polymetamorphic history of Variscan and/or Alpine ages (Loomis, 1972; Massonne, 2014; Platt et al., 2003; Torres-Roldán, 1981), and display clear features of extensive migmatization (Barich et al., 2014). While earlier studies on these rocks proposed that anatexis started in the field of sillimanite during decompression from peak pressures, the study of MI by Barich et al. (2014) demonstrated that melt was already present in the system at peak conditions in the kyanite field (850 °C and 12–14 kbar), and that most garnet grew in the presence of melt (see Section 6.1).

8.4. Melt-fluid immiscibility

The immiscibility between two melts or a melt and a fluid phase (e.g., Lowenstern, 1994) is a well known phenomenon in fluid inclusion studies from igneous systems, and is responsible for important processes of geochemical differentiation and formation of ore deposits (review in Audetat and Lowenstern, 2014). Melt-fluid immiscibility in anatectic systems occurs when the quantity of fluid exceeds the amount that is soluble/miscible in the melt at the pressure and temperature of interest. In fact, besides the nature of the fluids/melts involved, the solubility of fluids in melts is a function of pressure and temperature (e.g. Holtz and Johannes, 1994; Holtz et al., 2001). In the case of granitic melts produced by the anatexis of metasedimentary protoliths, the fluid is most commonly H_2O: if pure, immiscibility would correspond to the H_2O-saturated melting conditions, where free H_2O coexist with a melt phase. Although reported (see the compilation of Weinberg and Hasalová, 2015), these conditions are not deemed likely in the Earth's crust (Clemens and Watkins, 2001).

The situation can be significantly different when other fluid components, like the carbonic species CO_2 and CH_4 that show lower solubility in granitic melts, are involved. The presence of carbonic species is necessarily met in graphite-bearing rocks (Cesare and Maineri, 1995; Ohmoto and Kerrick, 1977). Immiscibility between melt and CO_2, or more rarely with N_2 or CH_4 (or with salt rich *brines*), is implicit in the common reports of CO_2-rich fluid inclusions in *HT* graphitic granulites (e.g., Satish-Kumar, 2005). Here, fluid inclusions would witness the fluid immiscible with a former melt, whose existence is compatible with the petrological history of the rock and with microstructures indicating its former presence. However, direct microstructural evidence of melt-fluid immiscibility in granulites or migmatites has not been reported until attention was paid to crustal xenoliths and enclaves in rapidly quenched lavas, where the preservation of the anatectic glass is favored by rapid cooling.

In the scapolite-bearing granulite xenoliths from diatremes of Pamir (Chupin et al., 2006a; Madyukov et al., 2011), the evidence of immiscibility between rhyodacitic melts and almost pure CO_2 is provided by clear-cut microstructures of "immiscible trapping", i.e., by the coexistence in the same fluid inclusion array of inclusions displaying all proportions from 100% fluid to 100% melt. These microstructures are observed in garnet and in scapolite, inferred to have crystallized during anatexis at c. 1000 °C and 15 kbar.

Immiscibility, recorded in inclusions in cordierite, garnet and plagioclase, occurred during anatexis at lower pressures in the graphitic crustal enclaves from both El Hoyazo and Mazarrón (Cesare et al., 2007; Ferrero et al., 2011). The mineral hosts preserve spectacular microstructural evidence of immiscible trapping, where a peraluminuous felsic rhyolitic melt coexists with a CO_2-dominated (>85 mol%) fluid, with minor amounts of N_2 and CH_4, and traces of CO and H_2. In the fluid inclusions, the absence of H_2O and the low density, incompatible with the estimated trapping conditions of 5–7 kbar and 800–900 °C, suggest that post-entrapment re-equilibration and fluid leakage occurred. This was confirmed by the TEM-based study of Ferrero et al. (2011), who showed the presence in garnet of partially annealed sub-μm cracks, containing small cavities, which may have been the pathways for fluid escape out of the inclusions associated with decrepitation during decompression by magma uprise.

A similar scenario, with re-equilibration and leakage of fluid inclusions after entrapment at c. 800 °C and 5 kbar, has been proposed for fluid-melt immiscibility in garnet from La Galite (Ferrero et al., 2014). Here the rocks do not contain graphite, the melt is a metaluminous granite, and the fluid within inclusions is dominated by CO_2, with minor H_2O, N_2 and CH_4.

These examples highlight, on the one hand, the potential of peritectic phases to preserve in their fluid and melt inclusions the evidence for immiscibility; on the other hand, however, they also show the limitations of the use of fluid inclusion data from xenoliths in lavas, where decompression during magma uprise induces the most favorable conditions for decrepitation (Touret and Huizenga, 2012) with the modification of composition and density of fluid inclusions.

8.5. Melting in ultrahigh-pressure rocks

Several studies reported in the last 15 years the presence of polycrystalline multiphase inclusions from UHP terrains such as the Dabie–Sulu orogen (e.g. Chen et al., 2014; Gao et al., 2012, 2013) and Kokchetav Massif (Hwang et al., 2001; Korsakov and Hermann, 2006). Mostly hosted in garnet and omphacite, these inclusions have been interpreted as crystallized portions of homogeneous melt/silica-rich fluid produced by phengite breakdown during decompression (Auzanneau et al., 2006) at P below the quartz–coesite transition, i.e. <27–28 kbar at 800–900 °C (Bose and Ganguly, 1995). The study of crystallized MI in UHP granulites of the Orlica-Śnieżnik Dome (Bohemian Massif) has provided instead direct evidence for partial melting at the metamorphic peak under near-UHP conditions, corresponding to 27 kbar and ≥875 °C (Ferrero et al., 2015). The presence of melt at the metamorphic peak is likely to promote rapid exhumation of deeply subducted rocks (Hermann et al., 2001; see also Ferrero et al., 2015). This process has been proposed by Labrousse et al. (2011) for the Western Gneiss Region, where indeed *nanogranites* have been identified in UHP garnets (Ganzhorn et al., 2014), thus providing crucial constraints on the geodynamic behavior of the deepest portions of orogens.

The relationship between melt and host, i.e. whether or not the host is a peritectic phase, is generally not discussed in the published case studies of polycrystalline inclusions in UHP rocks, and the melt is often inferred to have infiltrated the host *after* its crystallization, along cracks and cleavages (e.g. Hwang et al., 2004; 2009). In the Orlica-Śnieżnik granulites melt entrapment and garnet formation are constrained as coeval by strong microstructural criteria supporting the primary nature of the MI, and by the results of experimental re-homogenization via piston cylinder apparatus. The re-homogenized MI have both composition and water content similar to the experimental results available in literature for HP and UHP rocks, confirming that *nanogranites* are "ideal natural charges of melt" regardless of the pressure of formation (Ferrero et al., 2015).

A few case studies have reported the presence of localized melting within previously solid inclusions in garnet porphyroblasts of natural rocks (e.g. Lang and Gilotti, 2007), whose occurrence is also supported by experimental studies (Perchuk et al., 2005; 2008). This process generates polycrystalline inclusions with remnants of hydrous phases, i.e. phengite or amphibole and epidote (Perchuk et al., 2005) plus crystal phases consistent with melt crystallization (Lang and Gilotti, 2007), and occasionally newly crystallized garnet with euhedral faces (Perchuk et al., 2008). Although they attest for the presence of melt at some point of the rock history, such inclusions have a very different meaning with respect to the primary anatectic MI. While the latter are trapped as a homogeneous melt during host growth during widespread partial melting of the surrounding rock, the polycrystalline inclusions described above are products of in-situ melting, which takes place after garnet formation and only in the garnet interiors, with limited significance for the rest of the rock.

9. Problems and pitfalls

Like any other novel object and tool of research, also MI suffer from potential problems and pitfalls that might invalidate inferences and conclusions drawn from their studies. Clemens (2009) raised four main questions after the first report on *nanogranites* made by Cesare et al. (2009a): 1) what phase is trapped in the inclusions? 2) which is its actual composition? 3) has such composition been modified after entrapment? 4) is that composition representative of the bulk behavior of the rock? We discuss these problems and try to answer the questions, also on the basis of the new data collected in the following years.

9.1. Origin of the inclusions

The first question relates to the origin of the phase contained in the inclusions: could the MI represent something else than an (anatectic) melt trapped during melting of the host rock and growth of the mineral host, subsequently crystallized into a cryptocrystalline aggregate or quenched as glass? Could the MI be related to a different genetic process? Incidentally, we are unaware of occurrences of similar polycrystalline "MI" in rocks for which only a subsolidus history has ben documented, e.g., in upper greenschist-facies metapelites where garnet can be abundant.

Doubts on the origin proposed for the glassy inclusions in the enclaves from El Hoyazo were also raised by Vernon (2007), who called into question the entrapment of an anatectic melt phase, and proposed that inclusions were the result of "melting in response to loss of stability of a mineral assemblage" that "may conceivably produce melt droplets dispersed all through the grains of the unstable mineral if inclusions were originally present, which is a common situation in metamorphic assemblages". Because the genetic process is "instability of inclusion-rich cores during the melting, rather than incorporation of melt droplets during growth", he concluded that "glass inclusions must have formed later" than garnet.

Such radically alternative hypothesis has been discussed by Cesare (2008), who showed how it was untenable on the basis of microstructural, mass balance and thermodynamic constraints. Referring to that paper for the full details, it can be recalled that melting in a system composed of a pre-existing solid inclusion (I) in a host (H) may be either eutectic (I + H = M) or incongruent (I + H = M + P), where M is the melt and P is a peritectic phase. In the case of eutectic melting it can be observed that there is no known single mineral (I) that can produce a granitic eutectic melt (M) if included in garnet (H). Therefore the rhyolitic glass inclusions in the garnet from El Hoyazo cannot have formed by the process proposed by Vernon (2007). In the same occurrence, the absence of any peritectic phases systematically associated with the melt inclusions also rules out an incongruent melting of pre-existing solid inclusions (see e.g. the results of remelting experiments of garnet inclusions from Perchuk et al., 2008 discussed in Section 9.5). Cesare (2008) concluded that "the only way by which "inclusion melting" could take place is that H, rather than a single mineral, includes an aggregate of reactant phases that always happen to occur in exactly the right modal proportions to enable the reaction to be complete congruent melting".

The above discussion concerned glassy inclusions in host minerals from rapidly cooled enclaves in lavas. But could the phase originally trapped in MI be confidently considered a melt even when we observe a cryptocrystalline aggregate, as in most migmatites and granulites? We believe that the number of case studies collected and characterized since the first discovery of *nanogranites* provides a solid, systematic and even overwhelming basis for a positive answer. The first important fact is that MI, when well preserved from deformation and microfracturing, can be experimentally remelted to a homogeneous glass without interaction with the host or formation of peritectic phases (Fig. 10d). In addition, successful homogenization is achieved for many or most of the inclusions in a sample, and rehomogenization is achieved at *P–T* conditions consistent with the anatectic history of the rocks. The second fact is that the composition of the remelted MI is homogeneous within a sample and compatible with an anatectic melt formed in the host (see Section 7). In addition, glassy MI, although much less abundant than *nanogranites*, are often present in the same clusters, and have similar compositions to the analyzed rehomogenized *nanogranites*.

Finally, are there valid alternative explanations? The possibility raised by Clemens (2009) that MI may contain some "silicothermal" aqueous-silicic fluids (Wilkinson et al., 1996), although clearly not supported by data from any of the natural occurrences of migmatites and granulites reported so far, would not invalidate the proposed trapping process. On the contrary, similar fluids are expected to play a role, and to be found, at (U)HP conditions (Frezzotti and Ferrando, 2015), above the second critical end point (Hermann et al., 2013), where a separation between granitic melt and aqueous fluid is not present anymore.

In summary, we believe there is at present no tenable alternative to the interpretation of cryptocrystalline polymineralic inclusions (*nanogranitoids*), such as those described here, as the products of crystallization of former melt inclusions and that the concerns on the origin of MI do not find support. This line of reasoning is in perfect analogy with the common acceptance of crystallized inclusions ("stone-cavities" of Sorby, 1858) in deep-seated intrusive rocks as former MI (Bodnar and Student, 2006; Roedder, 1984).

9.2. Reliability of chemical data from MI

A second problem concerns the reliability of chemical data obtained from MI to represent the actual composition of the trapped melt. Analyzing the phenomenon of Na loss during EMP analysis of hydrous felsic glasses, and discussing the unusual, highly potassic character of the compositions obtained by Cesare et al. (2009a) from MI in the UHT granulites of the Kerala Khondalite Belt, Clemens (2009) questioned their reliability and suggested caution in the interpretation of chemical data obtained from MI.

The analysis of small volumes of glasses is a well-known challenge, especially for alkalis and Na in particular (e.g. Morgan and London, 1996, 2005), and affects not only the characterization of small inclusions but at the same fashion also experimental charges with low melt percentages (e.g., Garcia Casco et al., 2003; Nair and Chacko, 2002).

Beam-induced Na loss can be prevented or monitored (and then corrected) in several ways, including: a) reducing the areal current density by using small beam currents and broad – 20 μm – beam diameters or, when this is not possible, b) applying correction factors determined from the simultaneous analysis of secondary glass standards of similar and well-known composition (Morgan and London, 1996, 2005), or c) using a N_2-cooled SEM cryostage (Stevens et al., 1997; see also Section 5.2). In some experiments, the measurement of Na in the melt was discarded, and Na_2O was calculated by mass-balance (Patino Douce and Johnston, 1991).

The small size of MI generally requires the use of a focused beam, and the analytical strategy adopted in most works and discussed above at Section 5.2 implies some uncertainties for Na, and for other major elements as well. Analyzing glassy MI at El Hoyazo, Acosta-Vigil et al. (2007) used a beam diameter of 5 μm. During the analysis of the small MI in migmatites and granulites (Bartoli et al., 2013b; 2014; Cesare et al., 2003a; Ferrero et al., 2015) beam diameters of ≈1 μm were used. In all cases, however, Na loss was monitored through the analysis of secondary glass standards, and Na loss varied between ≈0 and 25% relative. The fact that final recalculated Na_2O concentrations in MI are similar to those in experimental glasses, and that also reported ASI values are similar to those in experimental glasses at equilibrium with peraluminous minerals (Section 7), means that Na loss during EMP analysis does not represent an obstacle for providing reliable analyses of the MI. In addition, uncertainties provided by MI compositions using these analytical strategies are similar to those reported in most studies of natural and experimental glasses (Gardien et al., 1995; Koester et al., 2002; Le Breton and Thompson, 1988; Patiño Douce and Harris, 1998; Pickering and Johnston, 1998).

It is important also to point out that considering the currently available dataset obtained from several migmatite occurrences, the highly potassic compositions (normative Or/Ab > 4) reported by Cesare et al. (2009a) are an exceptional finding, and that MI with Or/Ab ratios from 0.5 to 2 are the most frequently found (Fig. 13b). Nevertheless, melts with normative Or/Ab > 4 have been reported both in experiments and nature (Maheshwari et al., 1996; Patiño Douce and Johnston, 1991). Also Ca-rich, K-poor compositions have been measured (Kali Gandaki, Jubrique; Carosi et al., 2015; Acosta-Vigil et al., under review), probably reflecting melting under fluid-present

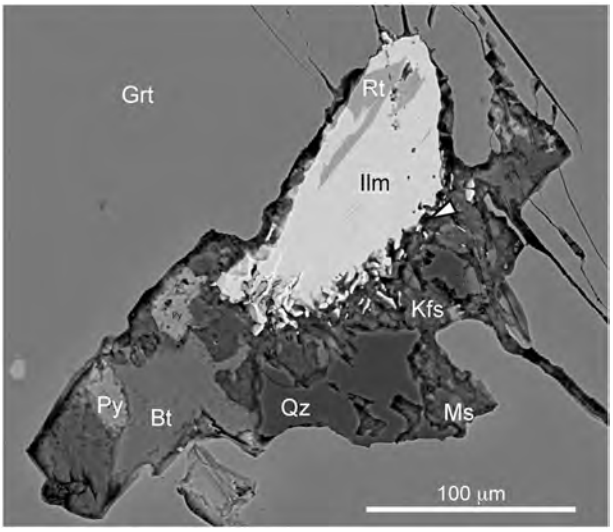

Fig. 15. Fractured MI in a strongly deformed garnet from Jubrique granulites. Fracturing allows fluid expulsion in the early HT stages, but also fluid access, retrogression and hydration in the late-stage evolution and weathering of rocks. This is attested by the resorbed aspect of crystals within the MI, and by the presence of low-T minerals like pyrite and chlorite.

conditions and in accordance with experimental evidence (García-Casco et al., 2003; Patiño Douce and Harris, 1998).

Available data indicate that differences exist among the measured compositions of MI in each of the case studies analyzed (see Section 7, Fig. 13b). Not only are melt compositions different among samples, but broadly homogeneous within each sample, as shown by the low standard deviations of EMP averages (Table 2). When compared with glasses obtained from the experimental melting of metapelitic/metapsammitic compositions at P < 13 kbar (compiled by Bartoli et al., 2013b), the chemical data obtained from remelted MI display similar degrees of homogeneity (see also Fig. 13b), suggesting similar analytical accuracy. In addition, standard deviations of the mean concentration of major elements for each MI case study are similar or just slightly larger than those from glasses considered as compositionally homogeneous (compare with Acosta-Vigil et al., 2003).

9.3. Are MI compositions affected by post-entrapment modifications?

Like fluid and melt inclusions from all geological settings, also MI in migmatites and granulites can be affected by post-entrapment modifications of various types, that may hinder the ability of MI to record the chemical and physical conditions of trapping, i.e., to preserve the composition of the primary anatectic melt as it was trapped by the host.

Excluding decrepitation and microfracturing, which almost inevitably lead to extensive hydration and chemical exchange with the matrix outside the host (Fig. 15; see also, e.g., Liu et al., 2013; Hiroi et al., 2014), making MI unusable for remelting and reconstructing the primary melt compositions, several changes can occur also in those MI which are thought to behave as "closed", considering as part of the closed system also the chemically reactive part of the host that constitutes the unfractured walls of the cavity. The modifications that can occur include (Audetat and Lowenstern, 2014): a) the crystallization of the inclusion, usually starting at the walls (*sidewall crystallization*), b) the nucleation of bubbles during cooling and crystallization, and c) the diffusional re-equilibration of the MI with the host phase. During the crystallization of a MI, the host at the inclusion wall can either show overgrowths formed from the melt, or behave as an inert nucleation site for other daughter phases, or can be partially replaced by retrograde, host-consuming reactions. As discussed above, the latter process, unexpected for MI in igneous systems, should instead occur in the case that the host is a peritectic mineral (Bartoli et al., 2013a). Overgrowth or resorption of inclusion walls can be detected microstructurally, by optical or electronic microscopy, as alterations of the planar facets of the negative crystal shaped inclusions. Bodnar and Student (2006) noted how MI in plutonic rocks are poorly defined and lack sharp borders, as an effect of sidewall crystallization. On the contrary, MI in migmatites and granulites, when preserved from microcracking, commonly exhibit perfect negative crystal shapes (Figs. 1 and 6). This observation suggests that resorption of garnet (the most common mineral host) at MI walls is an uncommon process.

The presence of bubbles affects the volatile content of the glass in inclusions (Moore et al., 2015) because some volatile species may diffuse into the bubble, leading to measured fluid contents in the glasses lower than in the originally trapped melts. When volatiles diffuse into the bubble, the process can be reversed by heating and rehomogenizing the inclusion (see below).

Volatiles, in particular H_2O, may also be lost to/through the host in an irreversible way, although the exact processes by which such loss takes place are still unclear (Audétat and Lowenstern, 2014). Huge H_2O variations have been induced experimentally (e.g., Hauri, 2002; Massare et al., 2002; Portnyagin et al., 2008; Severs et al., 2007) in MI hosted both in olivine and in quartz. However, as noted by Audetat and Lowenstern (2014) the evidence from natural MI is different, and there are many studies showing that original H_2O contents of melts can be preserved since entrapment. Presenting the first nanoSIMS data on the H_2O content of MI in garnet from migmatites, Bartoli et al. (2014) discussed why these types of MI should not be prone to diffusional re-equilibration as much as those in volcanic environments because of: i) the lower temperatures resulting in up to 5–7 orders of magnitude slower H_2 diffusivities, ii) the lack of driving force for pressure diffusion, due to the lack of significant pressure gradients between external matrix and inclusion, and iii) the often larger size of peritectic hosts in migmatites and granulites, implying longer diffusion distances (a few mm to several cm) between mineral boundaries and MI. Because of these large differences in physical parameters, Bartoli et al. (2014) estimated that the times for H_2 equilibration by diffusion in MI from anatectic terranes would be >10 order of magnitude greater than in magmatic systems.

Diffusional exchange also involves cations, as recognized by Clemens (2009) who pointed out that the biotite from the *nanogranite* inclusions in the UHT granulites of the Kerala Khondalite Belt is extremely magnesian ($X_{Mg} = 0.8$, Cesare et al., 2009a), unlike any mica in felsic igneous rocks. Such composition is most likely the product of retrograde Fe–Mg exchange with garnet ("ReERs" of Kohn and Spear, 2000) during cooling of the rock after crystallization of the MI. The small size of biotite and the large volume of host garnet constitute the most favorable conditions for retrograde exchange to proceed extensively. For the same reasons, it is expected that during experimental heating for MI rehomogenization, the reversal of such retrograde Fe–Mg exchange will readily establish the original Fe-richer biotite composition, and that if the melting temperature is close to that of trapping, the Fe and Mg contents of the melt so obtained will be close to the primary values (Clemens, 2009). Similar arguments can be proposed for other diffusion exchanges between other minerals (or the glass) and the host phase.

In summary, although compared with fluid inclusions MI are more dynamic and active systems where various post-entrapment processes may induce chemical and volumetric changes, they can nonetheless represent reliable recorders of the chemical composition of melt at trapping conditions when they meet the three "Roedder's Rules" in the way discussed by Bodnar and Student (2006): if the MI homogenize – completely and without interaction with the host – in a narrow temperature interval, and if the remelted composition is homogeneous, then one can be reasonably certain that MI record the original formation conditions. The case studies described here, coming from different migmatite/granulite terrains from different P–T conditions, show that these conditions can be and have been met, and that with a careful preliminary selection of the samples containing MI to be rehomogenized,

the chemical data on anatectic melts so obtained are as reliable as those gained from glasses in partial melting experiments.

9.4. Are MI compositions representative of the bulk melt in the rock?

Once it has been shown that the composition of MI can be reliably analyzed to provide primary anatectic melt compositions, the final point that deserves discussion is whether these compositions reflect those of the bulk melt present in the host rock at the time of entrapment. Alternative possibilities are that MI compositions reflect local melts, such as boundary layers formed adjacent to growing crystals (e.g., Baker, 2008) or transient, locally controlled disequilibrium melt compositions (Clemens, 2009). These alternatives deal with two issues: the extent of equilibrium between melt and adjacent mineral(s); and local compositional heterogeneities, dictated by the adjacent growing peritectic mineral – boundary layers – or by the nearby reactants contributing to the melt.

Concerning compositional heterogeneities locally controlled by the mineral phases occurring in the microdomain, often observed in experimental runs, these do not seem to have an important role on the major element compositions of MI. This conclusion is supported by the studies of Acosta-Vigil et al. (2007) and Bartoli et al. (2013b) on MI from the enclaves of El Hoyazo and the migmatites of Ronda, respectively. In both cases, a large number of datapoints was collected from MI in garnet, plagioclase, cordierite and ilmenite (Table 2), from different host crystals found in several thin sections from several enclaves, or separated by crushing a dm-sized rock sample of migmatite. The low standard deviations of average analyses result in absolute uncertainties of calculated normative Qz, Ab and Or ≤ 3% (Bartoli et al., 2013b) and indicate that over distances of at least several cm the major element composition of MI is homogeneous, without evidence of local control. On the other hand, microdomain-controlled conditions of mosaic equilibrium have been proposed to explain heterogeneities of H_2O in the MI from Ronda, where MI hosted in different garnet crystals show different average H_2O contents (Bartoli et al., 2014). Therefore, if a local control on MI composition exists, based on available data it appears to affect only the fluid content of the melt.

Concerning boundary layers, which may develop adjacent to crystals, especially when their growth is fast (see Baker, 2008; and Kent, 2008, for a review) the main open question is the relevance of the phenomenon to MI found in nature (Audétat and Lowenstern, 2014), as experiments have provided controversial indications. The evidence from natural MI in igneous rocks suggests that boundary-layer phenomena may be relevant only for small MI (<15 μm, Kuzmin and Sobolev, 2004), or in the presence of sieve or spongy microstructures.

The role of boundary layers for MI in anatectic rocks has been evaluated by Acosta-Vigil et al. (2010, 2012a) for the case study of El Hoyazo. Regarding major elements, mass balances show that boundary layer phenomena are not controlling the differences in composition among MI in the several minerals and matrix glasses. Regarding the trace elements, boundary layer phenomena are negligible for the incompatible elements, as MI in plagioclase and garnet show remarkably similar concentrations, e.g., for Li, Rb, Cs, B, Be, Zn, As, Zr, Th, and U. Considering that these analyses come from several plagioclase and garnet crystals distributed on several thin sections of different Grt–Bt–Sil enclaves, this points to a melt reservoir with a well-defined geochemical character, and indicates that MI composition is broadly representative of the bulk melt in the system at the time of entrapment (Acosta-Vigil et al., 2010). Conversely, the trace elements compatible or very slightly incompatible in the host are strongly depleted in the MI, e.g., Sr, Ba and Eu in MI within Pl, and Y and the heavy REE in MI within garnet. This indicates that the concentrations of these elements have been modified by interaction with the host (Acosta-Vigil et al., 2010). Acosta-Vigil et al. (2012a) concluded, first, that concentrations of incompatible elements in the MI were produced during entrapment and, second, that they are due to disequilibrium distribution during rapid mineral growth, rather than to equilibrium growth during generation of boundary layers.

Most of the contributions on the extent of equilibrium during crustal anatexis relate to trace element partitioning and the current view seems to favor disequilibrium melting as the most common scenario (e.g., Bea, 1996). However, the first detailed study of this issue using MI from the anatectic enclaves of El Hoyazo, shows that melt equilibrated with its residue during anatexis, except for the incompatible elements in melts at the contact with the growing peritectic host (for a detailed discussion, see Acosta-Vigil et al., 2012a).

Having concluded that MI are in general neither local nor disequilibrium features, can these tiny objects tell us anything about crustal magmas and S-type granites? It is well known that after their production, anatectic melts commonly undergo a prolonged and complex series of processes ending with the crystallization of a leucosome or a granitic intrusion (e.g., Brown, 2013). Physically, these processes involve melt segregation and collection, extraction (or injection), transport and emplacement into upper crustal levels. These processes are accompanied by other chemical phenomena, such as homogenization of the melts produced within a single rock source, mixing of magmas from compositionally different rock sources, entrainment of peritectic or residual material, fractional crystallization, melt loss and melt-residue interaction upon cooling. Collectively, these processes result in final products – granites and leucosomes in migmatites – that depart markedly from the original anatectic melts as they were produced at the source (e.g. Chappell et al., 1987; Clemens and Stevens, 2012; Sawyer, 1996, 2008; Stevens et al., 2007; Taylor et al., 2014).

In this scenario, MI appear to be the only tool by which one can trace at the source region the compositions of the melt. Potentially, for example, MI in peritectic garnet (e.g., Ferrero et al., 2014) or in ilmenite (e.g., Acosta-Vigil et al., 2007) entrained in granites (Stevens et al., 2007) can provide the original composition of the anatectic melt, and can help to constrain the chemical evolution that modifies magmas after their production.

Likewise, MI are probably the only way to solve the controversy about the fluid-absent vs. water-fluxed nature of melting (Clemens and Stevens, 2015 vs. Weinberg and Hasalová, 2015) in a specified migmatite outcrop, as they are the only method to obtain in situ, with the cautions discussed by Bartoli et al. (2014) and in this paper, the precise H_2O content of the anatectic melt.

10. Perspectives

Since their first detailed microstructural and compositional description in regionally metamorphosed migmatites and granulites, in 2009, MI have become a matter of considerable scientific interest and will likely become a routine object of study in crustal petrology. Most MI have been found in terranes already intensively studied in the past decades, indicating that anatectic MI have been overlooked until now because they simply were not searched for. Moreover, the growing list (Table 1) of high-grade metamorphic basements containing MI indicates that they are more common than expected, opening the possibility to perform a detailed geochemical characterization of natural anatectic melts from different geodynamic settings. Since the preservation of MI depends on several factors (e.g., host microfracturing, percolation of fluids, retrograde reactions consuming host phase; see Section 9.3), MI should be targeted in the most chemically inert and mechanically strong mineral hosts (e.g., garnet, ilmenite, rutile, spinel, zircon) from the least deformed rock domains.

Although anatectic MI in migmatites and granulites have already provided new and significant advances in our understanding of crustal anatexis (Section 8), MI studies in the near future will impact deeply on our views of the differentiation of the silicate Earth.

One topic of application will be granite petrogenesis. There are conflicting views about whether granites, in particular the I-type granites which are the most abundant ones, image heterogeneous crustal

sources or result from the combination of crustal and mantle inputs (Castro, 2008; Clemens et al., 2011; Kemp, 2007, 2009). So far this dispute has been tackled by means of whole rock geochemistry and Hf–O isotope composition of zircons (Brown, 2013). Because anatectic MI seem to be valuable strongboxes where the pristine geochemical signatures of granitoid melts can be recorded and preserved, the geochemical (trace elements and in particular isotopes) characterization of these embryos of granite, produced from different crustal sources and at different tectonic settings, will lead in the next decade to significant advances in our understanding of granite petrogenesis.

Another topic will be the formation and differentiation of the early continental crust. The oldest continental crust is mainly composed of granitoid rocks known as tonalite–trondhjemite–granodiorite (TTG; e.g., Moyen and Martin, 2012), which are generally believed to have formed by partial melting of a basaltic crust (Moyen, 2011). However, the nature of the mafic source rocks (amphibolites vs. eclogites) and the tectonic environment in which their melting occurred still remain controversial (Arndt, 2013; Foley et al., 2002; Moyen, 2011; Polat, 2012; Rapp et al., 2003). These uncertainties renew the debate about when Earth adopted a plate tectonics mode of behavior (Arndt, 2013; Bedard, 2006; Kerrich and Polat, 2006). The finding and study of MI in Archean anatectic rocks will be central to comprehend better the formation and reworking of the continental crust (in terms of nature of source regions, melting reactions, fluid regimes and P–T conditions of melting) in the early Earth, with broad implications for the crucial question of when plate tectonics first became active.

A third field will be melting during UHT and UHP metamorphism. The inconsistency among most of the current models on the thermal evolution of orogens, which do not generally predict ultrahigh-temperature (UHT) conditions (>900 °C), and the common presence of UHT rocks in many orogenic belts, raises the need for better information on the prograde history of UHT granulites (Korhonen et al., 2014). The occurrence of MI in key minerals of UHT rocks such as sapphirine, and their detailed characterization (experimental remelting, trace element analysis — including Zr, LREE) will provide alternative thermal constraints for this type of rocks.

The study of UHP metamorphism has considerable interest for understanding how mass transfer and element recycling operates in the deepest part of the orogens (Hermann et al., 2013). As deeply subducted rocks often reach temperatures compatible with partial melting reactions (Hermann et al., 2013), and as the melt-fluid phase boundary gradually disappears between 25 and 35 kbar (Hermann et al., 2006), the investigation of melting in HP/UHP rocks through *nanogranites* studies inevitably blends with that of the fluids released during deep subduction (see recent review by Frezzotti and Ferrando, 2015). By increasing the studies of MI from HP to UHP rocks, this fruitful contamination between fields will provide a comprehensive view of the melting processes at different levels in the subducting slab, clarifying the nature and timing of the melting reactions, and the evolution of melt composition during orogenesis, which influences the chemical differentiation of the continental crust.

11. Concluding remarks

MI do represent an equivalent of the “Rosetta Stone” (Clemens, 2009) unlocking the secrets of anatexis of migmatites and granulites. Being written in small print, this message has been just overlooked for too long. However, we have shown here that a good optical microscope and well-prepared thin sections are all one needs to make the preliminary, essential observations that allow to decide if MI are present and suitable for a subsequent, detailed study.

A thorough characterization of anatectic melts preserved in MI requires a time-consuming preparation and use of cutting-edge techniques in addition to more routine ones, but the results so obtained are very satisfactory and open new perspectives in crustal petrology.

The small-size of MI and of daughter minerals crystallized in them still poses some limitations to a full and fast chemical analysis of these objects. However, in a few years from now, the rapid improvement of analytical techniques will have overcome these problems: it is time to go back to your thin sections of migmatites and granulites, and take another look with a different perspective!

Supplementary data to this article can be found online at http://dx.doi.org/10.1016/j.lithos.2015.09.028.

Acknowledgments

Many thanks to Dave Pattison and Maria Luce Frezzotti for their reviews of the manuscript. We are grateful to D. Baker, B. Bodnar, M. Brown, M.L. Frezzotti, M.T. Gomez-Pugnaire, L. Hollister, H. Marschall, J-F. Moyen, S. Poli, E. Salvioli-Mariani, F.P. Sassi, E. Sawyer, C. Szabo, J. Touret, G. Venturelli, R.H. Vernon, D. Vielzeuf, for discussion, advice and support on various aspects of our research, and to Lithos Editors for soliciting this contribution.

This research benefitted from funding from the Italian Ministry of Education, University, Research (grant PRIN 2010TT22SC to BC; Progetto SIR RBSI14Y7PF to OB), from Padova University (Piscopia — Marie Curie Fellowship GA No. 600376 to AAV, Progetti per Giovani Studiosi 2013 to OB, Progetto di Ateneo CPDA107188/10 to BC), from the Ministerio de Ciencia e Innovación of Spain (grant CGL2007-62992 to AAV), and from the Alexander von Humboldt Foundation, the German Federal Ministry for Education and Research and the Deutsche Forschungsgemeinschaft (Project FE 1527/2-1 to SF). The research leading to these results has received funding from the European Commission, Seventh Framework Programme, under Grant Agreement n° 600376.

References

Acosta, A., 1998. Estudio de los fenómenos de fusión cortical y generación de granitoides asociados a las peridotitas de Ronda. Unpublished PhD Thesis, Universidad de Granada, p. 305.

Acosta-Vigil., A., Barich, A., Bartoli, O., Garrido, C.J., Cesare, B., Remusat, L., Poli, S., Raepsaet, C. (under review) The composition of nanogranitoids in migmatites overlying the Ronda peridotites (Betic Cordillera, S Spain): the anatectic history of a polymetamorphic basement. Contributions to Mineralogy and Petrology, under review.

Acosta-Vigil, A., Buick, I., Cesare, B., London, D., Morgan VI, G.B., 2012a. The extent of equilibration between melt and residuum during regional anatexis and its implications for differentiation of the continental crust: a study of partially melted metapelitic enclaves. Journal of Petrology 53, 1319–1356.

Acosta-Vigil, A., Buick, I., Hermann, J., Cesare, B., Rubatto, D., London, D., Morgan VI, G.B., 2010. Mechanisms of crustal anatexis: a geochemical study of partially melted metapelitic enclaves and host dacite, SE Spain. Journal of Petrology 51, 785–821.

Acosta-Vigil, A., Cesare, B., London, D., Morgan VI, G.B., 2007. Microstructures and composition of melt inclusions in a crustal anatectic environment, represented by metapelitic enclaves within El Hoyazo dacites, SE Spain. Chemical Geology 235, 450–465.

Acosta-Vigil, A., London, D., Morgan VI, G.B., 2006a. Experiments on the kinetics of partial melting of a leucogranite at 200 MPa H_2O and 690–800 °C: compositional variability of melts during the onset of H_2O-saturated crustal anatexis. Contributions to Mineralogy and Petrology 151, 539–557.

Acosta-Vigil, A., London, D., Morgan VI, G.B., 2012b. Chemical diffusion of major and minor components in granitic liquids: implications for the rates of homogenization of crustal melts. Lithos 153, 308–323.

Acosta-Vigil, A., London, D., Morgan VI, G.B., Dewers, T.A., 2003. Solubility of excess alumina in hydrous granitic melts in equilibrium with peraluminous minerals at 700–800 °C and 200 MPa, and applications of the aluminum saturation index. Contributions to Mineralogy and Petrology 146, 100–119.

Acosta-Vigil, A., London, D., Morgan VI, G.B., Dewers, T.A., 2006b. Dissolution of quartz, albite, and orthoclase in H_2O-saturated haplogranitic melts at 800 °C and 200 MPa: diffusive transport properties of granitic melts at crustal anatectic conditions. Journal of Petrology 47, 231–254.

Acosta-Vigil, A., Rubatto, D., Bartoli, O., Cesare, B., Meli, S., Pedrera, A., Azor, A., Tajčmanová, L., 2014. Age of anatexis in the crustal footwall of the Ronda peridotites, S Spain. Lithos 210–211, 147–167.

Albuquerque, C.A.R., 1971. Petrochemistry of a series of granitic rocks from northern Portugal. Bulletin of the Geological Society of America 82, 2783–2798.

Álvarez-Valero, A.M., Cesare, B., Kriegsman, L.M., 2005. Formation of elliptical garnets in a metapelitic enclave by melt-assisted dissolution and reprecipitation. Journal of Metamorphic Geology 23, 65–74.

Álvarez-Valero, A.M., Cesare, B., Kriegsman, L.M., 2007. Formation of spinel–cordierite–feldspar–glass coronas after garnet in metapelitic xenoliths: reaction modelling and geodynamic implications. Journal of Metamorphic Geology 25, 305–320.
Álvarez-Valero, A.M., Jagoutz, O., Stanley, J., Manthei, C., El Maz, A., Moukadri, A., Piasecki, A., 2014. Crustal attenuation as a tracer for the emplacement of the beni Boussera ultramafic massif (Betico-Rifean Belt). Geological Society of America Bulletin 126, 1614–1624.
Álvarez-Valero, A.M., Kriegsman, L.M., 2008. Partial crustal melting beneath the Betic Cordillera (SE Spain): the case study of Mar Menor volcanic suite. Lithos 101, 379–396.
Álvarez-Valero, A.M., Kriegsman, L.M., 2010. Chemical, petrological and mass balance constraints on the textural evolution of pelitic enclaves. Lithos 116, 300–309.
Anderson, A.T., Davis, A.M., Lu, F., 2000. Evolution of bishop tuff rhyolitic magma based on melt and magnetite inclusions and zoned phenocrysts. Journal of Petrology 41, 449–473.
Anderson, A.J., McCarron, T., 2011. Three-dimensional textural and chemical characterization of polyphase inclusions in spodumene using a dual focused ion beam–scanning electron microscope (FIB–SEM). The Canadian Mineralogist 49, 541–553.
Arndt, N.T., 2013. Formation and evolution of the continental crust. Geochemical Perspectives 2 (3), 405–533.
Audetat, A., Lowenstern, J.B., 2014. Mel inclusions. In: Holland, H.D., Turekian, K.K. (Eds.), Treatise on Geochemistry, Second edition Elsevier, Oxford, pp. 143–173.
Auzanneau, E., Vielzeuf, D., Schmidt, M.W., 2006. Experimental evidence of decompression melting during exhumation of subducted continental crust. Contributions to Mineralogy and Petrology 152, 125–148.
Axler, J.A., Ague, J.J., 2015. Oriented multiphase needles in garnet from ultrahigh-temperature granulites, Connecticut, U.S.A. American Mineralogist 100, 2254–2271.
Bachmann, O., Wallace, P.J., Bourquin, J., 2010. The melt inclusion record from the rhyolitic Kos Plateau Tuff (Aegean Arc). Contributions to Mineralogy and Petrology 159, 187–202.
Baker, D.R., 2008. The fidelity of melt inclusions as records of melt composition. Contributions to Mineralogy and Petrology 156, 377–395.
Barbero, L., Villaseca, C., 1992. The Layos granite, Hercynian complex of Toledo (Spain): an example of parautochthonous restite-rich granite in a granulitic area. Transactions of the Royal Society of Edinburgh: Earth Sciences 83, 127–138.
Barbero, L., Villaseca, C., Rogers, G., Brown, P.E., 1995. Geochemical and isotopic disequilibrium in crustal melting: an insight from the anatectic granitoids from Toledo, Spain. Journal of Geophysical Research 100, 15745–15765.
Barbey, P., Brouand, M., Le Fort, P., Pêcher, A., 1996. Granite–migmatite genetic link: the example of the Manaslu granite and Tibetan Slab migmatites in central Nepal. Lithos 38, 63–79.
Barbey, P., Macaudiere, J., Nzenti, J.P., 1990. High-pressure dehydration melting of metapelites: evidence from the migmatites of Youndé (Cameroon). Journal of Petrology 31, 401–427.
Barich, A., Acosta-Vigil, A., Garrido, C.J., Cesare, B., Tajčmanová, L., Bartoli, O., 2014. Microstructures and petrology of melt inclusions in the anatectic sequence of Jubrique (Betic Cordillera, S Spain): implications for crustal anatexis. Lithos 206–207, 303–320.
Barker, F., 1979. Trondhjemites: definition, environment and hypotheses of origin. In: Baker, F. (Ed.), Trondhjemites, Dacites and Relatated Rocks. Elsevier, Amsterdam, pp. 1–12.
Barker, F., Arth, J.G., Stern, T.W., 1986. Evolution of the coast batholith along the Skagway Traverse, Alaska and British Columbia. American Mineralogist 71, 632–643.
Bartoli, O., 2012. When the continental crust melts: a combined study of melt inclusions and classical petrology on the Ronda migmatites. Unpublished PhD Thesis, Università degli Studi di Parma, p. 128. [unpublished data].
Bartoli, O., Acosta-Vigil, A., Cesare, B., 2015. High-temperature metamorphism and crustal melting: working with melt inclusions. Periodico di Mineralogia 84. http://dx.doi.org/10.2451/2015PM00xx.
Bartoli, O., Cesare, B., Poli, S., Acosta-Vigil, A., Esposito, R., Turina, A., Bodnar, R.J., Angel, R.J., Hunter, J., 2013a. Nanogranite inclusions in migmatitic garnet: behavior during piston cylinder re-melting experiments. Geofluids 13, 405–420.
Bartoli, O., Cesare, B., Poli, S., Bodnar, R.J., Acosta-Vigil, A., Frezzotti, M.L., Meli, S., 2013b. Recovering the composition of melt and the fluid regime at the onset of crustal anatexis and S-type granite formation. Geology 41, 115–118.
Bartoli, O., Tajčmanová, L., Cesare, B., Acosta-Vigil, A., 2013c. Phase equilibria constraints on melting of stromatic migmatites from Ronda (S. Spain): insights on the formation of peritectic garnet. Journal of Metamorphic Geology 31, 775–789.
Bartoli, O., Cesare, B., Remusat, L., Acosta-Vigil, A., Poli, S., 2014. The H_2O content of granite embryos. Earth and Planetary Science Letters 395, 281–290.
Baxter, E.F., Caddick, M.J., Ague, J.J., 2013. Garnet: common mineral, uncommonly useful. Elements 9, 415–419.
Bea, F., 1996. Controls on the trace element composition of crustal melts. Transactions of the Royal Society of Edinburgh: Earth Sciences 87, 33–41.
Bea, F., Montero, P., 1999. Behavior of accessory phases and redistribution of Zr, REE, Y, Th, and U during metamorphism and partial melting of metapelites in the lower crust: an example from the Kinzigite Formation of Ivrea-Verbano, NW Italy. Geochimica et Cosmochimica Acta 63, 1133–1153.
Bea, F., Pereira, M.D., Stroh, A., 1994. Mineral/leucosome trace-element partitioning in a peraluminous migmatite (a laser ablation-ICP–MS study). Chemical Geology 117, 291–312.
Bédard, J., 2006. A catalytic delamination-driven model for coupled genesis of Archaean crust and subcontinental lithospheric mantle. Geochimica et Cosmochimica Acta 70, 1188–1214.
Behrens, H., Roux, J., Neuville, D.R., Siemann, M., 2006. Quantification of dissolved H_2O in silicate glasses using confocal microRaman spectroscopy. Chemical Geology 229, 96–112.
Bento dos Santos, T.M., Munhá, J.M.U., Tassinari, C.C.G., Noronha, F.M., Guedes, A., Fonseca, P.E., Dias Neto, C., Doria, A., 2011. P–T-Fluid evolution and graphite deposition during retrograde metamorphism in Ribeira Fold Belt, SE Brazil: oxygen fugacity, fluid inclusions and CeOeH isotopic evidence. Journal of South American Earth Sciences 31, 93–109.
Bodnar, R.J., Student, J.J., 2006. Melt Inclusions in Plutonic Rocks: Petrography and Microthermometry. In: Webster, J.D. (Ed.), Melt inclusions in Plutonic Rocks. Mineralogical Association of Canada Short Course 36, pp. 1–26.
Bose, K., Ganguly, J., 1995. Quartz–coesite transition revisited: reversed experimental determination at 500–1200 °C and retrieved thermochemical properties. American Mineralogist 80, 231–238.
Braun, I., Raith, M., Ravindra Kumar, G.R., 1996. Dehydration–melting phenomena in leptynitic gneisses and the generation of leucogranites: a case study from the Kerala Khondalite Belt, southern India. Journal of Petrology 37, 1285–1305.
Brown, M., 2013. Granite: from genesis to emplacement. Geological Society of America Bulletin 125, 1079–1113.
Carosi, R., Montomoli, C., Langone, A., Turina, A., Cesare, B., Iaccarino, S., Fascioli, L., Visonà, D., Ronchi, A., Man Rai, S., 2015. Eocene partial melting recorded in peritectic garnets from kyanite-gneiss, Greater Himalayan Sequence, central Nepal. In: Mukherjee, S., Carosi, R., van der Beek, P.A., Mukherjee, B.K., Robinson, D.M. (Eds.), Tectonics of the Himalaya. Geological Society, London, Special Publications 412, pp. 111–129.
Castro, A., 2008. The off-crust origin of granite batholiths. Geoscience Frontiers 5, 63–75.
Cesare, B., 1999. Multi-stage pseudomorphic replacement of garnet during polymetamorphism: 1 micro-structures and their interpretation. Journal of Metamorphic Geology 17, 723–734.
Cesare, B., 2008. Crustal melting: working with enclaves. In: Sawyer, E.W., Brown, M. (Eds.), Working with Migmatites, Short Course 38. Mineralogical Association of Canada, Quebec City, pp. 37–55.
Cesare, B., Acosta-Vigil, A., 2011. Using melt inclusions for understanding crustal melting processes. McGraw-Hill Yearbook of Science & Technology 355–359.
Cesare, B., Acosta-Vigil, A., Ferrero, S., Bartoli, O., 2011. Melt Inclusions in Migmatites and Granulites paper 2 In: Forster, M.A., Fitz Gerald, J.D. (Eds.), The Science of Microstructure — Part II, Electronic edition. Journal of the Virtual Explorer 38 (paper 2).
Cesare, B., Ferrero, S., Salvioli-Mariani, E., Pedron, D., Cavallo, A., 2009a. Nanogranite and glassy inclusions: the anatectic melt in migmatites and granulites. Geology 37, 627–630.
Cesare, B., Gómez-Pugnaire, M.T., 2001. Crustal melting in the Alboran domain: constraints from the xenoliths of the Neogene Volcanic Province. Physics and Chemistry of the Earth, Part A 26, 255–260.
Cesare, B., Gómez-Pugnaire, M.T., Rubatto, D., 2003a. Residence time of S-type anatectic magmas beneath the Neogene Volcanic Province of SE Spain: a zircon and monazite SHRIMP study. Contributions to Mineralogy and Petrology 146, 28–43.
Cesare, B., Maineri, C., 1999. Fluid-present anatexis of metapelites at El Joyazo (SE Spain): constraints from Raman spectroscopy of graphite. Contributions to Mineralogy and Petrology 135, 41–52.
Cesare, B., Maineri, C., Baron Toaldo, A., Pedron, D., Acosta-Vigil, A., 2007. Immiscibility between carbonic fluids and granitic melts during crustal anatexis: a fluid and melt inclusion study in the enclaves of the Neogene Volcanic Province of SE Spain. Chemical Geology 237, 433–449.
Cesare, B., Marchesi, C., Hermann, J., Gomez-Pugnaire, M.T., 2003b. Primary melt inclusions in andalusite from anatectic graphitic metapelites: implications for the position of the Al_2SiO_5 triple point. Geology 31, 573–576.
Cesare, B., Mazzoli, C., Raffaele, S., Spiess, R., Sassi, F.P., 2010. Beauty and complexity of metamorphism: case studies from the frontal part of the Adria microplate. Rendiconti Lincei 21, S73–S94.
Cesare, B., Meli, S., Nodari, L., Russo, U., 2005. Fe^{3+} reduction during biotite melting in graphitic metapelites: another origin of CO_2 in granulites. Contributions to Mineralogy and Petrology 149, 129–140.
Cesare, B., Salvioli Mariani, E., Venturelli, G., 1997. Crustal anatexis and melt extraction during deformation in the restitic xenoliths at El Joyazo (SE Spain). Mineralogical Magazine 61, 15–27.
Cesare, B., Rubatto, D., Gómez-Pugnaire, M.T., 2009b. Do extrusion ages reflect magma generation processes at depth? An example from SE Spain. Contributions to Mineralogy and Petrology 157, 267–279.
Chabiron, A., Pironon, J., Massare, D., 2004. Characterization of H_2O in synthetic rhyolitic glasses and natural melt inclusions by Raman spectroscopy. Contributions to Mineralogy and Petrology 146, 485–492.
Chappell, B.W., White, A.J.R., 1992. I- and S-type granites in the Lachlan Fold Belt. Transactions of the Royal Society of Edinburgh: Earth Sciences 83, 1–26.
Chappell, B.W., White, A.J.R., Wyborn, D., 1987. The importance of residual source material (restite) in granite petrogenesis. Journal of Petrology 28, 1111–1138.
Charoy, B., 1986. The genesis of the Cornubian batholith (South-West England): the example of the Carnmenellis pluton. Journal of Petrology 27, 571–604.
Chen, R.-X., Ding, B., Zheng, Y.-F., Hu, Z., 2015. Multiple episodes of anatexis in a collisional orogen: zircon evidence from migmatite in the Dabie orogeny. Lithos 212–215, 247–265.
Chen, Y.-X., Zheng, Y.-F., Gao, X.-Y., Hu, Z.C., 2014. Multiphase solid inclusions in zoisite-bearing eclogite: evidence for partial melting of ultrahigh-pressure metamorphic rocks during continental collision. Lithos 200–201, 1–21.
Chen, Y.-X., Zheng, Y.-F., Hu, Z., 2013. Petrological and zircon evidence for anatexis of UHP quartzite during continental collision in the Sulu orogen. Journal of Metamorphic Geology 31, 389–413.
Chupin, S.V., Chupin, V.P., Barton, J.M., Barton, E.S., 1998. Archean melt inclusions in zircon from quartzite and granitic orthogneiss from South Africa: magma compositions and probable sources of protoliths. European Journal of Mineralogy 10-6, 1241–1251.
Chupin, V.P., Kosukhin, O.N., 1982. Diagnostics and methods for studying melt inclusions in minerals of granitoids and pegmatites. Soviet Geology and Geophysics 23, 56–61.
Chupin, V.P., Kuzmin, D.V., Madyukov, I.A., 2006a. Melt inclusions in minerals of scapolite-bearing granulite (lower crustal xenoliths from diatremes of the Pamirs). Doklady Earth Sciences 407A (3), 507–511 (2006).

Chupin, V.P., Vetrin, V.R., Rodionov, N.V., Matukov, D.I., Berezhnaya, N.G., Sergeev, S.A., Mitrofanov, F.P., Smirnov, Yu.P., 2006b. Composition of melt inclusions and age of zircons from plagiogneisses of the archean complex penetrated by the Kola superdeep borehole (Baltic Shield). Doklady Akademii Nauk - Rossijskaya Akademiya Nauk 406 (4), 533–537.
Chupin, V.P., Kuzmin, D.V., Touret, J.L.R., 2001. High-pressure melt and fluid inclusions in minerals of garnet granulites/eclogites (eastern Pamir). In: Noronha, F., Dória, A., Guedes, A. (Eds.), Abstracts of ECROFI XVI (European Current Research on Fluid Inclusions), Porto 2001. Universidade do Porto, Faculdade de Ciências, Departamento de Geologia, Memória 7, pp. 95–98.
Chupin, V.P., Kuzmin, D.V., Madyukov, I.A., Rodionov, N.V., Lutkov, V.S., Touret, J.L.R., 2010. High-pressure magmatic inclusions in zircon and rock-forminh minerals of granulites/eclogites (xenoliths from diatremes of the Pamir). In: Sharygin, V.V. (Ed.), Abstracts vol. of ACROFI III & TBG XIV, Novosibirsk, 15–20 September, 2010. Publishing House of SB RAS, RAS SB, IGM, Novosibirsk, pp. 46–47 (2010).
Chupin, V.P., Tomilenko, A.A., Chupin, S.V., 1993. Origin of granulite complexes: results of study of melt and fluid inclusions in zircon and rock-forming minerals. Russian Geology and Geophysics 12, 103–116.
Clarke, D.B., et al., 2005. Occurrence and origin of andalusite in peraluminous felsic igneous rocks. Journal of Petrology 46, 441–472.
Clemens, J.D., 2009. The message in the bottle: "melt" inclusions in migmatitic garnets. Geology 37, 671–672.
Clemens, J.D., Stevens, G., 2012. What controls chemical variation in granitic magmas? Lithos 134–135, 317–329.
Clemens, J.D., Stevens, G., 2015. Comment on "Water-fluxed melting of the continental crust: A review" by R.F. Weinbert and P. Hasalová. Lithos 234–235, 100–101.
Clemens, J.D., Stevens, G., Farina, F., 2011. The enigmatic sources of I-type granites: the peritectic connexion. Lithos 126, 174–181.
Clemens, J.D., Watkins, J.M., 2001. The fluid regime of high-temperature metamorphism during granitoid magma genesis. Contributions to Mineralogy and Petrology 140, 600–606.
Clocchiatti, R., 1975. Les inclusions vitreuses des cristaux de quartz. Étude optique, thermooptique et chimique. Applications géologiques, Mémoires de la Société géologique de France 122, 1–96.
Collins, W.J., Flood, R.H., Vernon, R.H., Shaw, S.E., 1989. The Wuluma granite, Arunta Block, central Australia: an example of in situ, near-isochemical granite formation in a granulite facies terrane. Lithos 23, 63–83.
Currie, K.L., Paraji, G.E., 1981. Anatectic peraluminous granites from the Carmanville area, northeastern Newfoundland. Canadian Mineralogist 19, 147–162.
Danyushevsky, L.V., Della-Pasqua, F.N., Sokolov, S., 2000. Re-equilibration of melt inclusions trapped by magnesian olivine phenocrysts from subduction-related magmas: petrological implications. Contributions to Mineralogy and Petrology 138, 68–83.
Danyushevsky, L.V., McNeill, A.W., Sobolev, A.V., 2002. Experimental and petrological studies of melt inclusions in phenocrysts from mantle-derived magmas: an overview of techniques, advantages and complications. Chemical Geology 183, 5–24.
Darling, R.S., 2013. Zircon-bearing, crystallized melt inclusions in peritectic garnet from the western Adirondack Mounatins, New York State, USA. Geofluids 13, 453–459.
Darling, R.S., Chou, I.M., Bodnar, R.J., 1997. An occurrence of metastable cristobalite in high-pressure garnet granulite. Science 276, 91.
Day, W.C., Weiblen, P.W., 1986. Origin of Late Archaean granite: geochemical evidence from the Vermilion Granite Complex of northern Minnesota. Contributions to Mineralogy and Petrology 93, 283–296.
Di Martino, C., Forni, F., Frezzotti, M.L., Palmeri, R., Webster, J.D., Ayuso, R.A., Lucchi, F., Tranne, C.A., 2011. Formation of cordierite-bearing lavas during anatexis in the lower crust beneath Lipari Island (Aeolian arc, Italy). Contributions to Mineralogy and Petrology 161, 1011–1030.
Dolgov, Yu.A., Tomilenko, A.A., Chupin, V.P., 1984. Conditions of anatexis and metamorphism (according to the data on inclusions in minerals). Soviet Geology and Geophysics 25-8, 82–88.
Esposito, E., Klebesz, R., Bartoli, O., Klyukin, Y.I., Moncada, D., Doherty, A., Bodnar, R.J., 2012. Application of the Linkam TS1400XY heating stage to melt inclusion studies. Central European Journal of Geosciences 4 (2), 208–218.
Ferrando, S., Frezzotti, M.L., Dallai, L., Compagnoni, R., 2005. Remnants of supercritical silicate-rich aqueous fluids released during continental subduction. Chemical Geology 223, 68–81.
Ferrero, S., Bartoli, O., Cesare, B., Salvioli-Mariani, E., Acosta-Vigil, A., Cavallo, A., Groppo, C., Battiston, S., 2012. Microstructures of melt inclusions in anatectic metasedimentary rocks. Journal of Metamorphic Geology 30, 303–322.
Ferrero, S., Bodnar, R.J., Cesare, B., Viti, C., 2011. Reequilibration of primary fluid inclusions in peritectic garnet from metapelitic enclaves, El Hoyazo, Spain. Lithos 124, 117–131.
Ferrero, S., Braga, R., Berkesi, M., Cesare, B., Laridhi Ouazaa, N., 2014. Production of metaluminous melt during fluid-present anatexis: an example from the Maghrebian basement, La Galite Archipelago, central Mediterranean. Journal of Metamorphic Geology 32, 209–225.
Ferrero, S., Wunder, B., Walczak, K., O'Brien, P.J., Ziemann, M.A., 2015. Preserved near ultrahigh-pressure melt from continental crust subducted to mantle depths. Geology 43, 447–450.
Foley, S.F., Tiepolo, M., Vannucci, R., 2002. Growth of early continental crust controlled by melting of amphibolite in subduction zones. Nature 417, 637–640.
Frezzotti, M.L., 2001. Silicate melt inclusions in magmatic rocks: applications to petrology. Lithos 55, 273–299.
Frezzotti, M.L., Ferrando, S., 2015. The chemical behavior of fluids released during deep subduction based on fluid inclusions. American Mineralogist 100, 352–377.
Frezzotti, M.L., Peccerillo, A., Zanon, V., Nikogosian, I., 2004. Silica-rich melts in quartz xenoliths from Vulcano Island and their bearing on processes of crustal anatexis and crust–magma interaction beneath the Aeolian Arc, Southern Italy. Journal of Petrology 45, 3–26.
Gaetani, G.A., O'Leary, J.A., Shimizu, N., Bucholz, C.E., Newville, M., 2012. Rapid reequilibration of H_2O and oxygen fugacity in olivine-hosted melt inclusions. Geology 40, 915–918.
Ganzhorn, A.C., Labrousse, L., Prouteau, G., Leroy, C., Vrijmoed, J.C., Andersen, T.B., Arbaret, L., 2014. Structural, petrological and chemical analysis of syn-kinematic migmatites: insights from the Western Gneiss Region, Norway. Journal of Metamorphic Geology 32, 647–673.
Gao, X.Y., Zheng, Y.F., Chen, Y.X., 2012. Dehydration melting of ultrahigh-pressure eclogite in the Dabie orogen: evidence from multiphase solid inclusions in garnet. Journal of Metamorphic Geology 30, 193–212.
Gao, X.-Y., Zheng, Y.-F., Chen, Y.-X., Hu, Z., 2013. Trace element composition of continentally subducted slab-derived melt: insight from multiphase solid inclusions in ultrahigh-pressure eclogite in the Dabie orogen. Journal of Metamorphic Geology 31, 453–468.
Gao, X.-Y., Zheng, Y.-F., Chen, Y.-X., Hu, Z., 2014. Composite carbonate and silicate multiphase solid inclusions in metamorphic garnet from ultrahigh-P eclogite in the Dabie orogeny. Journal of Metamorphic Geology 32, 961–980.
García-Casco, A., Haissen, F., Castro, A., El-Hmidi, H., Torres-Roldán, R.L., Millán, G., 2003. Synthesis of staurolite in melting experiments of a natural metapelite: consequences for phase relations in low-temperature pelitic migmatites. Journal of Petrology 44, 1727–1757.
Gardien, V., Thompson, A.B., Grujic, D., Ulmer, P., 1995. Experimental melting of biotite + plagioclase + quartz ± muscovite assemblages and implications for crustal melting. Journal of Geophysical Research 100, 15581–15591.
Gardien, V., Thompson, A.B., Ulmer, P., 2000. Melting of biotite + plagioclase + quartz gneisses: the role of H_2O in the stability of amphibole. Journal of Petrology 41, 651–666.
Georgieva, M., Mogessie, A., Cherneva, Z., 2005. Mineral needles and melt inclusions in garnet from the Chepelare Area, central Rhodope, Bulgaria. Mitteilungen der Österreichische Mineralogische Gesellschaft 150.
Groppo, C., Rolfo, F., Indares, A., 2012. Partial melting in the Higher Himalaya Crystallines of eastern Nepal: the effect of decompression and implications for the "Channel Flow" model. Journal of Petrology 53, 1057–1088.
Guillot, S., Le Fort, P., 1995. Geochemical constraints on the bimodal origin of High Himalayan leucogranites. Lithos 35, 221–234.
Halter, W.E., Pettke, T., Heinrich, C.A., Rothen-Rutishauser, B., 2002. Major to trace element analysis of melt inclusions by laser-ablation ICP–MS: methods of quantification. Chemical Geology 183, 63–86.
Harley, S., Nandakumar, V., 2014. Accessory mineral behaviour in granulite migmatites: a case study from the Kerala Khondalite Belt, India. Journal of Petrology 55, 1965–2002.
Hartel, T.H.D., Pattison, D.R.M., 1996. Genesis of the Kapuskasing (Ontario) migmatitic mafic granulites by dehydration melting of amphibolite: the importance of quartz to reaction progress. Journal of Metamorphic Geology 14, 591–611.
Hartel, T.H.D., Pattison, D.R.M., Helmers, H., Maaskant, P., 1990. Primary granitoid-composition inclusions in garnet from granulite facies metapelite: direct evidence for the presence of a melt? Geological Association of Canada 15, 54 (abstract).
Hauri, E., 2002. SIMS analysis of volatiles in silicate glasses, 2: isotopes and abundances in Hawaiian melt inclusions. Chemical Geology 183, 115–141.
Hermann, J., Rubatto, D., Korsakov, A., Shatsky, V.S., 2001. Multiple zircon growth during fast exhumation of diamondiferous, deeply subducted continental crust (Kokchetav Massif, Kazakhstan). Contributions to Mineralogy and Petrology 141, 66–82.
Hermann, J., Rubatto, D., Trommsdorff, V., 2006. Sub-solidus Oligocene zircon formation in garnet peridotite during fast decompression and fluid infiltration (Duria, Central Alps). Mineralogy and Petrology 88, 181–206.
Hermann, J., Spandler, C., 2008. Sediment melts at sub-arc depths: an experimental study. Journal of Petrology 49, 717–740.
Hermann, J., Zheng, Y.-F., Rubatto, D., 2013. Deep fluids in subducted crust. Elements 9, 281–287.
Hiroi, Y., Yanagi, A., Kato, M., Kobayashi, T., Prame, B., Hokada, T., Satish-Kumar, M., Ishikawa, M., Adachi, T., Osanai, Y., Motoyoshi, Y., Shiraishi, K., 2014. Supercooled melt inclusions in lower-crustal granulites as a consequence of rapid exhumation by channel flow. Gondwana Research 25, 226–234.
Holness, M.B., Cesare, B., Sawyer, E.W., 2011. Melted rocks under the microscope: microstructures and their interpretation. Elements 7, 245–250.
Holness, M.B., Sawyer, E.W., 2008. On the pseudomorphing of melt-filled pores during the crystallization of migmatites. Journal of Petrology 49, 1343–1363.
Holtz, F., Johannes, W., 1991. Genesis of peraluminous granites: I. Experimental investigation of melt compositions at 3 and 5 kb and various H_2O activities. Journal of Petrology 32, 935–958.
Holtz, F., Johannes, W., 1994. Maximum and minimum water contents of granitic melts: implications for chemical and physical properties of ascending magmas. Lithos 32, 149–159.
Holtz, F., Johannes, W., Tamic, N., Behrens, H., 2001. Maximum and minimum water contents of granitic melts generated in the crust: a re-evaluation and implications. Lithos 56, 1–14.
Hwang, S.L., Shen, P., Chu, H.T., Yui, T.F., Lin, C.C., 2001. Genesis of microdiamonds from melt and associated multiphase inclusions in garnet of ultrahigh-pressure gneiss from Erzgebirge, Germany. Earth and Planetary Science Letters 188, 9–15.
Hwang, S.-L., Shen, P., Chu, H.-T., Yui, T.-F., Liou, J.-G., Sobolev, N.V., 2009. Kumdykolite, an orthorhombic polymorph of albite, from the Kokchetav ultrahigh-pressure massif, Kazakhstan. European Journal of Mineralogy 21, 1325–1334.
Hwang, S.L., Shen, P., Chu, H.T., Yui, T.F., Liou, J.G., Sobolev, N.V., Zhang, R.Y., Shatsky, V.S., Zayachkovsky, A.A., 2004. Kokchetavite: a new polymorph of $KAlSi_3O_8$ from the Kokchetav UHP terrain. Contributions to Mineralogy and Petrology 148, 380–389.

Inger, S., Harris, N.B.W., 1992. Geochemical constraints on leucogranite magmatism in the Langtang Valley, Nepal Himalaya. Journal of Petrology 34, 345–368.
Johannes, W., 1989. Melting of plagioclase-quartz assemblages at 2 kbar water pressure. Contributions to Mineralogy and Petrology 103, 270–276.
Johannes, W., Holtz, F., 1992. Melting of plagioclase in granite and related systems: composition of coexisting phases and kinetic observations. Transactions of the Royal Society of Edinburgh: Earth Sciences 83, 417–422.
Kawakami, T., Yamaguchi, I., Miyake, A., Shibata, T., Maki, K., Yokoyama, T.D., Hirata, T., 2013. Behavior of zircon in the upper-amphibolite to granulite facies schist/migmatite transition, Ryoke metamorphic belt, SW Japan: constraints from the melt inclusions in zircon. Contributions to Mineralogy and Petrology 165, 575–591.
Kelsey, D.E., Clark, C., Hand, M., 2008. Thermobarometric modelling of zircon and monazite growth in melt-bearing systems: examples using model metapelitic and metapsammitic granulites. Journal of Metamorphic Geology 26, 199–212.
Kemp, A.I.S., Hawkesworth, C.J., Collins, W.J., Gray, C.M., Blevin, P.L., 2009. Isotopic evidence for rapid continental growth in an extensional accretionary orogen: the Tasmanides, eastern Australia. Earth and Planetary Science Letters 284, 455–466.
Kemp, A.I.S., Hawkesworth, C.J., Foster, G.L., Paterson, B.A., Woodhead, J.D., Hergt, J.M., Gray, C.M., Whitehouse, M.J., 2007. Magmatic and crustal differentiation history of granitic rocks from Hf–O isotopes in zircon. Science 315, 980–983.
Kent, A.J.R., 2008. Melt inclusions in basaltic and related volcanic rocks. In: Putirka, K.D., Tepley, F.J.I. (Eds.), Minerals, Inclusions and Volcanic Processes. Reviews in Mineralogy and Geochemistry 69, pp. 273–331.
Kerrich, R., Polat, A., 2006. Archean greenstone-tonalite duality: thermo-chemical mantle convection models or plate tectonics in the early Earth global dynamics? Tectonophysics 415, 141–165.
Koester, E., Pawley, A.R., Fernandes, L.A.D., Porcher, C.C., Soliani Jr., E., 2002. Experimental melting of cordierite gneiss and the petrogenesis of syntranscurrent peraluminous granites in southern Brazil. Journal of Petrology 43, 1595–1616.
Kohn, M.J., Spear, F., 2000. Retrograde net transfer reaction insurance for pressure–temperature estimates. Geology 28 (12), 1127–1130.
Korhonen, F.J., Clark, C., Brown, M., Taylor, R.J.M., 2014. Taking the temperature of the Earth's hottest crust. Earth and Planetary Science Letters 408, 341–354.
Korsakov, A.V., Hermann, J., 2006. Silicate and carbonate melt inclusions associated with diamonds in deeply subducted carbonate rocks. Earth and Planetary Science Letters 241, 104–118.
Kotkova, J., Škoda, R., Machovič, V., 2014. Kumdykolite from the ultrahigh-pressure granulite of the Bohemian Massif. American Mineralogist 99, 1798–1801.
Kuzmin, D.V., Sobolev, A.V., 2004. Boundary layer contribution to the composition of melt inclusions in olivine. Geochimica et Cosmochimica Acta 68, A544.
Labrousse, L., Prouteau, G., Ganzhorn, A.C., 2011. Continental exhumation triggered by partial melting at ultrahigh pressure. Geology 39, 1171–1174.
Lang, H.M., Gilotti, J.A., 2007. Partial melting of metapelites at ultrahigh-pressure conditions, Greenland Caledonides. Journal of Metamorphic Geology 25, 129–147.
Lavaure, S., Sawyer, E.W., 2011. Source of biotite in the Wuluma pluton: replacement of ferromagnesian phases and disaggregation of enclaves and schlieren. Lithos 125, 757–780.
Le Breton, N., Thompson, A.B., 1988. Fluid-absent (dehydration) melting of biotite in metapelites in the early stages of crustal anatexis. Contributions to Mineralogy and Petrology 99, 226–237.
Le Losq, C., Neuville, D.R., Moretti, R., Roux, J., 2012. Determination of H_2O content in silicate glasses using Raman spectroscopy: implications for the study of explosive volcanism. American Mineralogist 97, 779–790.
Liu, Q., Hermann, J., Zhang, J., 2013. Polyphase inclusions in the Shuanghe UHP eclogites formed by subsolidus transformation and incipient melting during exhumation of deeply subducted crust. Lithos 177, 91–109.
Liu, P., Wu, Y., Liu, Q., Zhang, J., Zhang, L., Jin, Z., 2014. Partial melting of UHP calc-gneiss from the Dabie Mountains. Lithos 192–195, 86–101.
Loomis, T.P., 1972. Contact metamorphism of pelitic rocks by the Ronda ultramafic intrusion, Southern Spain. Geological Society of America Bulletin 83, 2449–2474.
Lowenstern, J.B., 2003. Melt inclusions come of age: volatiles, volcanoes and Sorby's legacy. In: De Vivo, B., Bodnar, R.J. (Eds.), Melt Inclusions in Volcanic Systems. Elsevier, pp. 1–22.
Madyukov, I.A., Chupin, V.P., Kuzmin, D.V., 2011. Genesis of scapolite from granulites (lower-crustal xenoliths from the Pamir diatremes): results of study of melt inclusions. Russian Geology and Geophysics 52, 1319–1333.
Maheshwari, A., Coltorti, M., Sial, A.N., Mariano, G., 1996. Crustal influences in the petrogenesis of the Malani rhyolite, southwestern Rajasthan: combined trace element and oxygen isotope constraints. Journal of the Geological Society of India 47, 611–619.
Malaspina, N., Hermann, J., Scambelluri, M., Compagnoni, R., 2006. Polyphase inclusions in garnet-orthopyroxenite (Dabie Shan, China) as monitors for metasomatism and fluid-related trace element transfer in subduction zone peridotite. Earth and Planetary Science Letters 249, 173–187.
Manley, C.R., 1996. Morphology and maturation of melt inclusions in quartz phenocrysts from the Badlands rhyolite lava flow, southwestern Idaho. American Mineralogist 81, 158–168.
Marchildon, N., Brown, M., 2002. Grain-scale melt distribution in two contact aureole rocks: implications for controls on melt localization and deformation. Journal of Metamorphic Geology 20, 381–396.
Massare, D., Metrichm, N., Clocchiatti, R., 2002. High-temperature experiments on silicate melt inclusions in olivine at 1 atm: inference on temperatures of homogenization and H_2O concentrations. Chemical Geology 183, 87–98.
Massonne, H.J., 2014. Wealth of P–T–t information in medium-high grade metapelites: example from the Jubrique Unit of the Betic Cordillera, S Spain. Lithos 208–209, 137–157.
Moore, L., Gazel, E., Tuohy, R., Lloyd, A., Esposito, R., Steele.MacInnis, M., Hauri, E.H., Wallace, P.J., Plank, T., Bodnar, R.J., 2015. Bubbles matter: an assessment of the contribution of vapor bubbles to melt inclusion volatile budgets. American Mineralogist 100, 806–823.
Montel, J.M., Abdelghaffar, A., 1993. Les granites tardimigmatitiques du Velay (Massif Central francais): principales caractéristiques pétrographiques et géochimiques. Géologie de la France 1, 15–28.
Montel, J.M., Vielzeuf, D., 1997. Partial melting of metagreywackes. Part II. Compositions of minerals and melts. Contributions to Mineralogy and Petrology 128, 176–196.
Morgan VI, G.B., Acosta-Vigil A, London, D., 2008. Diffusive equilibration between hydrous metaluminous–peraluminous haplogranitic liquid couples at 200 MPa (H_2O) and alkali transport in granitic liquids. Contributions to Mineralogy and Petrology 155, 257–269.
Morgan VI, G.B., London, D., 1996. Optimizing the electron microprobe analysis of hydrous alkali aluminosilicate glasses. American Mineralogist 81, 1176–1185.
Morgan VI, G.B., London, D., 2005. Effect of current density on the electron microprobe analysis of alkali aluminosilicate glasses. American Mineralogist 90, 1131–1138.
Mosca, P., Groppo, C., Rolfo, F., 2012. Structural and metamorphic features of the Main Central Trust Zone and its contiguous domains in the eastern Nepalese Himalaya. Electronic editionJournal of Virtual Explorer 41 (paper 2).
Moyen, J.-F., 2011. The composite Archaean grey gneisses: petrological significance, and evidence for a non-unique tectonic setting for Archaean crustal growth. Lithos 123, 21–36.
Moyen, J.-F., Martin, H., 2012. Forty years of TTG research. Lithos 148, 312–336.
Nabelek, P.I., Russ-Nabelek, C., Denison, J.R., 1992. The generation and crystallization conditions of the Proterozoic Harney Peak Leucogranite, Black Hills, South Dakota, USA: petrologic and geochemical constraints. Contributions to Mineralogy and Petrology 110, 173–191.
Nair, R., Chacko, T., 2002. Fluid-absent melting of high-grade semi-pelites: P–T constraints on orthopyroxene formation and implications for granulite genesis. Journal of Petrology 43, 2121–2141.
Ohmoto, H., Kerrick, D.M., 1977. Devolatilization equilibria in graphitic systems. American Journal of Science 277, 1013–1044.
Patiño Douce, A.E., Harris, N., 1998. Experimental constraints on Himalayan anatexis. Journal of Petrology 39, 689–710.
Patiño Douce, A.E., Johnston, A.D., 1991. Phase equilibria and melt productivity in the pelitic system: implications for the origin of peraluminous granitoids and aluminous granulites. Contributions to Mineralogy and Petrology 107, 202–218.
Pattison, D.R.M., Harte, B., 1988. Evolution of structurally contrasting migmatites in the 3-kbar *Ballachulish* aureole, Scotland. Journal of Metamorphic Geology 6, 475–494.
Perchuk, A.L., Burchard, M., Maresch, W.V., Schertl, H.P., 2005. Fluid-mediated modification of garnet interiors under ultrahigh-pressure conditions. Terra Nova 17, 545–553.
Perchuk, A.L., Burchard, M., Maresch, W.V., Schertl, H.P., 2008. Melting of hydrous and carbonate mineral inclusions in garnet host during ultrahigh pressure experiments. Lithos 103, 25–45.
Pickering, J.M., Johnston, D.A., 1998. Fluid-absent melting behaviour of a two mica metapelite: experimental constraints on the origin of Black Hill Granite. Journal of Petrology 39, 1787–1804.
Platt, J.P., Argles, T.W., Carter, A., Kelley, S.P., Whitehouse, M.J., Lonergan, L., 2003. Exhumation of the Ronda peridotite and its crustal envelope: constraints from thermal modelling of a P–T–time array. Journal of the Geological Society of London 160, 655–676.
Polat, A., 2012. Growth of Archean continental crust in oceanic island arcs. Geology 40, 383–384.
Portnyagin, M., Almeev, R., Matveev, S., Holtz, F., 2008. Experimental evidence for rapid H_2O exchange between melt inclusions in olivine and host magma. Earth and Planetary Science Letters 272, 541–552.
Rapp, R.P., Shimizu, N., Norman, M.D., 2003. Growth of early continental crust by partial melting of eclogite. Nature 425, 605–609.
Roedder, E., 1979a. Origin and significance of magmatic inclusions. Bulletin of Mineralogy 102, 487–510.
Roedder, E., 1979b. Fluid inclusions as samples of ore fluids. In: Barnes, H.L. (Ed.), Geochemistry of Hydrothermal Ore Deposits. Wiley, New York, pp. 684–737.
Roedder, E., 1984. Fluid Inclusions, Reviews in Mineralogy vol. 12. Mineralogical Society of America, Washington, DC.
Rubatto, D., Hermann, J., Buick, I.S., 2006. Temperature and bulk composition control on the growth of monazite and zircon during low-pressure anatexis (Mount Stafford, Central Australia). Journal of Petrology 47, 1973–1996.
Sawyer, E.W., 1996. Melt segregation and magma flow in migmatites: implications for the generation of granite magmas. Transactions of the Royal Society of Edinburgh: Earth Sciences 87, 85–94.
Sawyer, E.W., 1999. Criteria for the recognition of partial melting. Physics and Chemistry of the Earth 24, 269–279.
Sawyer, E.W., 2008. Atlas of migmatites. Mineralogical Association of Canada. The Canadian Mineralogist Special Publication 9, Quebec City.
Sawyer, E.W., 2010. Migmatites formed by water-fluxed partial melting of a leucogranodiorite protolith: microstructures in the residual rocks and source of the fluid. Lithos 116, 273–286.
Sawyer, E.W., Cesare, B., Brown, M., 2011. When the continental crust melts. Elements 7, 229–234.
Scaillet, B., France-Lanord, C., Le Fort, P., 1990. Badrinath–Gangotri plutons (Garhwal, India): petrological and geochemical evidence for fractionation processes in a high Himalayan leucogranite. Journal of Volcanology and Geothermal Research 44, 163–188.
Schiano, P., 2003. Primitive mantle magmas recorded as silicate melt inclusions in igneous minerals. Earth Science Reviews 63, 121–144.

Schmidt, M.W., Vielzeuf, D., Auzanneau, E., 2004. Melting and dissolution of subducting crust at high pressures: the key role of white mica. Earth and Planetary Science Letters 228, 65–84.
Severs, M.J., Azbej, T., Thomas, J.B., Mandeville, J.B., Bodnar, R.J., 2007. Experimental determination of H_2O loss from melt inclusions during laboratory heating: evidence from Raman spectroscopy. Chemical Geology 237, 358–371.
Silver, L.T., Chappell, B.W., 1988. The Peninsular Range Batholith: an insight into the evolution of the cordilleran batholiths of the southwestern North America. Transactions of the Royal Society of Edinburgh: Earth Sciences 79, 105–121.
Sobolev, A.V., Danyushevsky, L.V., 1994. Petrology and geochemistry of boninites from the north termination of the Tonga Trench: constraints on the generation conditions of primary high-Ca boninite magmas. Journal of Petrology 35, 1183–1211.
Sobolev, V.S., Kostyuk, V.P., 1975. Magmatic crystallization based on a study of melt inclusions. Fluid Inclusions Research 9, 182–253 (translated from original publication in Russian).
Sorby, H.C., 1858. On the microscopical structure of crystals, indicating origin of minerals and rocks. Quarterly Journal of the Geological Society of London 14, 453–500.
Stevens, G., Clemens, J.D., 1993. Fluid-absent melting and the roles of fluids in the lithosphere: a slanted summary? Chemical Geology 108, 1–17.
Stevens, G., Clemens, J.D., Droop, G.T.R., 1997. Melt production during granulite-facies anatexis: experimental data from "primitive" metasedimentary protoliths. Contributions to Mineralogy and Petrology 128, 352–370.
Stevens, G., Villaros, A., Moyen, J.-F., 2007. Selective peritectic garnet entrainment as the origin of geochemical diversity in S-type granites. Geology 35, 9–12.
Stöckhert, B., Duyster, J., Trepmann, C., Massonne, H.-J., 2001. Microdiamond daughter crystals precipitated from supercritical COH + silicate fluids included in garnet, Erzgebirge, Germany. Geology 29, 391–394.
Stöckhert, B., Trepmann, C., Massonne, H.J., 2009. Decrepitated UHP fluid inclusions: about diverse phase assemblages and extreme decompression rates (Erzgebirge, Germany). Journal of Metamorphic Geology 27, 673–684.
Sun, S.S., McDonough, W.F., 1989. Chemical and Isotopic Systematics of Oceanic Basalts: Implications for Mantle Composition and Processes. In: Sanders, A.D., Norry, M.J. (Eds.), Magmatism in the Ocean Basins. Geological Society, London, Special Publications 42, pp. 313–345.
Tait, S., 1992. Selective preservation of melt inclusions in igneous phenocrysts. American Mineralogist 77, 146–155.
Tajčmanová, L., Conolly, J.A.D., Cesare, B., 2009. A thermodynamic model for titanium and ferric iron solution in biotite. Journal of Metamorphic Geology 27, 153–165.
Taylor, J., Nicoli, G., Stevens, G., Frei, D., Moyen, J.-F., 2014. The processes that control the leucosome composition in metasedimentary granulites: perspectives from the Southern Marginal Zone migmatites, Limpopo Belt, South Africa. Journal of Metamorphic Geology 32, 713–742.
Thomas, R., Thomas, R., 1994. Fluid evolution in relation to the emplacement of the Variscan granites in the Erzgebirge region: a review of the melt and fluid inclusion evidence. In: Seltmann, R., Kampf, H., Moller, P., Seltmann, R., Kampf, H., Moller, P. (Eds.), Metallogeny of Collisional Orogens Focussed on the Erzgebirge and Comparable Metallogenetic Setting. Czech Geological Survey, pp. 70–81.
Thomas, R., 2000. Determination of H_2O contents of granite melt inclusions by confocal laser Raman microprobe spectroscopy. American Mineralogist 85, 868–872.
Thomas, R., Kamenetsky, V.S., Davidson, P., 2006. Laser Raman spectroscopic measurements of water in unexposed glass inclusions. American Mineralogist 91, 467–470.
Thomas, R., Klemm, W., 1997. Microthermometric study of silicate melt inclusions in Variscan granites from SE Germany: volatile contents and entrapment conditions. Journal of Petrology 38, 1753–1765.
Thompson, A.B., 1988. Dehydration melting of crustal rocks. Reconditi della Societa Italiana di Mineralogia e Petrologia 43, 41–60.
Thompson, A.B., 1990. Heat, Fluids, and Melting in the Granulite Facies. In: Vielzeuf, D., Vidal, Ph. (Eds.), Granulites and Crustal Evolution. NATO ASI Series 311, pp. 37–57.
Torres-Roldán, R.L., 1981. Plurifacial metamorphic evolution of the Sierra Bermeja peridotite aureole (Southern Spain). Estudios Geológicos 37, 115–133.
Touret, J.L.R., Huizenga, J.M., 2012. Fluid-assisted granulite metamorphism: a continental journey. Gondwana Research 21, 224–235.
Vannay, J.-C., Hodges, K.V., 1996. Tectonometamorphic evolution of the Himalayan metamorphic core between the Annapurna and Dhaulagiri, central Nepal. Journal of Metamorphic Geology 14, 635–656.
Vernon, R.H., Collins, W.J., 1988. Igneous microstructures in migmatites. Geology 16, 1126–1129.
Vernon, R.H., 2007. Problems in identifying restite in S-type granites of southeastern Australia, with speculations on sources of magma and enclaves. The Canadian Mineralogist 45, 147–178.
Vernon, R.H., 2011. Microstructures of melt-bearing regional metamorphic rocks. In: Van Reenen, D.D., Kramers, J.D., McCourt, S., Perchuk, L.L. (Eds.), Origin and Evolution of Precambrian High-Grade Gneiss Terranes, with Special Emphasis on the Limpopo Complex of Southern Africa. Geological Society of America Memoir 207, pp. 1–11.
Vidal, Ph., Cocherie, A., Le Fort, P., 1982. Geochemical investigations of the origin of the Manaslu leucogranite (Himalaya, Nepal). Geochimica et Cosmochimica Acta 46, 2279–2292.
Vielzeuf, D., Holloway, J.R., 1988. Experimental determination of the fluid-absent melting relations in the pelitic system. Contributions to Mineralogy and Petrology 98, 257–276.
Wang, J., Zhang, J., Wei, C., Rai, S., Wang, M., Qian, J., 2015. Characterising the metamorphic discontinuity across the Main Central Thrust Zone of eastern-central Nepal. Journal of Asian Earth Sciences 101, 83–100.
Watt, G.R., Burns, I.M., Graham, G.A., 1996. Chemical characteristics of migmatites: accessory phase distribution and evidence for fast melt segregation rates. Contributions to Mineralogy and Petrology 125, 100–111.
Watt, G.R., Harley, S.L., 1993. Accessory phase controls on the geochemistry of crustal melts and restites produced during water-undersaturated partial melting. Contributions to Mineralogy and Petrology 114, 550–566.
Weber, C., Barbey, P., 1986. The role of water, mixing processes and metamorphic fabric in the genesis of the Baume migmatites (Ardèche, France). Contributions to Mineralogy and Petrology 92, 481–491.
Weber, C., Barbey, P., Cuney, M., Martin, H., 1985. Trace element behavior during migmatization. Evidence for a complex melt-residuum–fluid interaction in the St. Malo migmatitic dome (France). Contributions to Mineralogy and Petrology 90, 52–62.
Webster, J.D., 2006. Melt Inclusions in Plutonic Rocks. Mineralogical Association of Canada Short Course Series vol. 36. Mineralogical Association of Canada, Montreal.
Weinberg, R.F., Hasalovà, P., 2015. Water-fluxed melting of the continental crust: a review. Lithos 212–215, 158–188.
White, A.J.R., Chappell, B.W., 1988. Some supracrustal (S-type) granites of the Lachlan Fold Belt. Transactions of the Royal Society of Edinburgh: Earth Sciences 79, 169–181.
Wilkinson, J.J., Rankin, A.H., Nolan, J., 1996. Silicothermal fluid: a novel medium for mass transport in the lithosphere. Geology 24, 1059–1062.
Yardley, B., Valley, J.W., 1997. The petrologic case for a dry lower crust. Journal of Geophysical Research, Solid Earth 102, 12173–12185.
Zajacz, Z., Halter, W., Malfait, W.J., Bachmann, O., Bodnar, R.J., Hirschmann, M.M., Mandeville, C.W., Morizet, T., Müntener, O., Ulmer, P., Webster, J.D., 2005. A composition-independent quantitative determination of the H_2O content in silicate glasses and silicate melt inclusions by confocal Raman spectroscopy. Contributions to Mineralogy and Petrology 150, 631–642.
Zeck, H.P., Williams, I., 2002. Inherited and magmatic zircon from Neogene Hoyazo cordierite dacite, SE Spain-Anatectic source rock provenance and magmatic evolution. Journal of Petrology 43, 1089–1104.
Zeng, L., Liang, F., Asimow, P., Chen, F.-Y., Chen, J., 2009. Partial melting of deeply subducted continental crust and the formation of quartzofeldspathic polyphase inclusions in the Sulu UHP eclogites. Chinese Science Bulletin 54, 2580–2594.